1. PHYSICAL AND MECHANICAL PROPERTIES OF REACTOR MATERIALS

(1503)

J. B. Conway,* P. N. Flagella†

The purpose of this program is to measure and evaluate high-temperature (to 3000°C) physical and mechanical properties of commercially available and newly developed materials being considered for use in fueled and non-fueled high-temperature reactor applications.

1.1 CREEP-RUPTURE STUDIES

A significant amount of creep-rupture data for wrought, unalloyed, tungsten and molybdenum have been obtained over the last few years at temperatures from 1600° to 3000°C. Results have shown that wrought material, fabricated by the powder-metallurgy process, does not consistently exhibit the same strength (rupture life), creep resistance (linear creep rate), and ductility (elongation at rupture). Powder-metallurgy material was found to be characterized by considerable duplexing of the structure with a significant portion of deformation related to grain boundary separation or cavitation leading to fracture in the grain boundaries.

Wrought, arc-cast material exhibited more consistent behavior. Extremely large grains formed in high-temperature tests and deformation occurred as crystallographic slip and grain boundary sliding. No void formation was observed in the grain boundaries. Arc-cast material was considerably more ductile with fracture being transgranular.

TUNGSTEN

Stress-Rupture and Creep

Stress-rupture and creep data for wrought, unalloyed, arc-cast tungsten sheet, identifying code W(3), were obtained over a broad range of temperatures and stresses. The results are summarized in Figures 1.1 and 1.2 and indicate a change in slope for both the stress-rupture and creep rate curves at 2200°C. The slope for the creep rate curve at low stresses is consistent with the isotherms for 2400°C and 2600°C. A similar change in slope is indicated for stress-rupture data at 2400°C but not at 2600°C. The mechanism associated with slope changes has not been identified.

Creep Rate Correlation

The creep data obtained for arc-cast tungsten, W(3), from 1600° to 3000°C were evaluated based on the proposed method of Sherby[1] for pure polycrystalline metals above one-half the absolute melting temperature. The results are presented in Figure 1.3 in terms of the ratio of steady-state creep rate ($\dot{\epsilon}_S$) to the diffusion coefficient (D) plotted as a function of creep stress (σ) divided by the elastic modulus (E). Correlation of the data

*Project leader.

†Principal investigator.

[1]O. D. Sherby, "Factors Affecting the High Temperature Creep of Polycrystalline Solids," Acta Met., Vol. 10, 1962, p. 135.

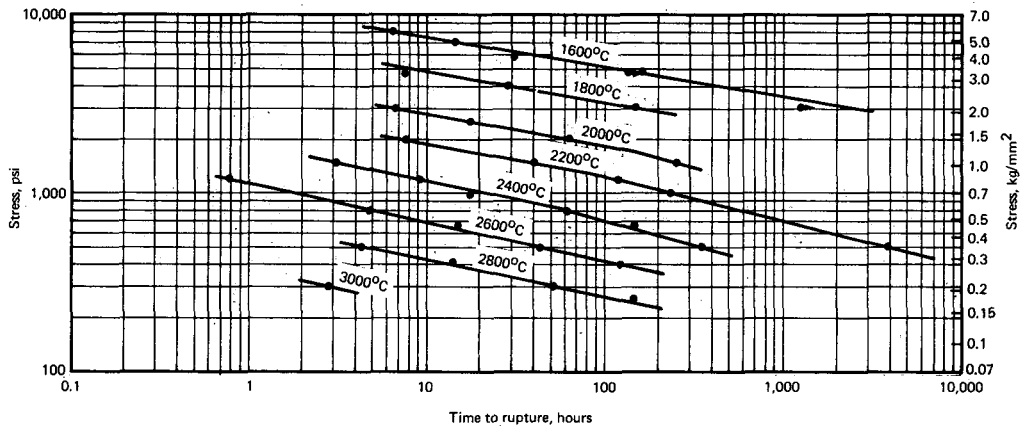

Fig. 1.1 — Stress-rupture test results for wrought, arc-cast unalloyed tungsten, W(3), sheet tested in hydrogen

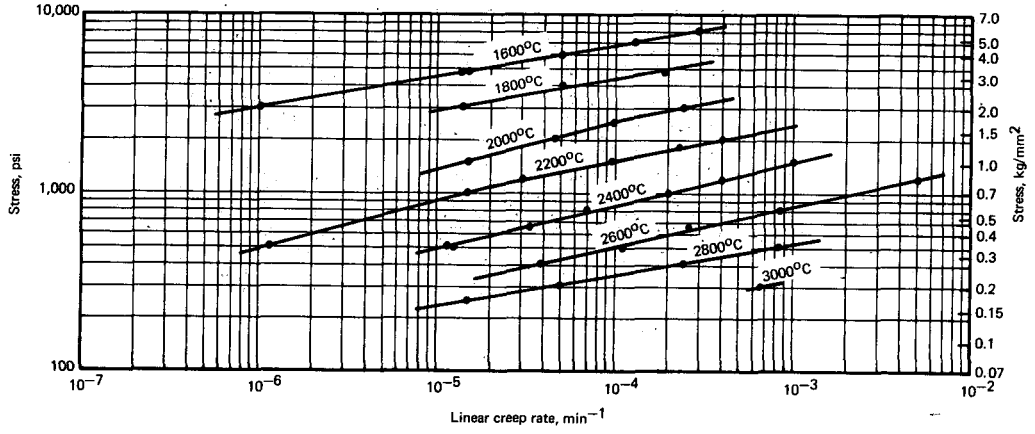

Fig. 1.2 — Creep rate test results for wrought, arc-cast unalloyed tungsten, W(3), sheet tested in hydrogen

in this manner appears to be quite good with the curve shape the same as that determined by Sherby for some other pure polycrystalline metals. The slope, n, of the linear portion of the curve is 4.2 and is consistent with Sherby's prediction that the value be approximately 5. This portion of the curve is associated with a creep process controlled by dislocation climb involving an equilibrium vacancy concentration. The non-linear portion of the curve (higher stresses) involves dislocation climb under conditions where vacancy concentration is greater than the equilibrium value.

Ductility

Evaluations of rupture elongation, for both powder-metallurgy (PM) and arc-cast (AC) tungsten, were made to obtain the results shown in Figure 1.4. (PM data are the result of testing three different vendor sources of material.) The PM sheet exhibited a decreasing trend in ductility with temperature from 1600° to 2800°C; the AC sheet showed a decrease in ductility from 1600° to 1800°C followed by a significant increase, peaking at 2200° to 2400°C, and then a decrease with further increasing temperature to 3000°C. Fracture in the PM sheet occurred only in the grain boundaries; no transgranular failures

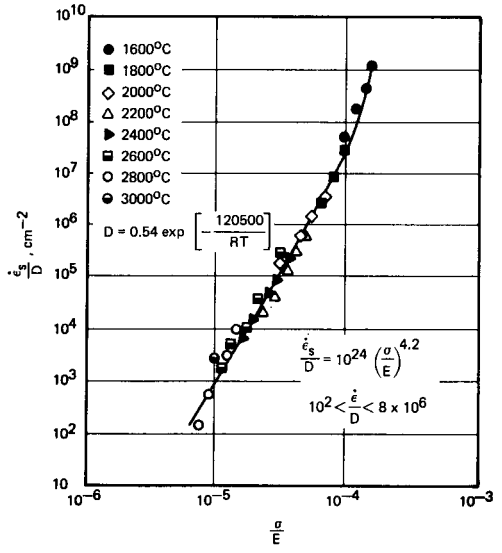

Fig. 1.3 — Ratio of steady-state creep rate ($\dot{\epsilon}_s$) to diffusion coefficient (D) versus ratio of stress (σ) to Young's modulus (E) for arc-cast W

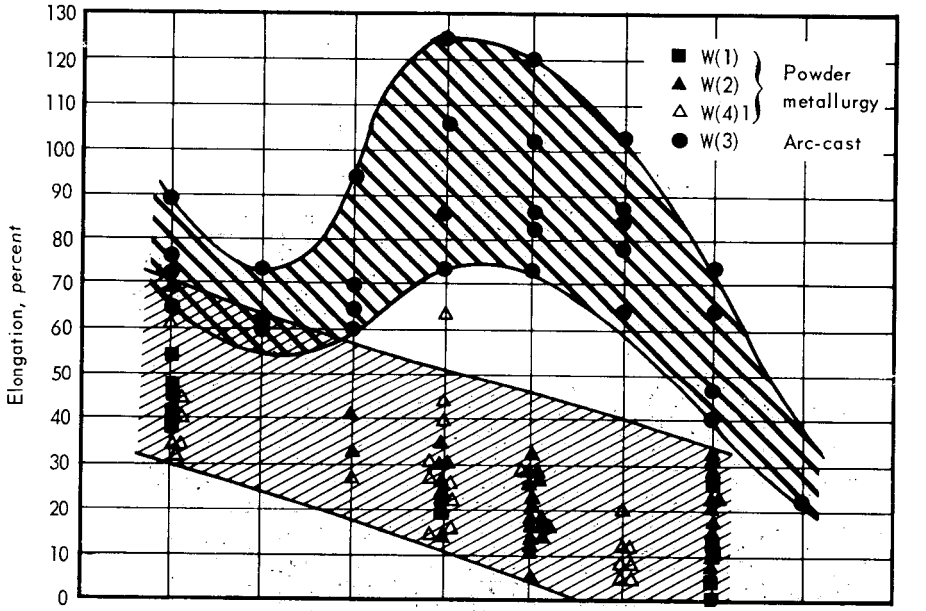

Fig. 1.4 — Elongation versus temperature for wrought powder-metallurgy and wrought arc-cast unalloyed W sheet tested in hydrogen

were observed. Failure in the AC sheet was principally transgranular with little or no grain boundary fissuring observed.

Although initial grain size appears to have an effect on the strength and ductility of these materials, the presence of many large grains after failure in the PM sheet indicates that some factor in addition to grain size must be exerting an effect. All fractures in the PM sheet occurred in grain boundaries indicating that the grain boundaries are weaker than the matrix at test conditions. The AC sheet grain boundaries remained strong and ductile leading to typical ductile transgranular deformation and ultimately resulting in "woody" tearing-type fractures with the grain boundaries appearing to play no direct part.

Reasons for reduction in ductility of the AC sheet at about 1800°C are not clear. Individual creep curves as well as instantaneous strain rate values plotted as a function of strain show a distinct discontinuity associated with the drop in ductility. Some inhibiting mechanism is apparently operative in the region of the second stage of creep (usually associated with a constant rate of dislocation flow).

Creep Analysis

Studies of creep data for arc-cast tungsten, W(3), were performed using the method proposed by Woodford[2] for constant-load tests. Although most analyses and interpretations of creep mechanisms are based on constant-stress tests, most experimental data for materials are obtained using the constant-load technique. For constant-load tests, actual stress on the specimen increases as strain increases since the cross-sectional area is decreasing. In both types of testing, the assumption is made that deformation occurs uniformly over the gage length until local necking is initiated.

A special computer program was written to analyze experimental strain – time data. This program was designed to yield calculated values of the instantaneous creep rate and instantaneous or true stress (the latter values are based on an assumption of constant volume deformation). For the portion of the creep curve beyond that corresponding to minimum creep rate, a plot of instantaneous creep rate versus instantaneous stress was found to be linear on logarithmic coordinates (Figure 1.5). For each temperature, then, a relationship of the form $\dot{\epsilon} = A\sigma^n$ is indicated; where $\dot{\epsilon}$ is the instantaneous creep rate beyond the minimum, σ is the instantaneous or true stress, and A and n are constants. Based on this approach, the following expression was obtained relating $\dot{\epsilon}$ to the initial stress, σ_o, and the strain, ϵ, in a constant-load creep test:

$$\dot{\epsilon} = \frac{d\epsilon}{dt} = A\sigma^n = A[\sigma_o(1 + \epsilon)]^n . \qquad (1.1)$$

Integration at constant σ_o and solving for time, t, yields:

$$t = B(1 + \epsilon)^{1-n} + C \qquad (1.2)$$

where C is the constant of integration and n is the slope of the plot shown in Figure 1.5 at any given temperature.

For a given value of σ_o, this expression defines a linear relationship between t and $(1 + \epsilon)^{1-n}$ for the region beyond the minimum creep rate. A typical plot of this type is shown in Figure 1.6 for the tungsten data at 2400°C for which n = 4.291. Linearity is noted at all σ_o values. It has been found in this analysis that the value of C [i.e., the

[2]D. A. Woodford, "Constant-Load Creep Data Interpreted in Terms of the Stress Dependence of Dislocation Velocity," Trans. Met. Soc. of AIME, Vol. 239, May 1967, p. 655.

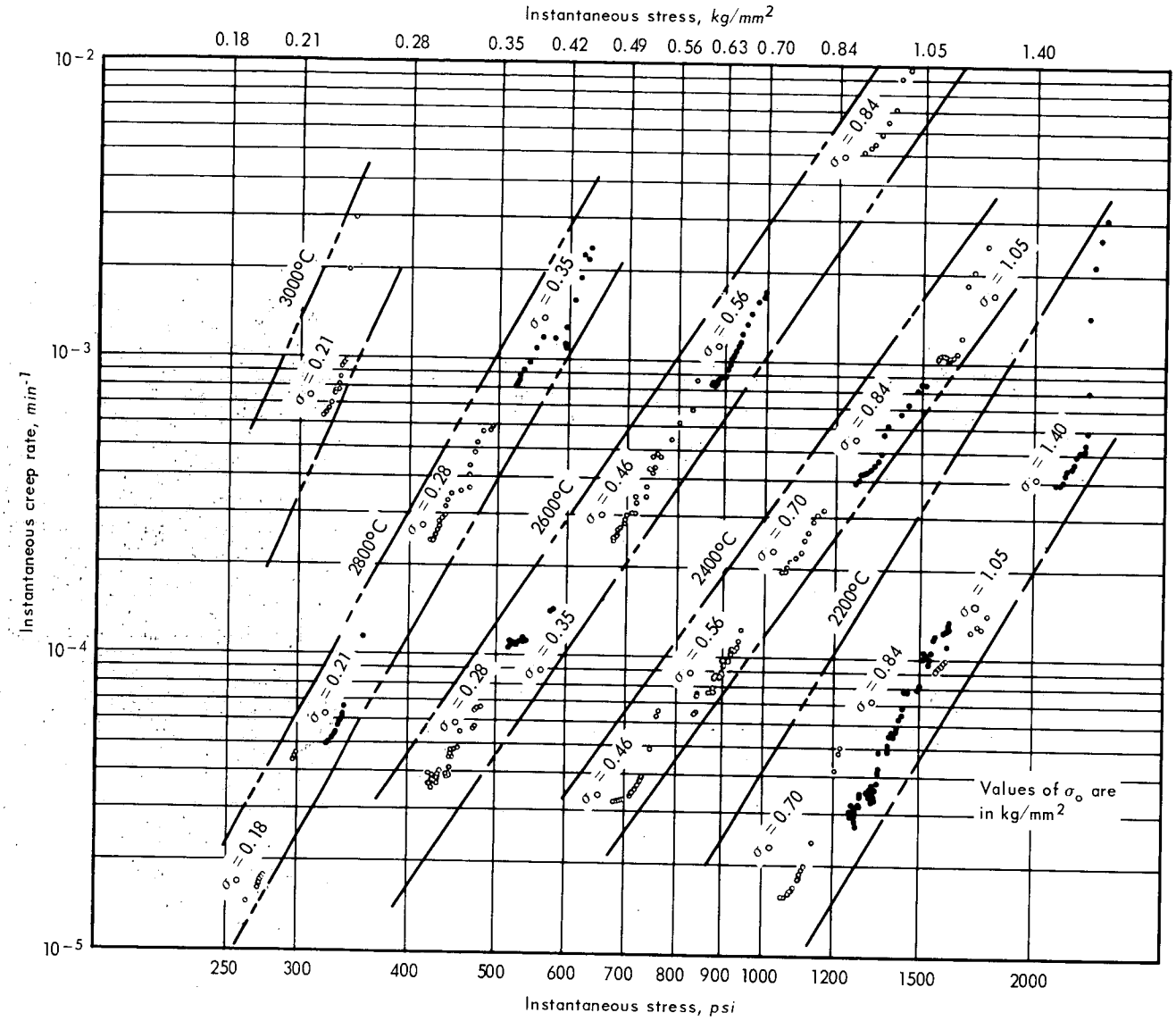

Fig. 1.5 — Creep rate versus instantaneous stress for W at various temperatures and initial stress (σ_o) values

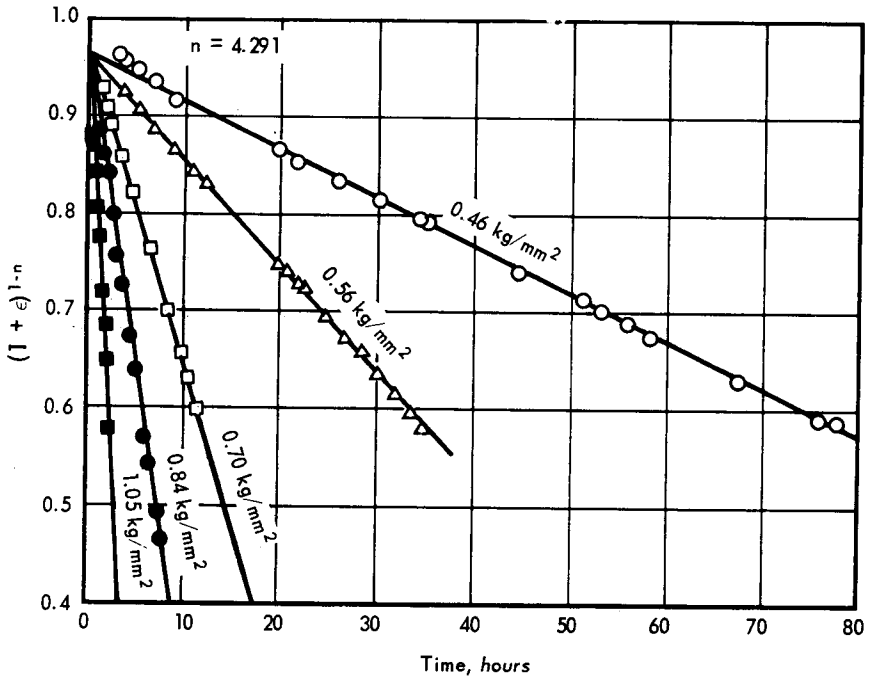

Fig. 1.6 — Tungsten W(3) data at 2400°C analyzed in terms of $(1 + \epsilon)^{1-n}$ versus time

intercept in Figure 1.6 at $(1 + \epsilon)^{1-n} = 0$] at any given temperature is related to σ_o according to:

$$C = D\sigma_o^m \tag{1.3}$$

leading to:

$$\epsilon = \frac{1}{(E - F\sigma_o^m t)^p} - 1 \tag{1.4}$$

Expressions of this type for the tungsten data obtained in this study are:

T = 2400°C

$$\epsilon = \frac{1}{(0.95 - 6.1708 \times 10^{-15}\ \sigma_o^{4.225}\ t)^{0.30386}} - 1 \tag{1.5}$$

T = 2600°C

$$\epsilon = \frac{1}{(0.95 - 7.5289 \times 10^{-15}\ \sigma_o^{4.561}\ t)^{0.2922}} - 1 \tag{1.6}$$

T = 2800°C

$$\epsilon = \frac{1}{(0.94 - 1.6707 \times 10^{-16}\ \sigma_o^{5.557}\ t)^{0.2247}} - 1 \tag{1.7}$$

where:

ϵ is strain
t is time, hr
σ_o is initial stress, $kg/mm^2 \times 1422.3$

The experimental results obtained at 2400°C and those determined from the above equation are compared in Figure 1.7. The agreement is excellent when considering the problems and uncertainties associated with testing at 2400°C.

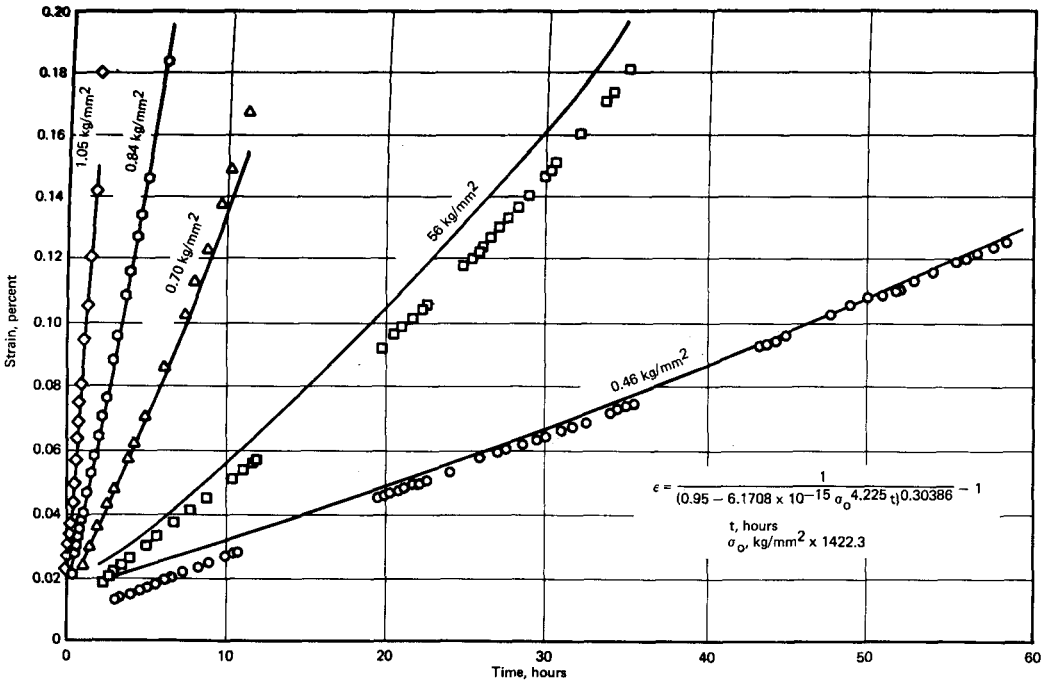

Fig. 1.7 — Strain versus time creep data for arc-cast tungsten tested at 2400°C in H_2 atmosphere

Hot Hardness

Wrought, arc-cast tungsten sheet, W(3), specimens were annealed in hydrogen at various temperatures for different times. Microhardness measurements were then made from room temperature to 1300°C. Results are given in Figure 1.8 for three specimens annealed at 1200°, 1400°, and 1600°C. As shown, a break in the curve occurs at approximately 300°C (0.16 T_m, where T_m represents the absolute melting temperature) consistent with data reported previously[3] for unalloyed tungsten. Also shown is a decrease in hardness with increasing annealing temperature over the total temperature range investigated. These differences are apparently related to the grain size differences resulting from the annealing treatments. Figure 1.9 compares the grain size and typical indents obtained in determining the microhardness of specimens annealed at 1200°C and 1600°C. The specimen receiving the highest-temperature anneal (1600°C) had such large grains that the indent and resulting symmetrical deformation pattern were contained within a single grain. The specimen annealed at 1200°C shows a relatively fine-grained structure with no deformation pattern apparent. Average grain sizes associated with the data given in Figure 1.8 are 20, 28, and 88 microns for annealing temperatures of 1200°, 1400°, and 1600°C, respectively.

Microstructural Studies (R. C. Rau, S. F. Bartram, P. N. Flagella)

Microstructural studies, using optical and electron microscopy and X-ray diffraction techniques, were performed on high-purity polycrystalline tungsten after creep-rupture testing at stress levels ranging from 0.18 to 5.62 kg/mm^2 over the temperature range from

[3] "AEC Fuels and Materials Development Program Progress Report No. 67," GE-NMPO, GEMP-67, June 30, 1967, p. 55.

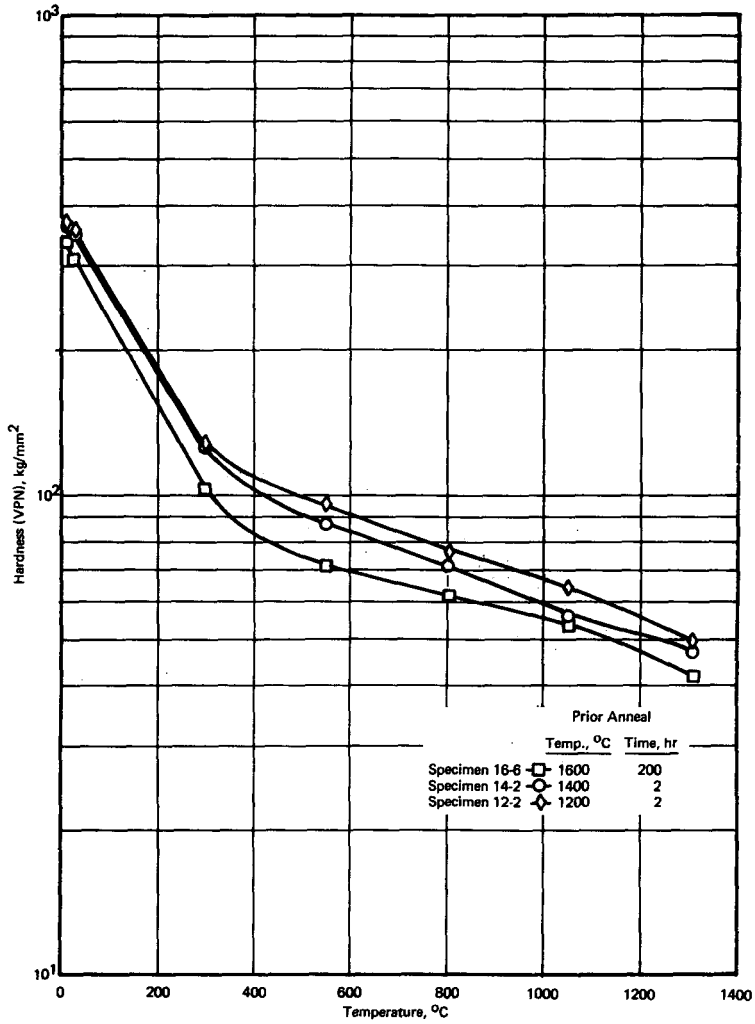

Fig. 1.8 — Hot microhardness of wrought, arc-cast tungsten sheet, W(3), after various annealing treatments

1600° to 3000°C. The objectives of these studies were (1) to characterize the dislocation microstructure in arc-cast tungsten as a function of stress and temperature, and (2) to determine the failure mechanisms in arc-cast and powder-metallurgy processed tungsten.

Dislocation Microstructures in Arc-Cast Tungsten – Development of dislocation substructures in metals during high-temperature deformation plays an important role in determining creep resistance. This substructure consists of dislocation networks or tangles, which form low-angle subgrain boundaries between slightly misoriented regions of material, and free dislocations located within the subgrains. In the present investigation, subgrain sizes, dislocation densities, and subgrain boundary tilt angles were determined in arc-cast, unalloyed tungsten and have been correlated with high-temperature creep conditions. Although the specimens used in this study had all been tested to failure, microstructural examinations were carried out on regions somewhat removed from the fracture to avoid third-stage creep effects and thus concentrate on effects related more nearly to secondary creep.

Material used for this study was 1.5-mm-thick wrought, arc-cast, polycrystalline tungsten, W(3), sheet. Creep-rupture specimens with 6.4-mm gage widths and 25.4-mm gage

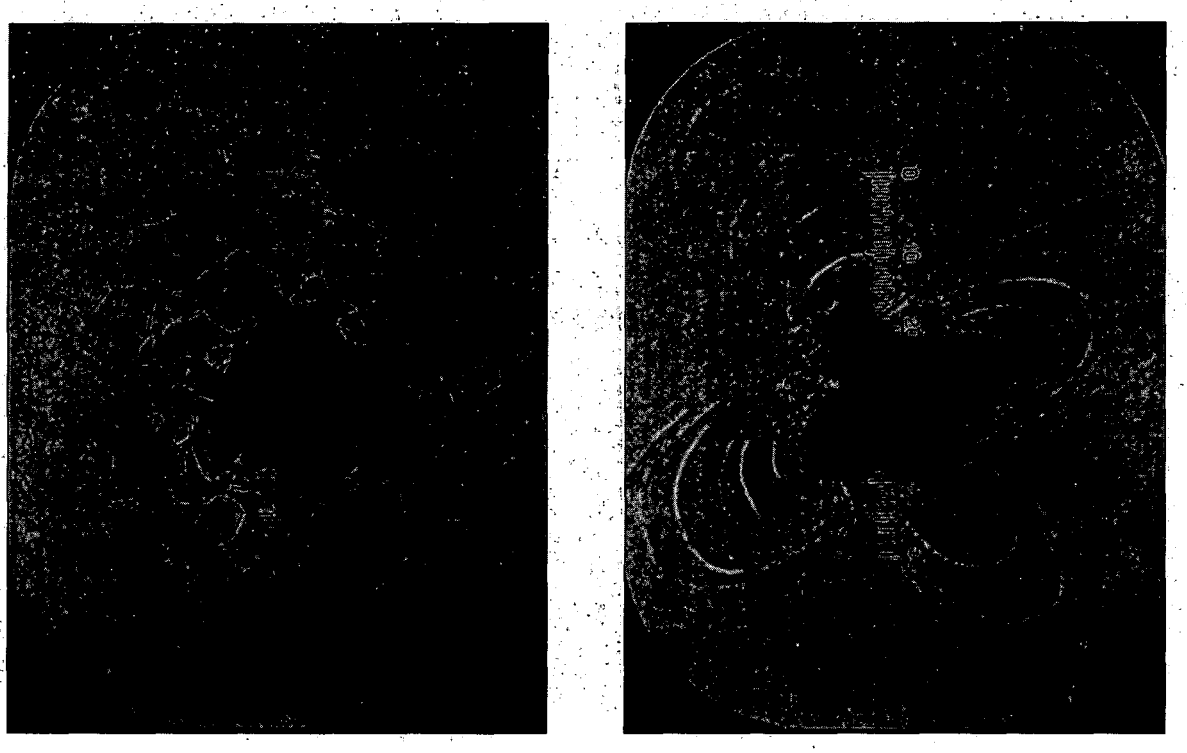

1200°C anneal for 2 hours.
Indent at 1308°C.

1600°C anneal for 200 hours.
Indent at 1310°C.

Fig. 1.9 — Photomicrographs of wrought, arc-cast unalloyed tungsten sheet showing typical indents and microstructure after hot hardness testing (200X)

lengths were tested under constant load at temperatures ranging from 1600° to 3000°C and at stress levels ranging from 0.18 to 5.62 kg/mm^2 in a hydrogen atmosphere. All specimens were annealed at test temperature for 2 hours before stress was applied.

A number of experimental techniques were used in studying the substructure of the creep-tested specimens. Optical microscopy methods were used to determine subgrain sizes and free dislocation densities. These measurements were made using electrolytically polished and etched surfaces parallel to the stress axis. To gain increased resolution and magnification over that available by optical microscopy, replica electron microscopy techniques were used to study etch pits in some samples. Replication of the polished and etched surfaces involved a two-stage plastic/carbon technique, using chromium shadowing. Direct observations of the dislocation microstructures were made by transmission electron microscopy of thin foils prepared by a double-jet electrolytic thinning technique.[4] These observations were used primarily for determining the dislocation separations within subgrain boundaries and for direct measurements of tilt angles between subgrains. Finally, back-reflection Laue X-ray diffraction photographs were used for indirect determinations of subgrain sizes and subgrain boundary tilt angles. This method, described previously,[5] has the advantage over direct microscopic methods of providing bulk measurements integrated over a volume of the sample. A summary of the results for the tungsten samples examined is given in Table 1.1.

[4]R. L. Ladd and R. C. Rau, "Immersed Double-Jet Technique for Electrothinning Tungsten for Transmission Electron Microscopy," Rev. Sci. Instrum., Vol. 38, 1967, p. 1162.

[5]"AEC Fuels and Materials Development Program Progress Report No. 71," GE-NMPO, GEMP-1002, December 29, 1967, pp. 18–28.

TABLE 1.1

MICROSTRUCTURAL DATA ON ARC-CAST TUNGSTEN

Sample Number	Creep Testing Conditions: Temperature, °C	Stress, kg/mm²	Stress, psi	Subgrain Diameter, mm: Optical	Subgrain Diameter, mm: X-Ray	Free Dislocation Density, 10^4 per mm²: Optical	Free Dislocation Density, 10^4 per mm²: Electron	Subgrain Boundary Tilt Angle, degrees	Dislocation Separation in Sub-Boundaries, Å: X-Ray	Dislocation Separation in Sub-Boundaries, Å: Electron	Dislocation Density in Sub-Boundaries, 10^5 per mm²
W(3)-69	1600	5.62	8000	~0.01	<0.01		4.7			525	
-71	1600	3.37	4800	~0.01	<0.01	3.5					
-50	1800	3.37	4800	0.013	0.057	7.4	12.8	0.294		780	
-87	1800	2.46	3500	0.075	0.084	1.0		0.207	897	1340	2.73
-52	1800	2.11	3000							1507	
-53	2000	2.11	3000	0.028	0.090	3.5		0.364	505	1070	4.47
-58	2000	1.76	2500			0.3					
-39	2000	1.41	2000	0.083	0.096	0.30	0.96	0.265	721		3.05
-46	2000	1.41	2000	0.075	0.077		1.5	0.365	512		5.22
-45	2000	1.05	1500	0.14	0.10	1.3		0.257	712	500	2.83
-13	2200	1.41	2000	0.067	0.10	2.6	11.1	0.321	589		3.48
-16	2200	0.70	1000	0.10	0.12	1.3		0.522	355	1250	4.79
-38	2400	1.05	1500	0.05	0.092	4.2	3.4	0.333	567		4.00
-21	2400	0.70	1000			0.71					
-85	2400	0.56	800	0.10	0.21	0.42		0.160	1152	633	8.42
-24	2400	0.56	800			1.2					
-22	2400	0.46	650			0.53					
-19	2600	0.84	1200	0.057	0.16	0.9	4.9	0.366	510		2.55
-27	2600	0.28	400	0.40	0.55	1.6		0.342	531		6.85
-28	2800	0.35	500	0.18	0.33	1.1		0.220	828		7.36
-36	2800	0.21	300	0.27	0.30	0.32		0.344	529		12.64
-49	3000	0.21	300	0.31	0.42	1.3		0.272	678		7.14

Optical microscope examination of the tested specimens showed that the structure almost invariably consisted of very large grains, often covering the entire width and thickness of the pieces. This large grain size was verified by Laue back-reflection X-ray photographs, and permitted such photographs to be obtained from single grains. A few exceptions to this large-grained microstructure were specimens tested at the lower temperatures (1600°C and 1800°C) and higher stress levels (>3 kg/mm^2). In these specimens, the typical large-grained microstructure occurred at the surfaces, but a fine-grained polycrystalline texture was retained in the interior.

Substructure developed within the large grains during testing consisted of subgrain boundaries and free dislocations, both of which are revealed by etch pits, as shown in the optical micrographs of Figure 1.10. Typical back-reflection Laue photographs are shown in Figure 1.11. The pattern in Figure 1.11a shows typical clusters of small spots corresponding to the subgrain reflections from a single large tungsten grain, while that in Figure 1.11b shows spotty Debye-Scherrer rings from small randomly oriented grains in a low-temperature, high-stress specimen. Such a pattern, which must be produced by grains having a mean dimension of about 10^{-2}mm, cannot be used for subgrain measurements.

Subgrain diameters measured by direct optical examination are listed in column five of Table 1.1; those determined indirectly from the Laue photographs are listed in column six. The agreement between the results is considered quite good, although the subgrain diameters indicated by X-ray tend to be slightly larger than those measured with the microscope. This is probably due to overlap and coincidences of spots in the Laue pat-

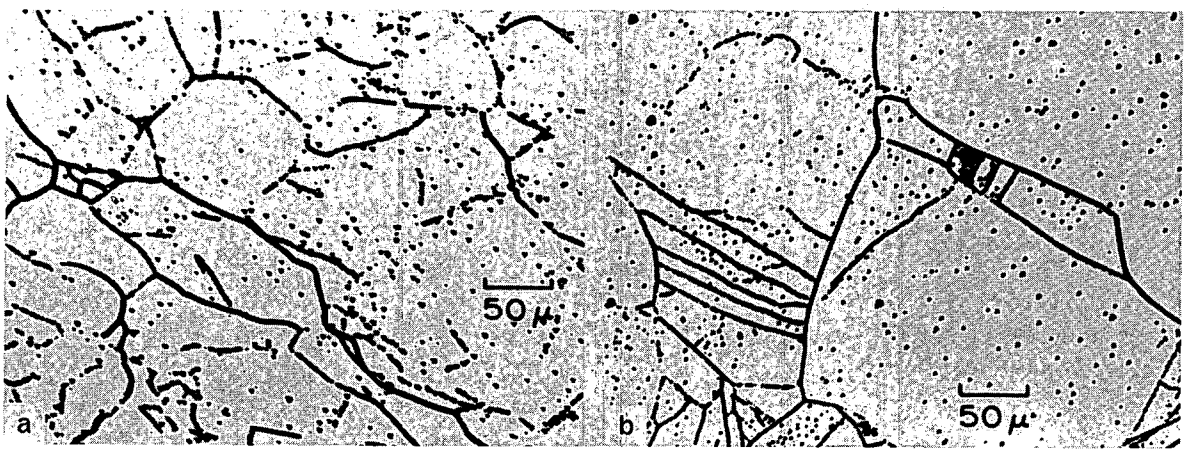

Fig. 1.10 — Optical micrographs showing etch pits delineating subgrain boundaries and free dislocations in tungsten
(a) Specimen tested at 2000°C and 1.05 kg/mm^2.
(b) Specimen tested at 3000°C and 0.21 kg/mm^2.

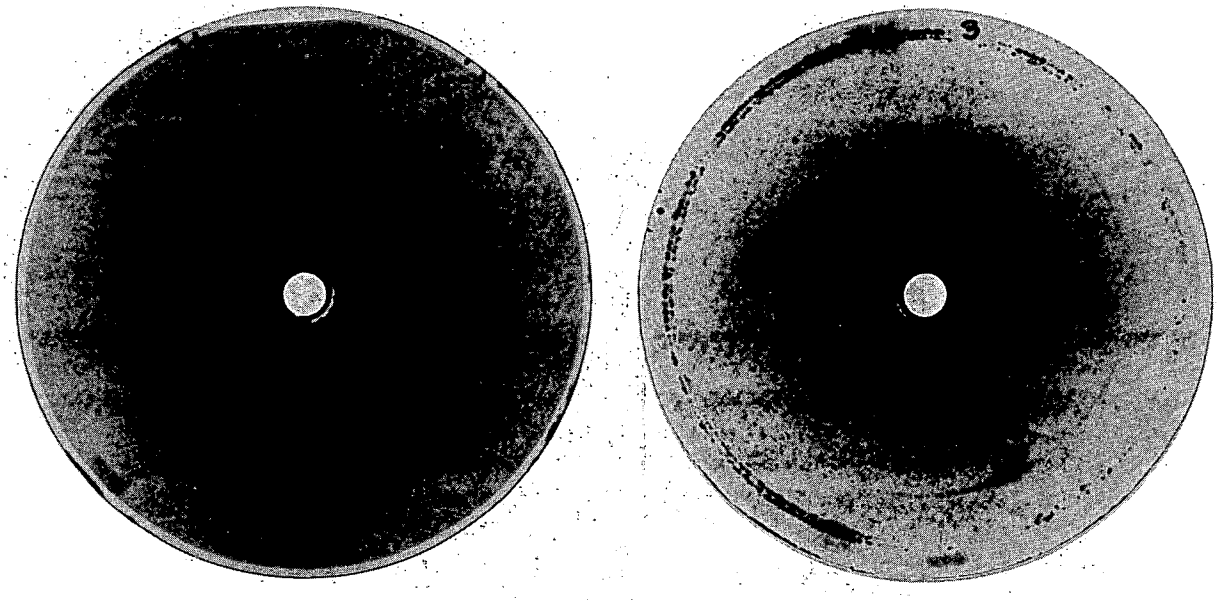

Fig. 1.11 — Typical back-reflection Laue photographs of creep tested tungsten. (a) Diffraction spot clusters due to slightly misoriented subgrains in specimen tested at 2600°C and 0.84 kg/mm^2. (b) Spotty Debye-Scherrer rings from polycrystalline region of specimen tested at 1600°C and 5.62 kg/mm^2.

terns, leading to low estimates of spot densities within the clusters and therefore high calculated subgrain diameters.

The subgrain sizes in tungsten are independent of test temperature and show an inverse relationship to creep stress, as indicated in Figure 1.12. This log-log plot shows a nearly linear dependence, similar to that obtained for aluminum,[6] iron,[7] and steels[8,9] tested at various stress levels. In a recent review, Sherby and Burke[10] correlated subgrain sizes, L, with stress, σ, for a number of metals, and showed that the data seem to obey a power relation of the type

$$\sigma = KL^{-\beta}, \tag{1.8}$$

where β is almost equal to unity. The tungsten data of Figure 1.12 appear to follow a similar relation.

Free dislocation densities were determined by counting the etch pits within subgrains in areas such as those seen in the optical micrographs of Figure 1.10. In addition, free etch pits in some specimens were counted from composite replica electron micrographs such as that shown in Figure 1.13. Results obtained from the two counts are listed in columns seven and eight, respectively, of Table 1.1. Unlike subgrain sizes, which are a function only of creep stress, the free dislocation density depends upon both temperature and stress. The relationship is illustrated in Figure 1.14. As shown by this plot, the number of etch pits, or the density of free dislocations, increases with increasing stress at constant temperature and increases with increasing temperature at constant stress. To maintain a fixed concentration of free dislocations, the temperature must be decreased if the stress is increased.

The relationship of the free dislocation density (ρ) to stress appears similar to that observed for the linear creep rate ($\dot{\epsilon}_s$) as a function of stress (power law at constant temperature) for this same material. Good correlation of the creep rate data was obtained when $\dot{\epsilon}_s$ was divided by the diffusion coefficient (Figure 1.3) as suggested by Sherby[11] for polycrystalline solids. When the same technique is applied to the dislocation density data, good correlation is also obtained, as shown in Figure 1.15. The same stress dependency (4.2) is obtained for the diffusion compensated ρ as for the diffusion compensated $\dot{\epsilon}_s$ parameter. This linear portion of the curve is believed to result from creep by dislocation climb or by the motion of jogged screw dislocations involving an equilibrium concentration of vacancies. Barrett[12] indicates that slip models based on the glide of jogged screw dislocations can predict an approximate power law region with $\dot{\epsilon}_s \propto \sigma^5$ but require the ρ to be a strong function of stress (σ^3 or σ^4). The present data appear to support this model, at least for the high-temperature, low-stress region. The dislocation densities in the low-temperature, high-stress region, showing a deviation from the power law dependence, are apparently influenced by excess vacancies.

[6] I. S. Servi and N. J. Grant, "Structure Observations of Aluminum Deformed in Creep at Elevated Temperatures," Trans. of AIME, Vol. 191, 1951, p. 917.

[7] A. Goldberg, "Influence of Prior Cold Work on the Creep Resistance and Microstructure of a 0.05% Carbon Steel," J. Iron and Steel Inst., Vol. 204, 1966, p. 268.

[8] F. Garofalo, O. Richmond, W. F. Domis, and F. von Gemmingen, "Strain-Time, Rate-Stress and Rate-Temperature Relations During Large Deformations in Creep," Joint International Conference on Creep, The Institution of Mechanical Engineers, London, 1963, p. 1-31.

[9] F. Garofalo, W. F. Domis, and F. von Gemmingen, "Effect of Grain Size on the Creep Behavior of an Austenitic Iron-Base Alloy," Trans. Met. Soc. of AIME, Vol. 230, 1964, p. 1460.

[10] O. D. Sherby and P. M. Burke, "Mechanical Behavior of Crystalline Solids at Elevated Temperatures," Progress in Materials Science, Vol. 13, No. 7, 1967, p. 325.

[11] O. D. Sherby, "Factors Affecting the High Temperature Creep of Polycrystalline Solids," Acta Met., Vol. 10, 1962, p. 135.

[12] C. R. Barrett, "On the Stress Dependence of High Temperature Creep," Trans. of AIME, Vol. 239, 1967, p. 1726.

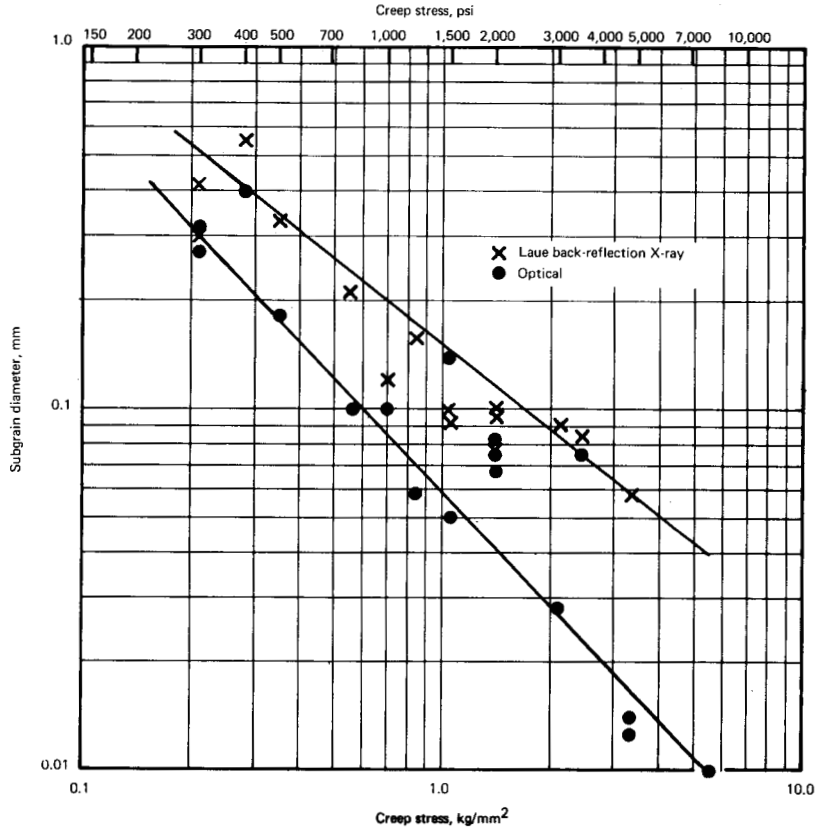

Fig. 1.12 – Effect of stress on the subgrain diameter of arc-cast tungsten as the result of creep-rupture testing from 1600° to 3000°C

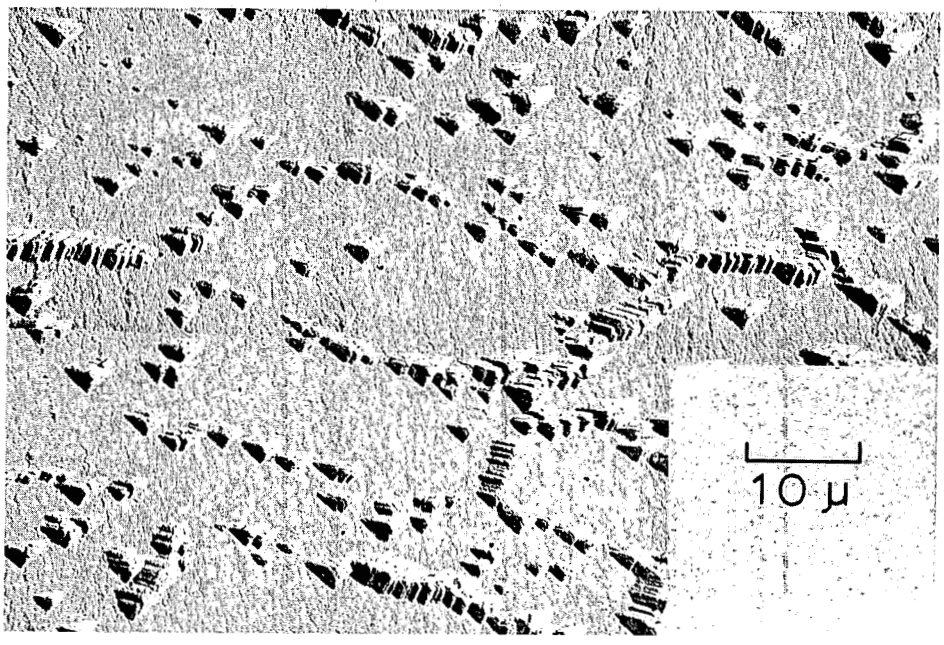

Fig. 1.13 – Composite replica electron micrograph of overlapping areas used for etch-pit counting. Tungsten tested at 1600°C and 5.62 kg/mm^2.

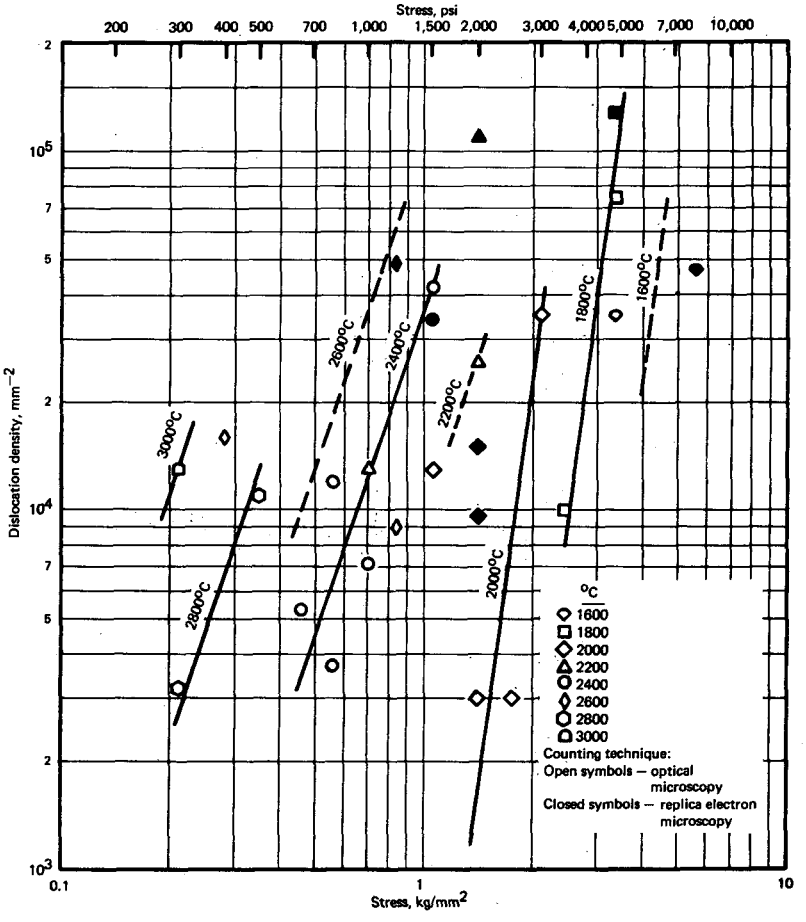

Fig. 1.14 — Number of free etch pits (dislocations) as a function of stress and temperature for wrought, arc-cast tungsten after creep tests from 1600° to 3000°C

Average misorientation angles between subgrains, determined by the back-reflection Laue technique, are listed in column nine of Table 1.1. The values obtained range from 0.16 to 0.52 degree, with the average for all samples being 0.31 degree. If the actual number of subgrains present has been underestimated, because of overlap of Laue spots, the calculated tilt angles may be somewhat too large, but the error should not exceed about 0.05 degree. These values are in good agreement with subgrain misorientations reported for other creep tested metals.[13,14] To check the values of tilt angle directly, measurements of misorientations between subgrains in one sample were made from selected area electron diffraction patterns obtained with the electron microscope. Values obtained by this technique ranged from 0.17 to 0.47 degree, with the average being 0.29 degree, in good agreement with the X-ray results.

From the tilt angles, the average dislocation separation within the subgrain boundaries was calculated. This separation, S, is given by the expression[15]

[13]F. Garofalo, L. Zwell, A. S. Keh, and S. Weissmannn, "Substructure Formation in Iron During Creep at 600°C," Acta Met., Vol. 9, 1961, p. 721.

[14]R. W. Guard, "Discussion of Parker and Washburn Paper on the Role of the Boundary in Creep Phenomena," Creep and Recovery, American Society for Metals, 1957, p. 251.

[15]S. Amelinckx and W. Dekeyser, "The Structure and Properties of Grain Boundaries," Solid State Phys., Vol. 8, 1959, p. 325.

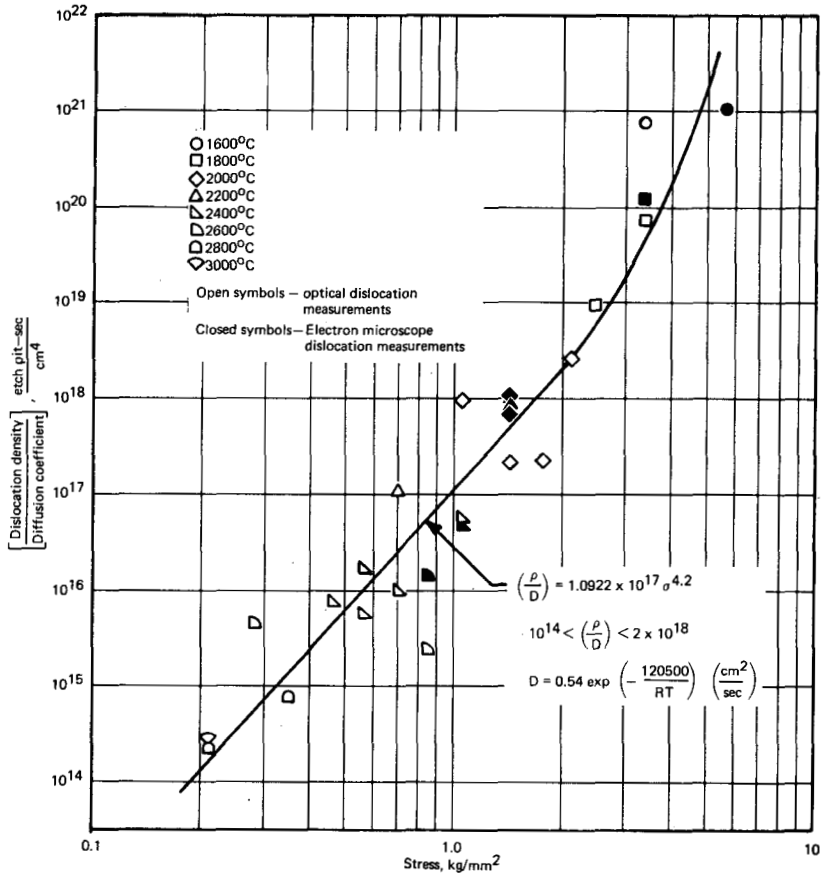

Fig. 1.15 – Correlation of diffusion-compensated dislocation density as a function of stress for wrought, arc-cast unalloyed tungsten, W(3), creep tested at temperatures from 1600° to 3000°C

$$S = \frac{b}{2 \sin \theta/2} \tag{1.9}$$

where b is the length of the Burgers vector of the dislocations and θ is the tilt angle. At small angles this expression reduces to

$$S = \frac{b}{\theta} \tag{1.10}$$

where θ is expressed in radians. Using this expression and the tilt angles tabulated in column nine of Table 1.1, the separation distances given in column ten were obtained.

Direct observations of subgrain boundary dislocation configurations and measurements of separations between the dislocations were made by transmission electron microscopy. Two subgrain boundaries analyzed crystallographically are shown in Figures 1.16 and 1.17, while typical measurements of dislocation separations are listed in column 11 of Table 1.1. Although these measured separations represent a small number of individual dislocation networks and cannot be considered good statistical values, they nevertheless verify the accuracy of the calculated values given in column ten.

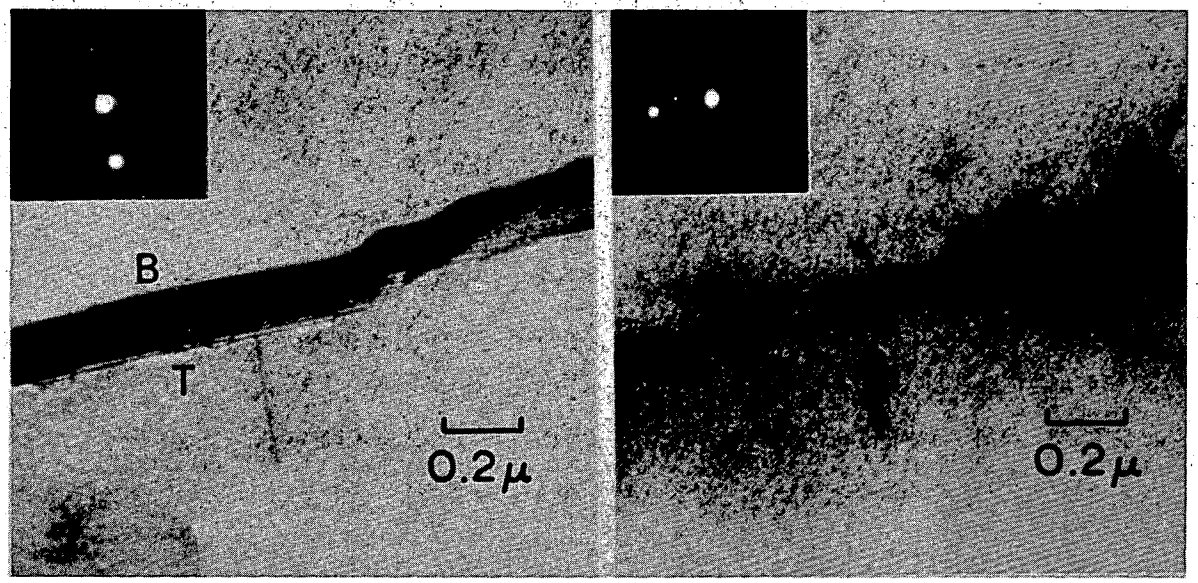

Fig. 1.16 — Transmission electron micrographs of nearly pure tilt boundary in tungsten tested at 1800°C and 2.11 kg/mm^2. (a) Operating reflection (110); intersections of the boundary with the bottom and top surfaces of the foil are indicated by B and T, respectively. (b) Operating reflection ($1\bar{1}0$).

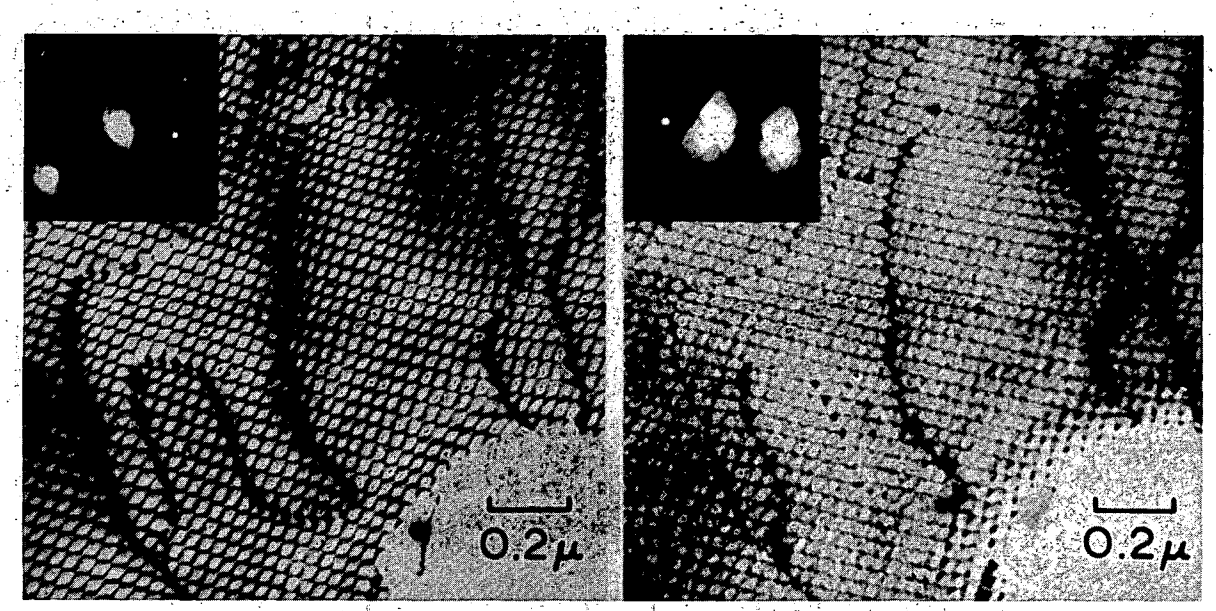

Fig. 1.17 — Transmission electron micrographs of twist boundary in tungsten at 1800°C and 3.37 kg/mm^2. (a) Operating reflection ($0\bar{2}0$). (b) Operating reflection (110).

Finally, from the subgrain diameter and tilt angle data, the dislocation density, ρ, in the subgrain boundaries was calculated from the expression[16]

$$\rho = \frac{2\theta}{Lb}, \tag{1.11}$$

where θ is the tilt angle in radians, L is the subgrain diameter, and b is the Burgers vector of the dislocations. This calculation thus gives the number of dislocations per unit area which are tied up in the subgrain boundary networks, rather than the number of free or mobile dislocations which can contribute to deformation under stress. The total number of subgrain boundary dislocations must obviously increase with increasing tilt angles and decreasing subgrain sizes.

Subgrain boundary dislocation densities were calculated from the subgrain diameters and tilt angles derived from the Laue photographs, columns six and nine, respectively, of Table 1.1, and are given in column 12 of that table. The data reveal that the number of dislocations in the subgrain boundaries tends to increase with decreasing stress at constant temperature and gradually increases as the temperature is raised. These observations indicate that during creep, free mobile dislocations within the subgrains move to and accumulate in the subgrain boundaries. Since dislocation movement during high-temperature creep is primarily diffusion controlled, longer times (i.e., lower stresses) and higher temperatures would be expected to increase the number of dislocations occupying subgrain boundaries.

The two subgrain boundaries shown in Figures 1.16 and 1.17 represent the two basic types of subgrain misorientations which can occur in body-centered cubic (bcc) metals. Figure 1.16 shows a nearly pure tilt boundary formed when subgrain misorientation occurs by a rotation about an axis in the boundary plane, while Figure 1.17 shows a twist boundary formed when such misorientation occurs about an axis perpendicular to the boundary plane. Most observed boundaries are formed by a combination of these two basic rotations.

Tilting experiments in the electron microscope reveal that the tilt boundary shown in Figure 1.16 lies on a $(11\bar{1})$ plane, inclined approximately 45 degrees from the (001) foil plane. Intersections of this boundary with the bottom and top surfaces of the foil are denoted B and T, respectively, in Figure 1.16a. It can be seen that the parallel set of closely spaced straight dislocations comprising this boundary is imaged in strong contrast in Figure 1.16a, where the (110) reflection is operating (i.e., $\bar{g} = [1\bar{1}0]$), but is at extinction in Figure 1.16b where the $(1\bar{1}0)$ reflection is operating (i.e., $\bar{g} = [1\bar{1}0]$, $\bar{g} \cdot \bar{b} = 0$). This diffraction contrast behavior is consistent with dislocations having a Burgers vector $b = a/2[11\bar{1}]$, indicating that they are edge dislocations and that the boundary is composed primarily of extra half-planes inserted on the $(11\bar{1})$ boundary plane. The fact that a second set of widely spaced dislocations, visible in both micrographs, is superimposed on this network of parallel edge dislocations indicates that the boundary is not a pure tilt boundary, but has a small amount of twist character.

Several direct measurements across the tilt boundary of Figure 1.16 indicate that the misorientation between the subgrains is about 0.83 degree of arc, i.e., a higher than average subgrain misorientation. The measured separation of the edge dislocations in Figure 1.16a is approximately 105 Å. Making a geometrical correction for the measured slope of the boundary plane, the true spacing of the dislocations is then 183 Å. This is in very good agreement with the value of 188 Å calculated from equation (1.10) for a pure tilt boundary composed of a/2 <111> dislocations and having a tilt angle of 0.83 degree.

[16]D. McLean, "Creep Processes in Coarse-Grained Aluminum," J. Inst. Metals, Vol. 80, 1951–52, p. 507.

The twist boundary of Figure 1.17 is a very extensive planar boundary, lying on the (001) plane parallel to the plane of the foil. The extinction conditions illustrated by the photomicrographs of Figure 1.17 indicate that the network is composed of three sets of straight dislocations, two having Burgers vectors of the type a/2<111> and one having $\bar{b}$ = a <100>, as diagramed in Figure 1.18, plus a superimposed set of randomly oriented stranger dislocations which were not identified. One of the following two interactions has occurred to form the short a <100> dislocation segments:

$$a/2\,[111] + a/2\,[1\bar{1}\bar{1}] = a\,[100]$$

$$a/2\,[11\bar{1}] + a/2\,[1\bar{1}1] = a\,[100];$$

however, the diffraction conditions observed were not sufficient to differentiate between these two equivalent possibilities.

Similar networks have been identified in the bcc metals iron[17,18] and tantalum.[19] The observed mesh shape in Figure 1.17 agrees rather well with that calculated by Carrington, Hale, and McLean[17] for a network on {100}, from strictly theoretical considerations. It should be pointed out, however, that since this boundary does not lie on a {110} plane, it is not pure twist, but actually is a mixed boundary, i.e., it is not composed of pure screw dislocations. The <100> segments are in screw orientation, but the a/2 <111> segments have mixed edge and screw character.[15]

Using equation (1.10), the angle of misorientation between the two subgrains on either side of this boundary was calculated from the mesh size of the network. This gave a value of about 0.47 degree, in good agreement with a number of measurements on other boundaries and within the range of tilt angles determined by the back-reflection Laue method.

Failure Mechanisms in Arc-Cast and Powder Metallurgy Tungsten – Using replica electron microscopy, Stiegler et al.[20] studied the formation of voids or cavities at the grain boundaries of powder-metallurgy processed tungsten subjected to creep deformation at 1650°C and 2200°C. They found that at both test temperatures specimens generally failed in a brittle manner, and they attributed this failure to the growth and linking up of grain boundary cavities.

Recently, however, it has been shown that while powder-metallurgy tungsten creep-rupture tested at temperatures ranging from 1600° to 3000°C failed in a brittle, intergranular manner, specimens prepared from arc-cast material and tested under similar conditions failed in a ductile manner. High-temperature stress-rupture tests of molybdenum also showed similar differences in the failure behavior of powder-metallurgy and arc-cast material.[21] These results indicate that different mechanisms of failure are operating in the two types of materials. To determine this basic difference, optical microscopy and electron fractography studies of creep-rupture-tested powder metallurgy and arc-cast tungsten were undertaken.

The studies were performed using selected powder-metallurgy (W-4) and arc-cast (W-3) tungsten specimens. These specimens were formed from sheet material with initial thicknesses of 0.5 mm for powder-metallurgy specimens and 1.5 mm for arc-cast specimens.

[17] W. Carrington, K. F. Hale, and D. McLean, "Arrangements of Dislocations in Iron," Proc. Roy. Soc., A Vol. 259, 1960, p. 203.

[18] S. M. Ohr and D. N. Beshers, "Crystallography of Dislocation Networks in Annealed Iron," Phil. Mag., Vol. 8, 1963, p. 1343.

[19] D. Hull, I. D. McIvor, and W. S. Owen, "The Distribution of Dislocations in Annealed Tantalum," J. Less-Common Metals, Vol. 4, 1962, p. 409.

[20] J. O. Stiegler, K. Farrell, B. T. M. Loh, and H. E. McCoy, "Nature of Creep Cavities in Tungsten," Trans. ASM, Vol. 60, 1967, p. 494.

[21] P. N. Flagella, "High-Temperature Stress-Rupture Characteristics of Mo and Mo Alloys," AIAA Journal, Vol. 5, 1967, p. 281.

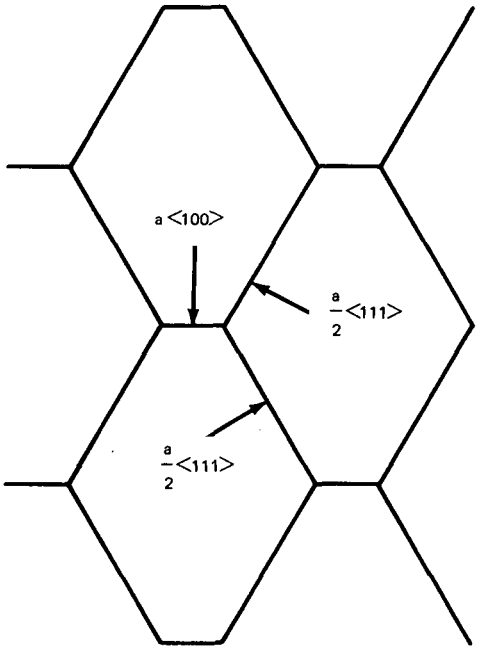

Fig. 1.18 — Schematic drawing of the three sets of dislocations comprising the twist boundary network of Figure 1.17

Specimens examined had been creep tested at 1600°, 2000°, 2200°, and 2600°C, with the results listed in Table 1.2.

For the fractographic study, fresh fracture surfaces in the highly stressed region near the original break were created by clamping the specimen in a vise with about 3 mm of the broken end protruding and sharply rapping the protruding end. These newly exposed surfaces were then replicated by the standard two-stage plastic/carbon technique, using chromium shadowing, and examined in the electron microscope.

After replication, these same pieces were mounted and mechanically polished for metallographic examination. The pieces were mounted edge-on, with the view perpendicular to

TABLE 1.2

TUNGSTEN SPECIMENS USED FOR STUDY OF FAILURE MECHANISM

Sample No.	Test Temperature, °C	Stress kg/mm²	Stress psi	Time to Rupture, hr	Elongation, %	Maximum Void Content, %	Measured Void Content, %	Ratio of Measured/Max. Void Content, %	Average Grain Size, microns
Powder Metallurgy									
W(4)-1-73	1600	4.22	6000	51.27	32	24.2	5.58	23.1	32.5
-79	2000	2.11	3000	23.17	27	21.3	2.46	11.5	38.0
-18	2200	1.41	2000	15.29	15	13.0	2.02	15.5	48.5
-10	2200	1.12	1600	60.65	17	14.5	2.11	14.6	48.5
-8	2600	0.84	1200	8.84	8	7.4	1.11	15.0	215.5
-7	2600	0.70	1000	25.08	5	4.8	0.90	18.8	264.0
Arc-Cast									
W(3)-48	1600	4.22	6000	30.90	76				
-53	2000	2.11	3000	6.70	70				
-14	2200	1.05	1500	40.70	106				
-25	2600	0.56	800	4.77	64				

the stress axis, and were examined and photographed in the as-polished condition. In this way, any stress-induced porosity was observed in its original state, unaltered by chemical attack. Following examination for porosity, some of the specimens were etched for grain size evaluation.

Optical microscopy of the as-polished surfaces showed an abundance of grain boundary cavities in the powder-metallurgy tungsten, and an almost total lack of such cavities in the arc-cast material. Representative micrographs are presented in Figure 1.19, where a and b are powder-metallurgy material, and c and d are arc-cast material.

As illustrated by these micrographs, the powder-metallurgy material consisted of fairly equiaxed grains, which increased in average size with increasing test temperature. Grain boundary separation and cavitation were very pronounced, especially along boundaries which were transverse to the stress direction. On the other hand, arc-cast material was composed of very large grains extending across the total thickness of the specimens and showed practically no tendency to form cavities. A rare instance of a grain boundary cavity in the arc-cast specimen tested at 1600°C is indicated by the arrow in Figure 1.19c.

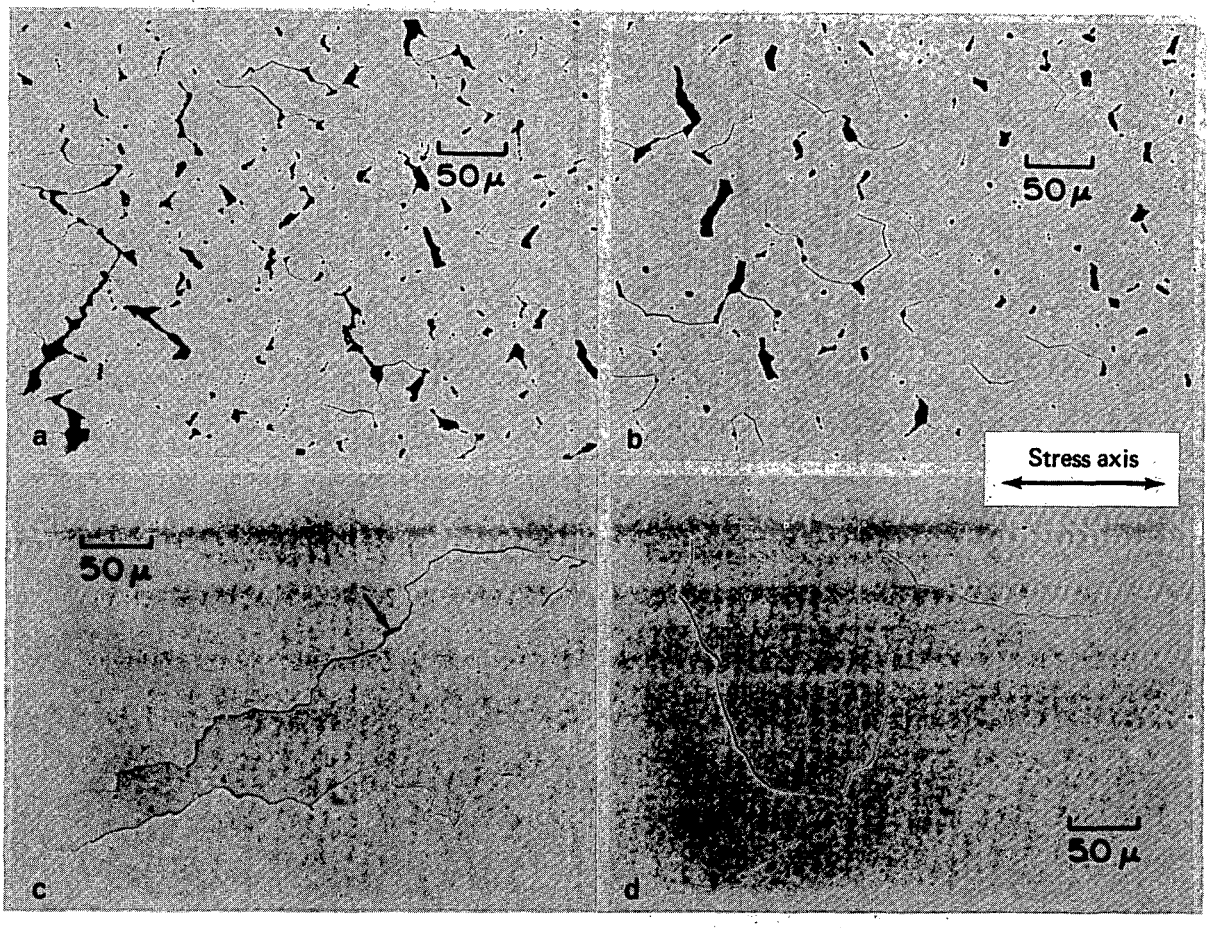

Fig. 1.19 – Optical micrographs of creep-rupture-tested tungsten in as-polished condition. (a) Powder-metallurgy specimen tested at 1600°C and 4.22 kg/mm^2. (b) Powder-metallurgy specimen tested at 2000°C and 2.11 kg/mm^2. (c) Arc-cast specimen tested at 1600°C and 4.22 kg/mm^2. (d) Arc-cast specimen tested at 2000°C and 2.11 kg/mm^2.

Replica electron microscopy of the powder-metallurgy samples showed that the fracture mode was almost totally intergranular, especially for the low-temperature, high-stress conditions, and that the exposed grain boundary surfaces contained a profusion of cavities. Typical examples are illustrated in Figure 1.20. At low temperatures the voids were usually irregular in shape, tending to be relatively flattened along the boundary surface and often containing elongated "fingers" suggestive of void coalescence, Figure 1.20a. Such cavities are termed wedged-shaped, or w-type,[22] and are believed to originate primarily by grain boundary sliding.[23,24] At higher temperatures, the shape of the cavities became more polyhedral, especially at low-stress levels, Figure 1.20b. These more rounded, or r-type[22] voids, are bounded by flat crystallographic facets which correspond to low-index planes of the cubic lattice.[25] Such polyhedral voids form under conditions where surface diffusion permits the cavities to reduce their surface tensions and assume equilibrium shapes. Although a few examples were seen of creep cavities aligned along grain boundary triple junctions, Figure 1.20c, there was nothing to indicate that such junctions were preferred sites for voids. In general, both w-type and r-type cavities tended to be distributed uniformly over the grain boundary surfaces, in agreement with the observations of Stiegler et al.[20]

In contrast to the powder-metallurgy material, replica electron micrographs of the arc-cast tungsten showed that the fracture at all temperatures was predominantly transgranular, as illustrated in Figure 1.21a. When grain boundary surfaces were seen, they were always relatively clean and contained only a few small irregularities suggestive of cavities, Figure 1.21b. In none of these samples was any evidence seen of cavity coalescence or polyhedral shaped voids.

An attempt was made to quantitatively correlate the observed microstructural features with the mechanical properties of the creep-tested specimens. This involved measurements of the open porosity and grain size in the powder-metallurgy specimens, Table 1.2. However, similar measurements could not be made on the arc-cast material because of the lack of porosity and the extremely large grain size.

For the powder-metallurgy tungsten, which failed with relatively little elongation in comparison with the arc-cast material, it was of interest to determine whether all of the elongation was caused by cavitation or whether other mechanisms also contributed. Accordingly, lineal measurements of open porosity were made from the as-polished surfaces at 250X magnification. These measurements were made parallel to the stress (elongation) direction at approximately 3 to 4 mm from the original fracture of each specimen in regions similar to those shown in Figures 1.19a and b. The averages of ten measurements made on each sample were converted to percentages of the length sampled, and are listed in column eight of Table 1.2.

Maximum possible void content in the stress direction, assuming that the total elongation was due to cavitation, was calculated from the measured elongations listed in column six of Table 1.2 using the relation:

$$\text{Max void content } (\%) = \frac{\text{elongation } (\%) \times 100}{100 + \text{elongation } (\%)}.$$

Comparison of the values listed in column seven of the table with the measured values of column eight shows that only a portion of the total elongation can be accounted for by the cavities. This relative proportion, however, remains essentially constant as the test

[22] F. Garofalo, Fundamentals of Creep and Creep-Rupture in Metals, Macmillan Series in Materials Science, New York, 1965, p. 213.

[23] C. Zener, Elasticity and Anelasticity of Metals, University of Chicago Press, Chicago, 1948, p. 158.

[24] H. C. Chang and N. J. Grant, "Mechanism of Intercrystalline Fracture," Trans. of AIME, Vol. 206, 1956, p. 544.

[25] K. Farrell, B. T. M. Loh, and J. O. Stiegler, "Morphologies of Bubbles and Voids in Tungsten," Trans. ASM, Vol. 60, 1967, p. 485.

Fig. 1.20 — Electron fractographs of powder-metallurgy tungsten. (a) Irregular creep cavities in specimen tested at 1600°C and 4.22 kg/mm^2. (b) Polyhedral shaped voids in specimen tested at 2600°C and 0.70 kg/mm^2. (c) Cavities along a grain boundary triple junction in specimen tested at 2600°C and 0.84 kg/mm^2.

temperature increases and overall ductility decreases. As shown in column nine of the table, the portion of the elongation due to cavities is about 16 percent of that expected if cavitation were the only source of deformation.

To determine if grain deformation had occurred during creep, lineal grain size measurements were made in the longitudinal (stress) and transverse directions both in the high-stress regions where porosity measurements had been made and in the unstressed holder ends of the specimens. These measurements showed the grains to be elongated approximately 40 percent in the stress direction in all specimens, but this elongation was the

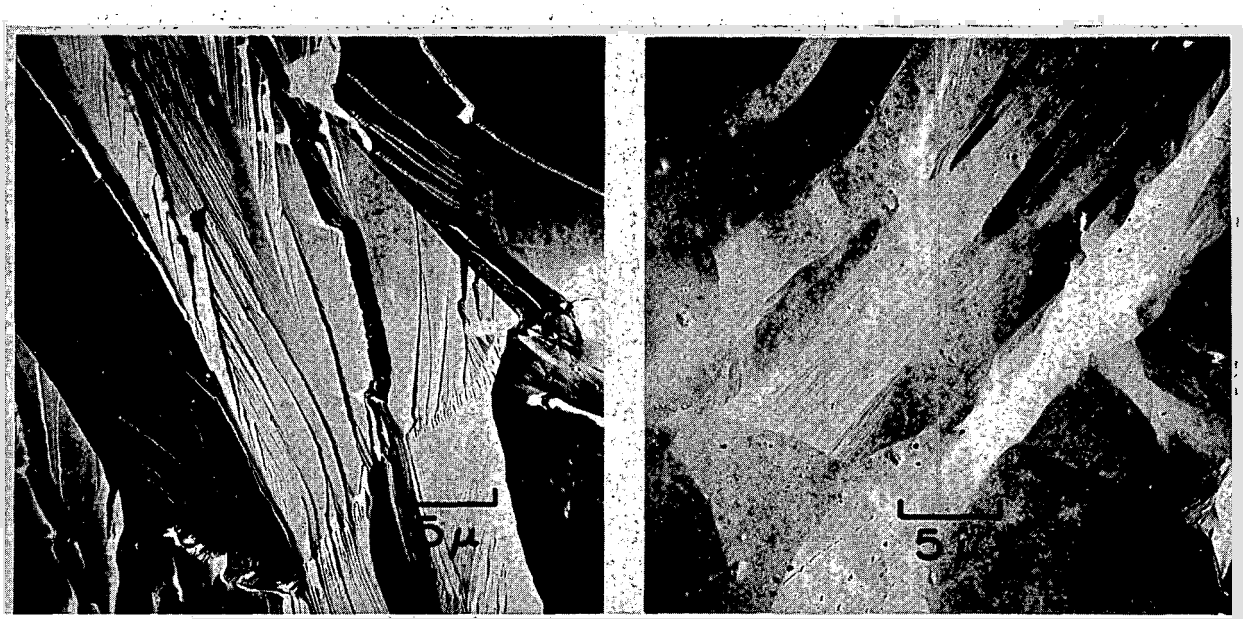

Fig. 1.21 — Electron fractographs of arc-cast tungsten. (a) Transgranular fracture in specimen tested at 2000°C and 2.11 kg/mm^2. (b) Grain boundary surface in specimen tested at 1600°C and 4.22 kg/mm^2.

same in unstressed regions as in highly stressed regions. This elongation is undoubtedly the result of prior fabrication history, since the specimens were formed with their lengths parallel to the rolling direction of the starting sheet material. The lack of measureable grain deformation during creep indicates that part of the bulk deformation must, therefore, be due to grain boundary sliding.

Although these observations illustrate the pronounced difference in failure mechanisms of powder-metallurgy and arc-cast tungsten, they do not indicate the underlying cause of this difference. Grain boundary failure, such as that observed in the powder-metallurgy material, can occur if the matrix is strengthened without a corresponding strengthening of the boundaries, or if the boundaries themselves are weakened.[26] Matrix hardening can be produced by a dispersion of impurities or precipitates while grain boundary weakening can occur with preferential precipitation in the boundaries, especially if a continuous film of precipitate forms. By the same reasoning, transgranular fracture, such as that observed in the arc-cast tungsten, will be favored if the grain boundaries are strengthened with respect to the matrix. Such strengthening can arise through a decrease in the amount of segregated impurities at grain boundaries, thus leading to increased grain boundary mobility and ductility. Alternatively, certain types of discontinuous precipitation at grain boundaries can strengthen those boundaries by blocking dislocation movement and preventing sliding.

In the present work, no direct evidence was observed of precipitation either within the matrix or along grain boundaries. The techniques employed, however, would not be expected to resolve very small precipitates. To detect such precipitates, transmission electron microscopy or replica electron microscopy of polished and etched surfaces would be required.

[26] Zener, loc. cit.

TUNGSTEN-BASE ALLOYS

W – 25Re

Recent creep-rupture studies of arc-cast W – 25Re (wt %) sheet material have extended the range of data reported previously[27] for this material. A complete summary of all the creep-rupture data generated for arc-cast W – 25Re in this program is presented in Figures 1.22 and 1.23. As reported,[27] arc-cast W – 25Re is stronger than arc-cast tungsten up to 2000°C and somewhat weaker than arc-cast tungsten at temperatures above 2000°C. It is important to note that the isotherms in Figures 1.29 and 1.30 are linear even though non-linear isotherms were observed in tests of powder-metallurgy W – 25Re. Apparently, different deformation mechanisms are involved in these two types of material. Two isotherms are shown for 2400°C, in Figure 1.31; two are shown to indicate that at this temperature, the stress-rupture properties of W – 25Re depend upon elongation at rupture.

W – 30Re – 30Mo

Stress-rupture and creep data were obtained for a number of different lots of wrought, powder-metallurgy (PM) W – 30Re – 30Mo (at. %) sheet material and one lot of wrought arc-cast (AC) material in sheet form. The PM material was produced at GE-NMPO under Task 1115, "Advanced Fast Breeder Reactor Fuel Element Cladding Development," and the AC material purchased commercially. A comparison of the stress-rupture and linear creep rate test results are shown in Figure 1.24 and 1.25. The AC material exhibits a greater rupture life than the PM material at both 1600°C and 2200°C for the stress levels investigated. This is probably related to the fact that the AC material is considerably more ductile, based on the elongation at rupture.

Photomicrographs of the PM sheet (lot 2) and the commercial AC sheet (lot 3) after creep-rupture testing are shown in Figure 1.26. Both materials tested at 1600°C and 3.37 kg/mm^2 show uniformly dispersed Re-rich sigma phase. The grain size for both is essentially the same, but intergranular separation is more predominant in the PM material. This is apparently the reason for the lower ductility. After testing at 2200°C and 0.56 kg/mm^2, the two materials are single phase, but the grain size in the AC material is approximately four times that of the PM material. Deformation appears to be primarily intergranular for the AC material, whereas cavitation or grain-boundary separation appears to contribute significantly to the deformation of the PM material. These factors may also account for the large difference in ductility for the two materials.

The linear creep rate data are essentially the same at 1600°C for the two types of material. At 2200°C, creep resistance of the AC material appears to be significantly greater at the lower stresses. This difference is apparently related to the difference in grain size at 2200°C which leads to different creep mechanisms. The PM material (lot 2) is fine grained (Figure 1.26) and has a stress versus creep rate slope of approximately 1; this indicates that diffusional creep[28] is the primary mechanism. The AC material (lot 3) has large grains at 2200°C (Figure 1.26) and gives a stress versus creep rate slope of approximatly 5; this indicates that dislocation climb is the primary creep mechanism.[29]

Special fabrication procedures were employed to produce high-purity W – 30Re – 30Mo sheet material. Creep-rupture tests were performed to compare this material with the previously produced (i.e., nonpurified) sheet material.[30] The in-process fabrication pro-

[27] "Sixth Annual Report – High-Temperature Materials Program, Part A," GE-NMPO, GEMP-475A, March 31, 1967, p. 13.

[28] Sherby, loc. cit.

[29] C. Herring, "Diffusional Viscosity of a Polycrystalline Solid," J. Appl. Phys., Vol. 21, 1950, p. 437.

[30] GEMP-67, p. 25.

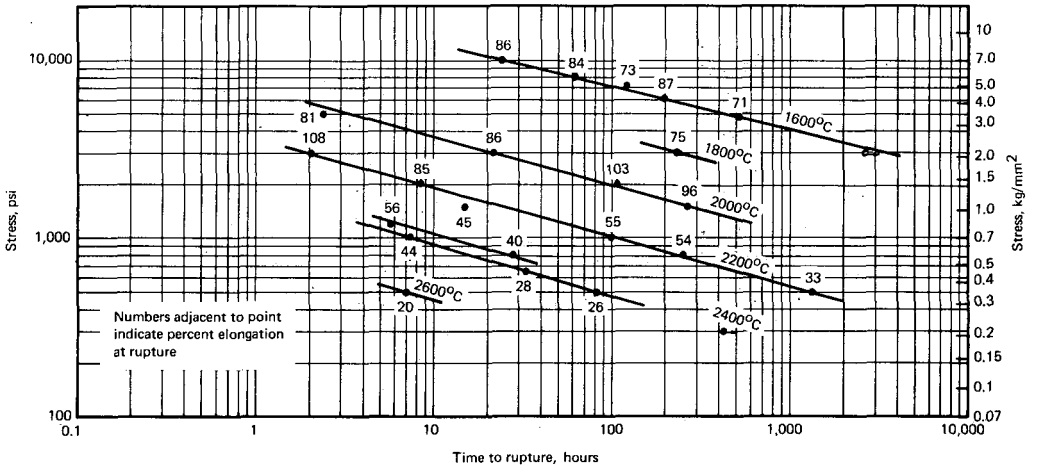

Fig. 1.22 — Stress-rupture data for arc-cast W — 25Re (wt %) alloy sheet tested in hydrogen

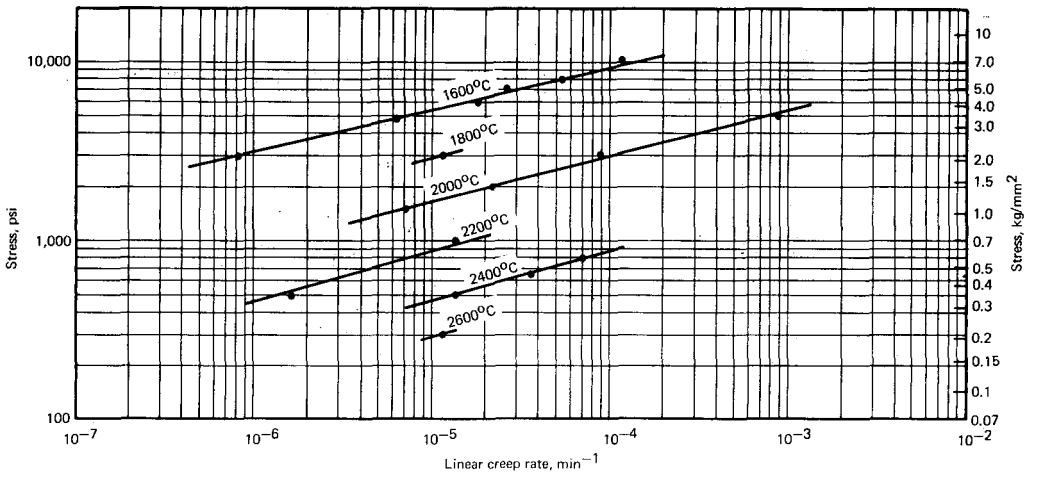

Fig. 1.23 — Linear creep rate data for arc-cast W — 25Re (wt %) alloy sheet tested in hydrogen

cedure was modified to produce four sheets (0.5-cm thick x 7 cm x 10 cm) of material, as shown in Table 1.3. Since the processing procedure differed slightly for each sheet, any effect on the mechanical properties could be determined. Specimens from each sheet were creep-rupture tested in hydrogen at 1600°C and 3.37 kg/mm^2 and at 2200°C and 0.56 kg/mm^2.

Typical creep curves, Figure 1.27, show no great difference in the rupture life, creep resistance, or ductility for the four sheets tested at the same conditions. Indication is that the variables associated with each sheet of high-purity material have a minor effect on the creep resistance and ductility, at least for the test conditions evaluated. Figure 1.27 also contains the results for AC and nonpurified PM material of the same nominal composition. The PM material, obtained as regular laboratory-produced sheet, was the least creep resistant of the group at both temperatures. Data for the commercial, recrystallized AC material show it to be somewhat more creep resistant than the regular nonpurified laboratory-produced sheet but considerably less creep resistant than the high-purity PM material.

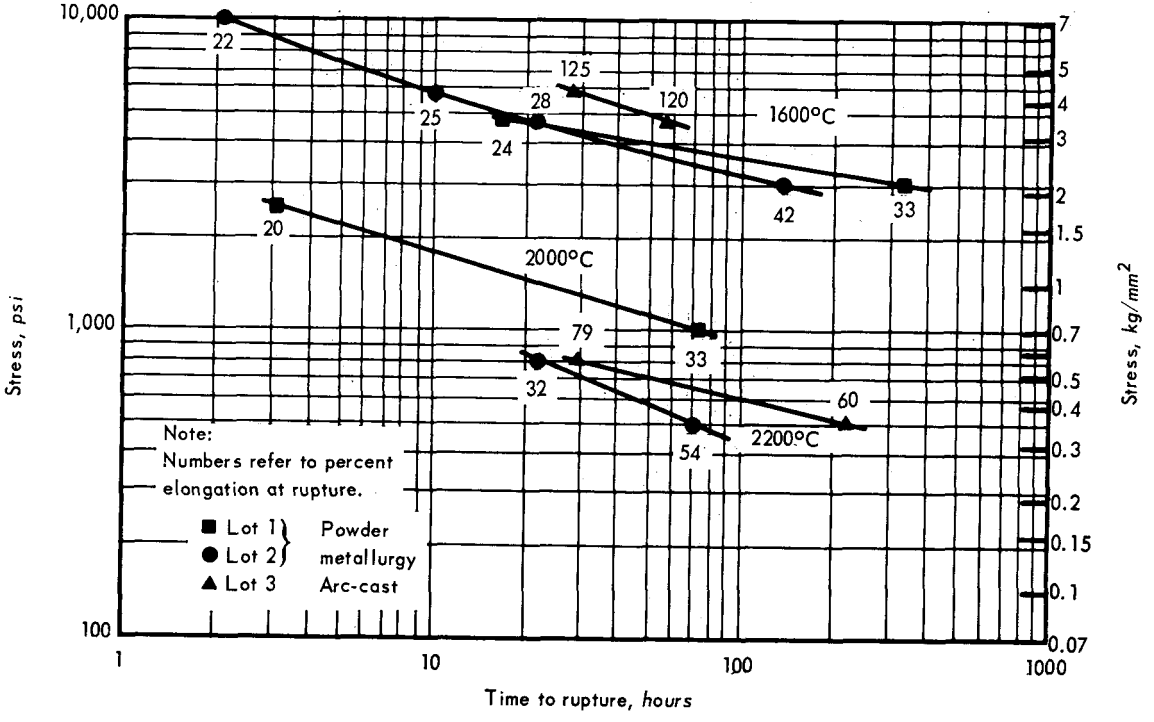

Fig. 1.24 – Stress-rupture results for W – 30Re – 30Mo (at. %) sheet tested in hydrogen

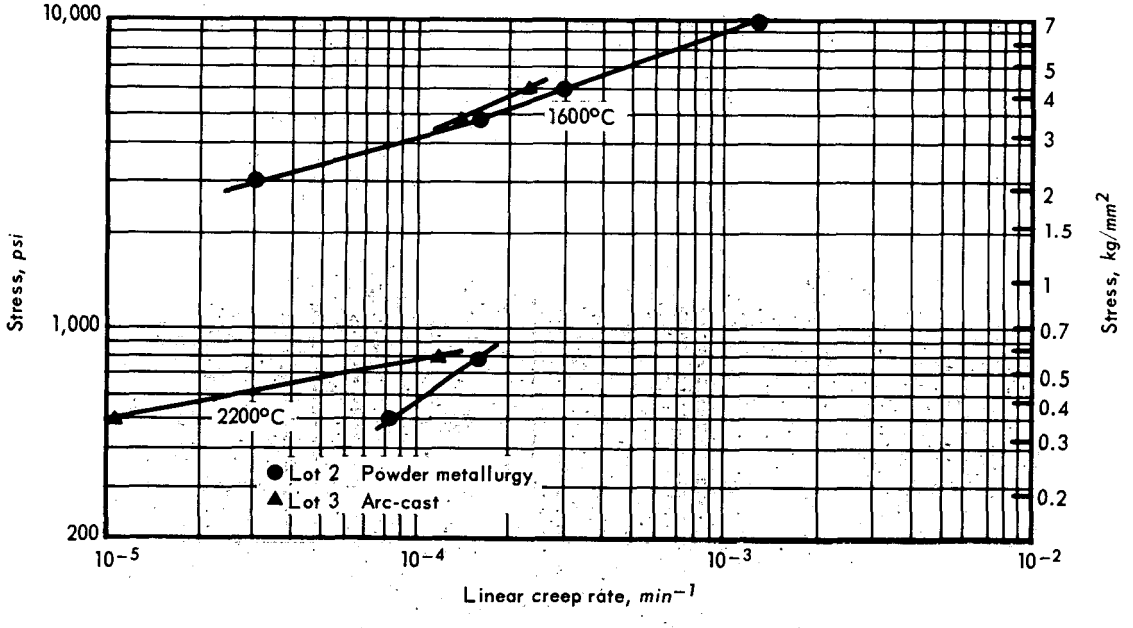

Fig. 1.25 – Creep rate results for W – 30Re – 30Mo (at. %) sheet tested in hydrogen

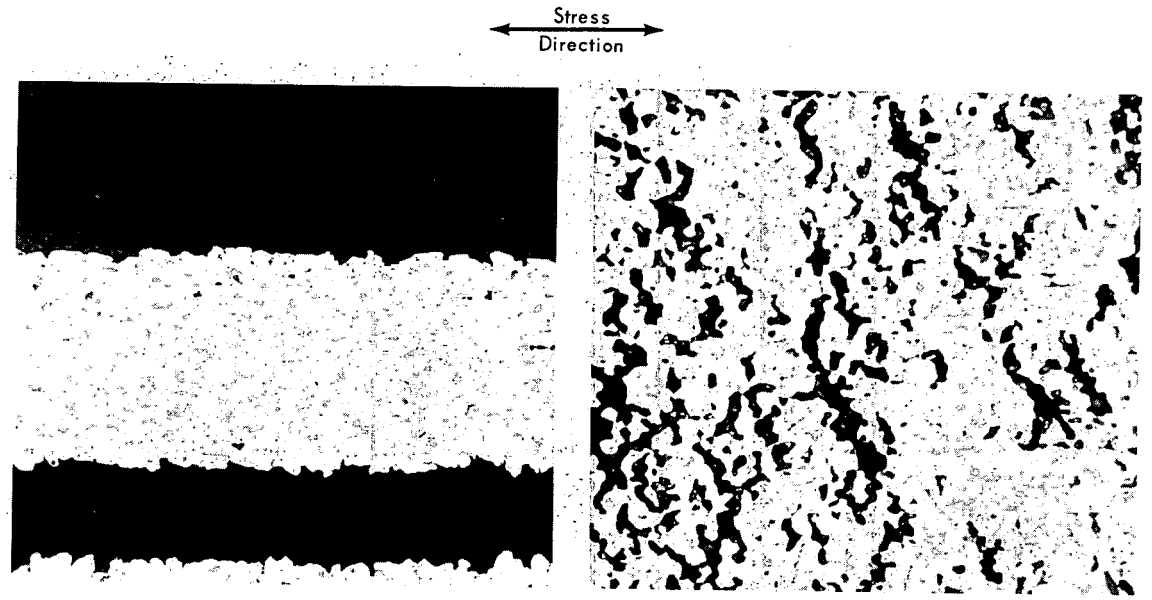

Arc cast — 306(3)-25 — Powder metallurgy — 306(8)-7

56.8 hours
120% elongation
15 microns
(Neg. 9022, as-polished)

1600°C, 3.37 kg/mm^2

21.6 hours
28% elongation
20 microns
(Neg. 8173, etched)

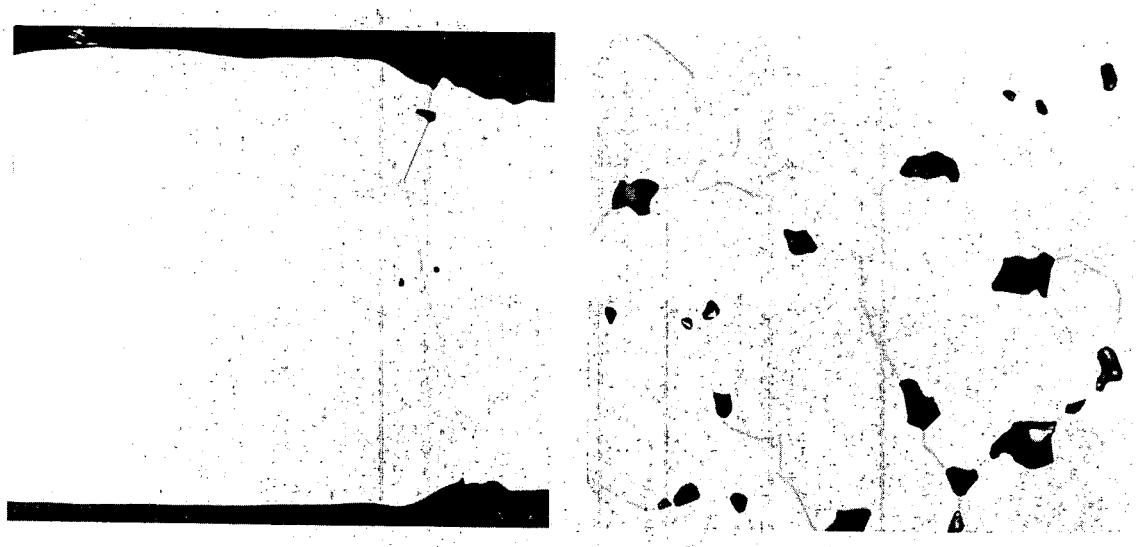

Arc cast — 306(3)-27 — Powder metallurgy — 306(8)-11

29.4 hours
79% elongation
265 microns
(Neg. 9026, etched)

2200°C, 0.56 kg/mm^2

22.0 hours
32% elongation
65 microns
(Neg. 8171, etched)

Fig. 1.26 — Photomicrographs of wrought W — 30Re — 30Mo (at. %) sheet after creep-rupture testing in hydrogen; numbers below each photomicrograph refer to time to rupture, elongation at fracture, and average grain size (250X)

TABLE 1.3

FABRICATION PROCEDURE USED TO PRODUCE HIGH-PURITY W – 30Re – 30Mo SHEET[a]

Sheet No.	Process
306(4)	Loose metal powders leached with 0.001 N HCl prior to blending. Not vapor treated.
306(5)	Same as 306(4) but powders leached with 0.001 N HNO_3.
306(6)	Same as 306(4) but compacted powders treated 150 hours at 1000°C in hydrogen–water vapor atmosphere prior to sintering.
306(7)	Same as 306(5) but treated as a compact similar to 306(6).

[a]All sheets were made from the identical metal powders and processed simultaneously.

Photomicrographs of the high-purity samples after testing at 1600°C and 2200°C are shown in Figures 1.28 and 1.29. No significant differences are noted between the samples tested at 2200°C. At 1600°C there appears to be some small variation in the second phase (sigma). Chemical analysis of the as-fabricated, high-purity sheet materials yielded the results given in Table 1.4. The major difference appears to be in the AC material where both the carbon and oxygen content are greater than any of the PM sheets. The special purification procedures apparently decrease the carbon content as the process is changed. These data along with the metallographic studies do not indicate the reason for the increased creep resistance of the high-purity material.

MOLYBDENUM

Stress-rupture data were previously reported[27] for wrought, arc-cast and wrought, powder-metallurgy, unalloyed molybdenum from 1200° to 2400°C in both hydrogen and argon atmospheres. Differences in the strength and structure for the two types of material were shown. It was also reported that essentially identical results were obtained for AC material purchased from a number of different vendor sources.

Additional data were obtained for AC material to evaluate the creep properties of unalloyed molybdenum.

Constant-load tests of wrought, AC molybdenum sheet (0.05 cm thick) were performed in hydrogen at temperatures from 1200° to 2400°C. Chemical analyses of the as-received material are given in Table 1.5. As shown, sheet material from two different vendor sources was evaluated. Test results are given in Tables 1.6 and 1.7; Table 1.8 gives the stress-rupture data previously reported for wrought, AC molybdenum rod material (0.40-cm gage diameter) along with the creep data obtained in these same tests. Figure 1.30 shows the stress-rupture curves obtained using the three sources of material; good agreement is apparent at 1600°C and 2200°C where duplicate tests were performed. Linear creep rate data for the three materials are presented in Figure 1.31. These data also show good agreement for the three materials at 1600°C and 2200°C. At 2400°C the creep rate curve decreases in slope. In fact, the data points at 2200°C and 0.141 kg/mm^2 (for M(9)4 material) deviate from the general trend, indicating a slope consistent with the data at 2400°C. The reason for this is not apparent but seems to be related to a unique behavior observed in an evaluation of the individual strain – time curves.

These creep curves, at constant temperature, are presented in Figure 1.32 as a function of the time required to give 10 percent strain. Plotting the curves in this way provides a comparison of the high- and low-stress tests at the same temperature. Additionally, tests at the same stress performed at different temperatures may also be compared conveniently. In this figure, creep curves obtained at 1200°C and 1600°C show a significant primary (first-

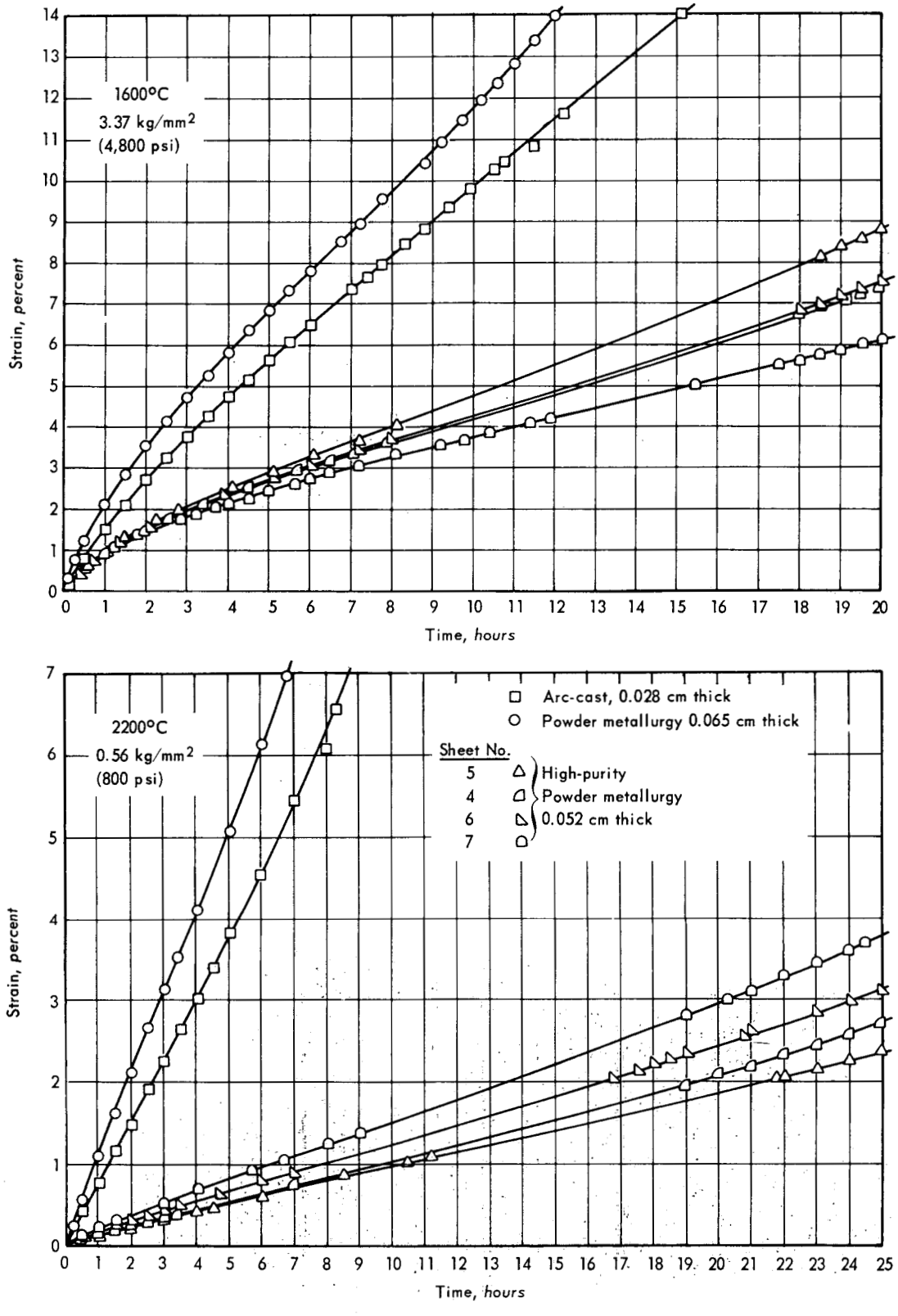

Fig. 1.27 — Creep curves for various lots of wrought W — 30Re — 30Mo (at. %) sheet tested in hydrogen

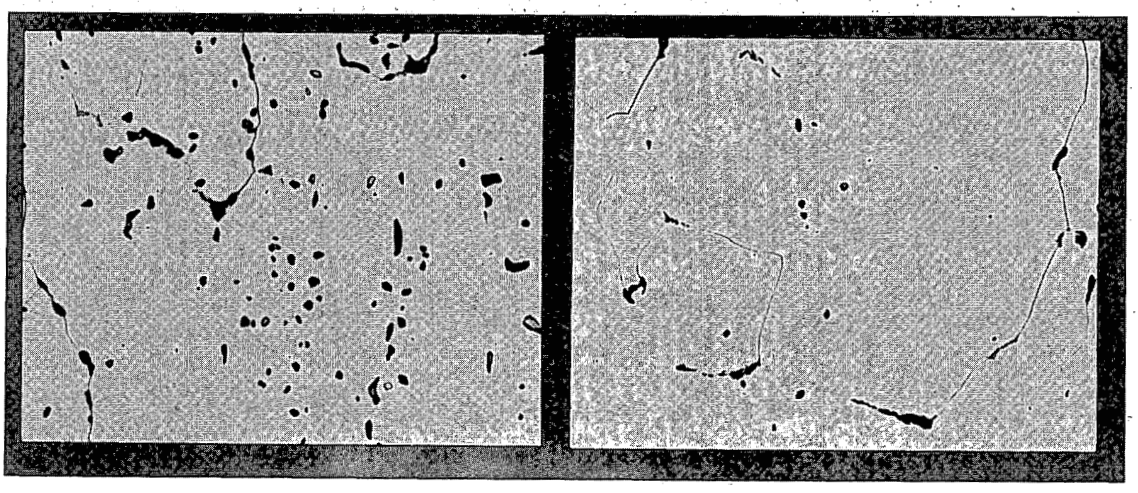

306(4)-12

43.7 hr
21.5% elongation
165 microns
(Neg. 9893)

306(5)-17

29.6 hr
15% elongation
135 microns
(Neg. 9894)

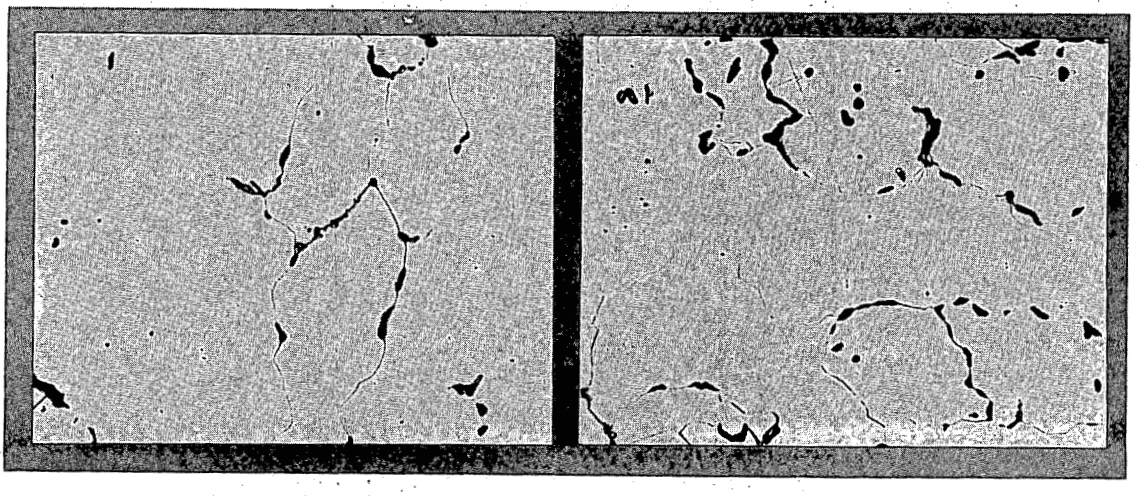

306(6)-18

37.8 hr
14.6% elongation
165 microns
(Neg. 9895)

306(7)-23

49.3 hr
21% elongation
145 microns
(Neg. 9896)

Fig. 1.28 – Photomicrographs of various lots of wrought, powder-metallurgy W – 30Re – 30Mo (at. %) sheet after creep-rupture testing at 1600°C and 3.37 kg/mm^2 in hydrogen; numbers below each photomicrograph refer to time-to-rupture, elongation at fracture, and average grain diameter. The figure in parentheses following the 306, under each photograph, is the lot number. (Etched, 250X)

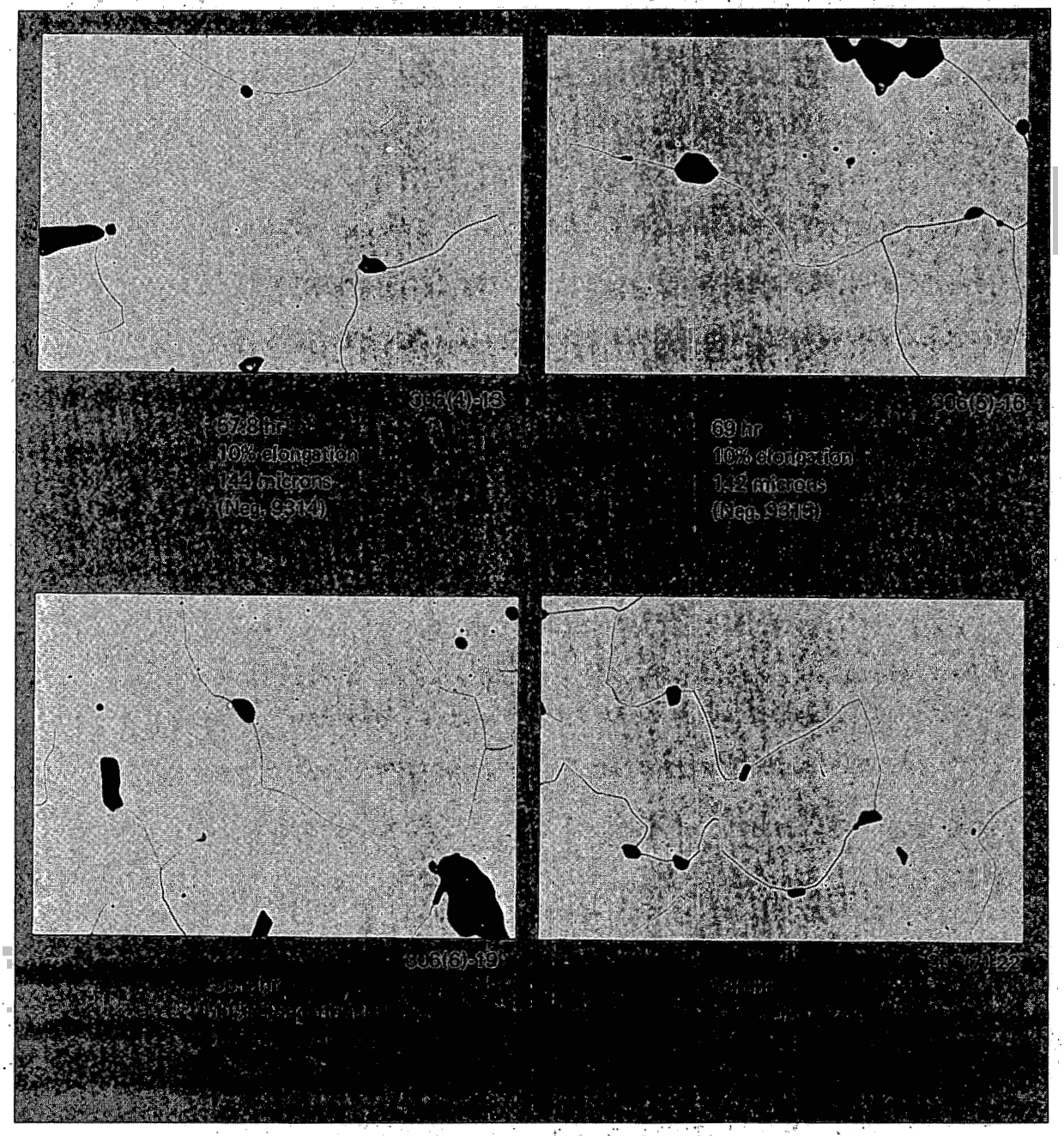

Fig. 1.29 – Photomicrographs of various lots of wrought, powder-metallurgy W – 30Re – 30Mo (at. %) sheet after creep-rupture testing at 2200°C and 0.56 kg/mm^2 in hydrogen; numbers below each photomicrograph refer to time-to-rupture, elongation at fracture, and average grain diameter. The figure in parentheses following the 306, under each photograph, is the lot number. (Etched, 250X)

TABLE 1.4

CHEMICAL ANALYSIS OF AS-FABRICATED W – 30Re – 30Mo SHEET SAMPLES FROM VARIOUS LOTS

Lot No.	Impurities, ppm C	O	H	N	Fabrication
2	19	4.9	0.5	0.3	PM regular laboratory process
3	<40	80	1.7	11	Per vendor } Commercial
	41	33	4	4	Per NMPO } AC
4	19	12	0.9	25	PM special purification procedures
5	16	9.8	1	0.2	
6	13	8.1	0.9	0.9	
7	7	11	0.9	4	

TABLE 1.5

CHEMICAL ANALYSIS OF AS-RECEIVED WROUGHT, ARC-CAST MOLYBDENUM

Material Source	Impurity Content, ppm C	H	O	N
M(6)4	140	1	17	19
M(9)4	250	1	22	5

TABLE 1.6

CREEP-RUPTURE RESULTS[a] FOR WROUGHT, ARC-CAST, UNALLOYED MOLYBDENUM SHEET,[b] M(6)4, TESTED IN HYDROGEN

Specimen No.	Test Conditions Temperature, °C	Stress, kg/mm^2	Time to Indicated Strain, hr 0.2%	0.5%	1%	2%	3%	5%	10%	Rupture Time, hr	Elongation, %	Linear Creep Rate, min^{-1}
4	1600	2.11	–	–	0.03	0.13	0.28	0.60	1.4	2.5	30	9.8×10^{-4}
5	1600	1.76	–	0.05	0.18	0.53	0.98	1.9	4.2	6.9	30	3.6×10^{-4}
6	1600	1.41	0.06	0.20	0.58	1.5	2.5	4.7	9.8	25.1	55	1.6×10^{-4}
7	1600	1.05	0.26	0.99	2.6	6.5	10.4	18.8	38.7	99.6	64	2.9×10^{-5}
16	1600	0.84	9.7	3.1	7.4	17.8	29.6	51.2	100.	247.	47	1.4×10^{-5}
3	1600	0.70	3.8	12.0	24.2	48.5	73.0	122.	234.	554.	45	6.8×10^{-6}
12	1600	0.56	8.5	26.5	57.5	124.	198.	345.	–	452.[c]	6.4[c]	2.3×10^{-6}
15	1600	0.35	90.5	255.	–	–	–	–	–	348.[c]	0.68[c]	2.9×10^{-7}
8	2200	0.56	–	–	–	–	–	0.02	0.09	0.22	40	–
9	2200	0.35	–	–	0.03	0.12	0.24	0.53	1.2	2.88	53	1.1×10^{-3}
10	2200	0.21	0.10	0.40	0.97	2.0	3.0	5.1	10.1	23.8	49	1.6×10^{-4}
11	2200	0.14	1.8	5.5	11.5	21.9	29.8	43.3	67.0	123.	52	1.3×10^{-5}
17T[d]	2200	0.10	10.0	28.0	55.0	95.0	126.	169.	232.	244.[c]	11.0[c]	2.7×10^{-6}

[a]Annealed at test temperature for 2 hours in hydrogen before testing.
[b]0.05-cm-thick sheet with 0.64-cm by 2.54-cm gage section.
[c]Test terminated prior to rupture at time and strain indicated.
[d]T denotes specimen transverse to rolling direction.

stage) creep as do the curves obtained at higher stresses at 2200°C. Curves for 0.141 kg/mm^2 and lower at both 2200°C and 24°C show no apparent primary or secondary stages of creep. The creep rates reported in Table 1.5 are essentially instantaneous creep rates in the region near time zero. This change in curve shape from the more conventional creep curves obtained at the higher stresses may be related to a change in creep mechanism at low stresses.

Sherby[31] showed that when the secondary creep rate, divided by the diffusion coefficient, is presented as a function of the stress divided by the modulus a single curve is obtained related to the mechanism of creep. The result of correlating the AC molybdenum data in this manner is presented in Figure 1.33. The 1600°C and 2200°C data show good correlation with a slope of 4.85; Sherby reported that a slope of 4 to 5 is normally obtained. The 1200°C data show a displacement that is not understood. The deviation of the data for 2400°C is apparently related to the effect of the creep-curve shape on the creep rate discussed above.

[31]Sherby, loc. cit.

TABLE 1.7

CREEP-RUPTURE RESULTS[a] FOR WROUGHT, ARC-CAST, UNALLOYED MOLYBDENUM SHEET,[b] M(9)4, TESTED IN HYDROGEN

Specimen No.	Test Conditions: Temperature, °C	Test Conditions: Stress, kg/mm²	Time to Indicated Strain, hr: 0.2%	0.5%	1%	2%	3%	5%	10%	Rupture: Time, hr	Rupture: Elongation, %	Linear Creep Rate, min^{-1}
40	1200	7.03	–	–	–	0.01	0.04	0.12	0.35	1.06	70	3.6×10^{-3}
41	1200	5.62	–	–	0.04	0.20	0.42	0.96	2.63	9.70	78	4.8×10^{-4}
42	1200	4.22	–	0.07	0.34	1.15	2.25	4.93	12.4	33.2	72	1.1×10^{-4}
44	1200	3.37	0.12	0.42	1.13	3.05	6.00	13.6	34.2	98.2	84	4.0×10^{-5}
36	1200	2.81	0.76	1.93	4.62	13.2	24.8	50.4	112.	214.	44	1.3×10^{-5}
43	1200	2.11	5.20	14.6	37.5	94.0	159.	278.	611.	1742.	52	2.4×10^{-6}
11	1600	1.41	0.01	0.08	0.33	1.03	1.88	3.71	8.33	17.5	34	1.8×10^{-4}
9	1600	1.05	0.65	1.35	2.67	5.30	8.60	14.8	29.7	59.3	57	5.0×10^{-5}
29	1600	1.05	0.26	0.82	2.09	5.50	9.00	16.0	33.0	81.7	51	4.8×10^{-5}
30	1600	0.844	1.20	2.80	6.00	14.0	23.4	42.2	87.2	241.	52	1.8×10^{-5}
10	1600	0.703	2.80	7.15	15.8	37.2	61.0	110.	228.	488.	35	6.8×10^{-6}
12	2200	0.352	–	0.01	0.04	0.15	0.27	0.55	1.25	3.40	78	1.2×10^{-3}
13	2200	0.281	–	0.03	0.15	0.48	0.87	1.71	3.72	9.92	52	4.0×10^{-4}
26	2200	0.211	0.11	0.58	1.35	2.90	4.45	7.45	13.6	32.1	73	1.1×10^{-4}
27	2200	0.176	0.54	1.76	3.82	7.93	11.9	19.5	35.0	89.0	82	4.1×10^{-5}
28	2200	0.141	5.45	14.5	27.0	49.0	68.5	99.4	145.	247.	50	7.2×10^{-6}
14	2200	0.141	5.00	11.1	20.3	37.2	53.3	77.3	108.	200.[d]	38	8.5×10^{-6}
49T	2400	0.211	–	0.02	0.04	0.12	0.20	0.36	0.76	1.88	48	2.0×10^{-3}
60	2400	0.190	0.02	0.06	0.14	0.30	0.56	0.78	1.52	3.89	52	1.0×10^{-3}
48T	2400	0.176	–	0.02	0.07	0.19	0.32	0.59	1.13	2.80	54	1.2×10^{-3}
23	2400	0.141	0.12	0.48	1.10	2.36	3.44	5.18	8.37	17.0	63	1.4×10^{-4}
53T	2400	0.120	0.63	1.90	3.81	6.86	9.25	13.0	19.2	28.3	46	4.4×10^{-5}
47T	2400	0.105	2.05	4.90	8.52	14.3	19.0	25.9	35.3	48.5	38	–
54T	2400	0.084	15.1	31.0	47.2	58.9	66.1	76.9	88.7	101.	32	2.6×10^{-6}

[a]Annealed at test temperature for 2 hours in hydrogen before testing.
[b]0.05-cm-thick sheet, 0.64-cm by 2.54-cm gage section.
[c]T denotes specimen transverse to rolling direction, all others parallel to rolling direction.
[d]Power failure at 88 hours caused increased strain rate.

TABLE 1.8

CREEP-RUPTURE RESULTS[a] FOR WROUGHT, ARC-CAST, UNALLOYED MOLYBDENUM ROD,[b] M(8)1, TESTED IN HYDROGEN

Specimen No.	Test Conditions: Temperature, °C	Test Conditions: Stress, kg/mm²	Time to Indicated Strain, hr: 0.2%	0.5%	1%	2%	3%	5%	10%	Rupture: Time, hr	Rupture: Elongation, %	Linear Creep Rate, min^{-1}
9	1600	1.76	–	0.02	0.12	0.44	0.82	1.60	3.30	5.18	64	4.5×10^{-4}
10	1600	1.41	0.01	0.14	0.49	1.40	2.37	4.35	7.47	11.7	72	1.7×10^{-4}
11	1600	1.05	0.11	0.74	2.30	5.60	8.92	13.4	23.3	58.2	53	5.0×10^{-5}
13	1600	0.844	1.88	3.48	7.40	16.7	26.7	48.7	105.	222.	82	1.4×10^{-5}
12	1600	0.703	5.20	17.0	26.5	45.0	68.5	120.	244.	357.[c]	15	7.0×10^{-6}
3	2200	0.316	–	0.02	0.07	0.24	0.44	0.82	1.60	2.66	86	8.9×10^{-4}
5	2200	0.246	0.02	0.09	0.17	0.76	1.33	2.52	5.20	9.60	78	2.8×10^{-4}
2	2200	0.197	0.26	0.79	1.67	3.43	5.19	8.70	11.6	17.0	44	9.3×10^{-5}
4	2200	0.162	1.05	3.32	6.11	11.56	17.0	26.2	31.5	50.0	38	3.1×10^{-5}
1	2200	0.141	2.66	6.00	10.6	19.2	27.8	48.5	77.5	145.	64	1.9×10^{-5}

[a]Annealed at test temperature for 2 hours in hydrogen before testing.
[b]0.41-cm-dia. by 2.54-cm-long gage section.
[c]Test terminated, no rupture.

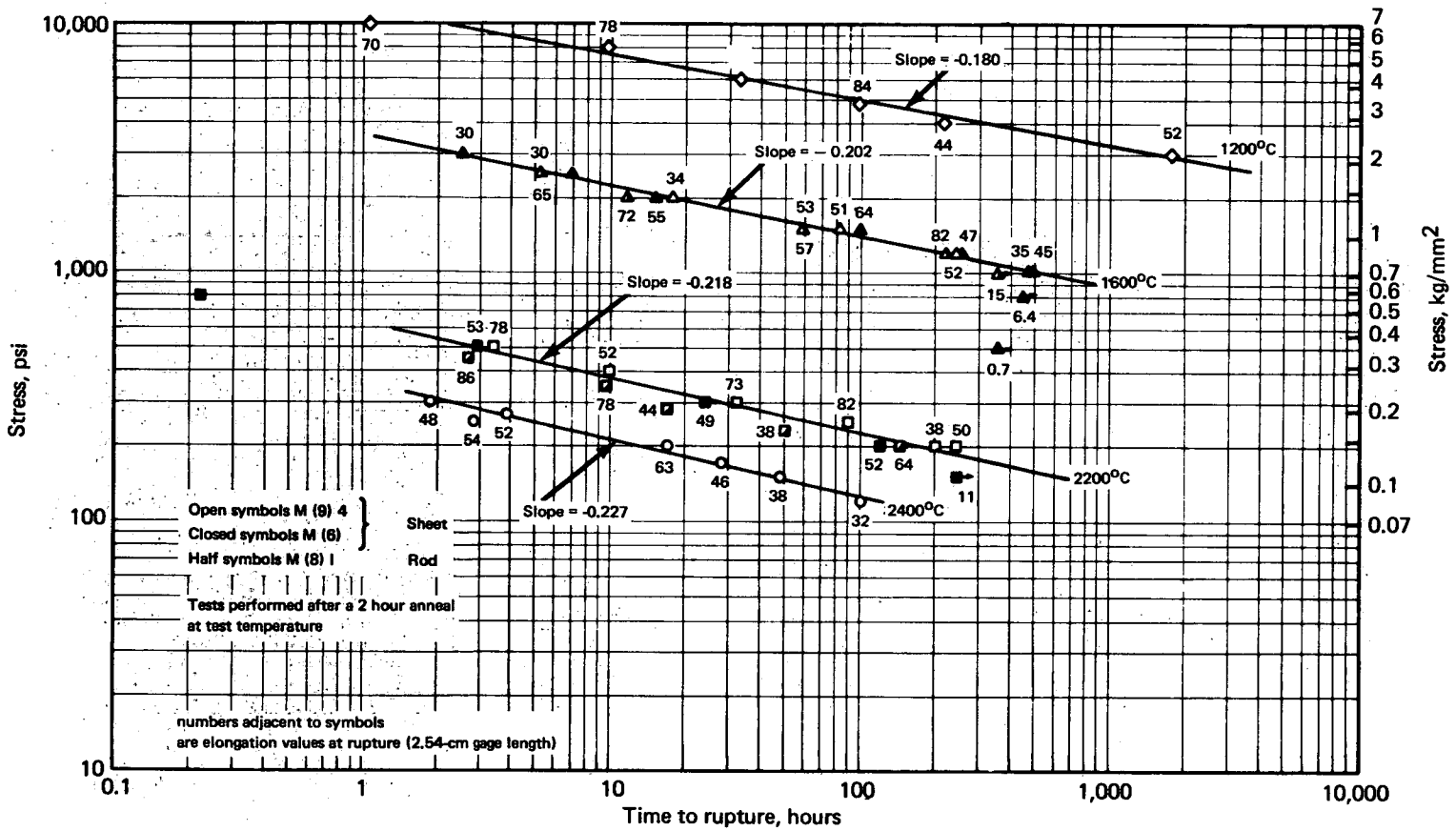

Fig. 1.30 — Stress-rupture results for wrought, arc-cast unalloyed molybdenum tested in hydrogen

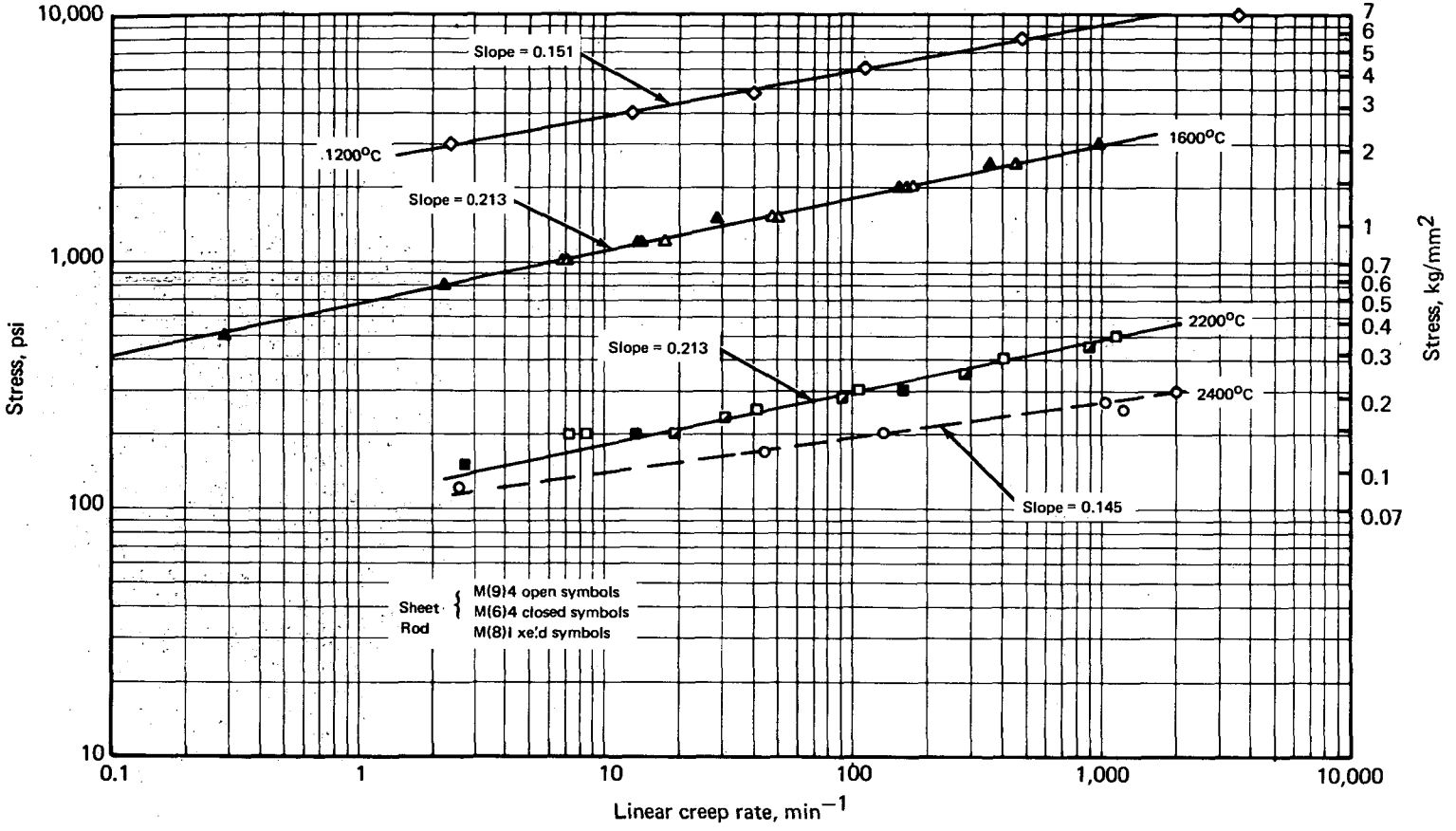

Fig. 1.31 — Creep rate results for wrought, arc-cast unalloyed molybdenum tested in hydrogen

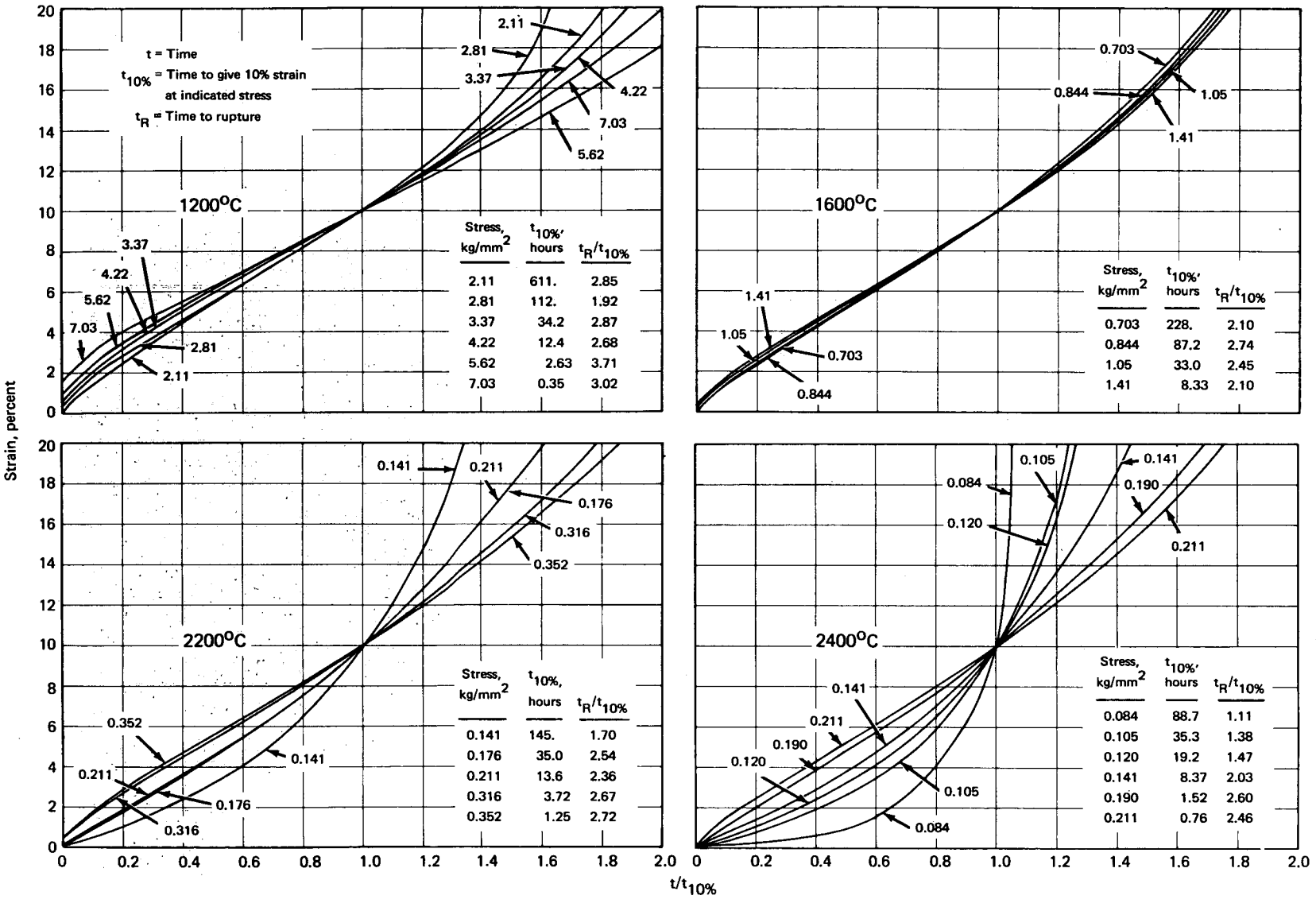

Fig. 1.32 – Constant load creep curves for wrought, arc-cast molybdenum sheet at 1200°, 1600°, 2200°, and 2400°C

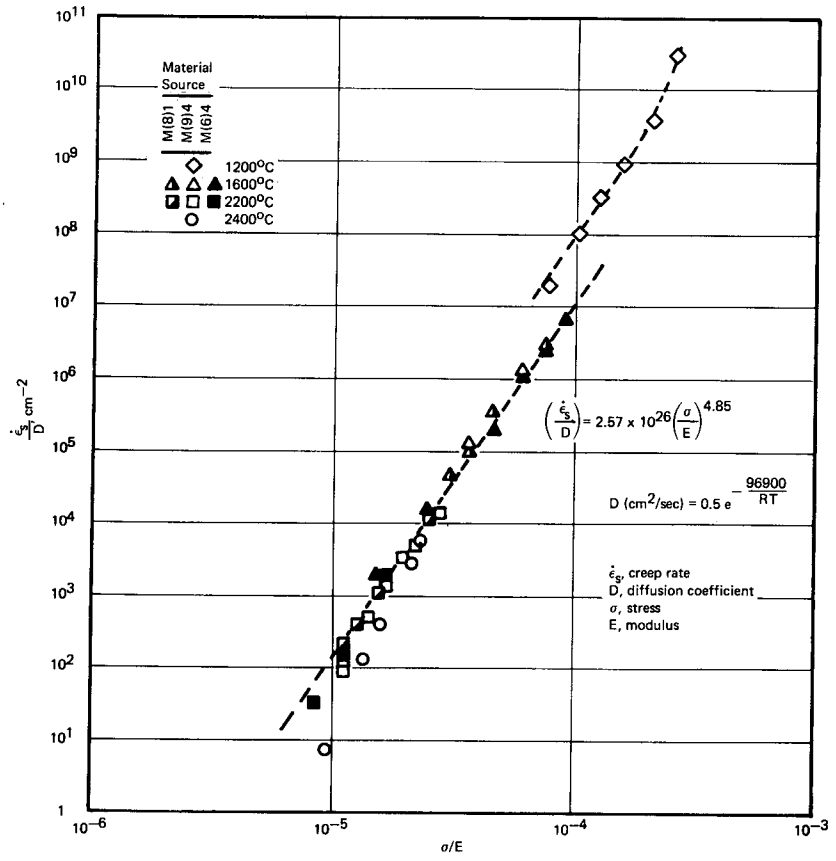

Fig. 1.33 – Correlation of linear creep rate data for arc-cast molybdenum tested in hydrogen

Monkman and Grant[32] reported that when the log of the time-to-rupture is plotted against the log of the linear creep rate, a straight-line relationship is obtained with a slope of minus m, in accordance with:

$$\log t_R = \log C - m \log \dot{\epsilon}_s \qquad (1.12)$$

where

t_R = rupture time
$\dot{\epsilon}_s$ = linear creep rate
m, C = constants

When m is equal to one, as it has been found to be for a number of materials, the equation becomes:

$$t_R = \frac{C}{\dot{\epsilon}_s} \qquad (1.13)$$

The data for molybdenum discussed above are shown in this form in Figure 1.34. The curves for both rod and sheet material are shown to possess a slope of minus 1 but are not coincident. This displacement is due to the consistent difference in rupture life (Figure 1.30) since

[32]F. C. Monkman and N. J. Grant, "An Empirical Relationship Between Rupture Life and Minimum Creep Rate in Creep Rupture Tests," Proc. ASTM, Vol. 56, 1956, p. 593.

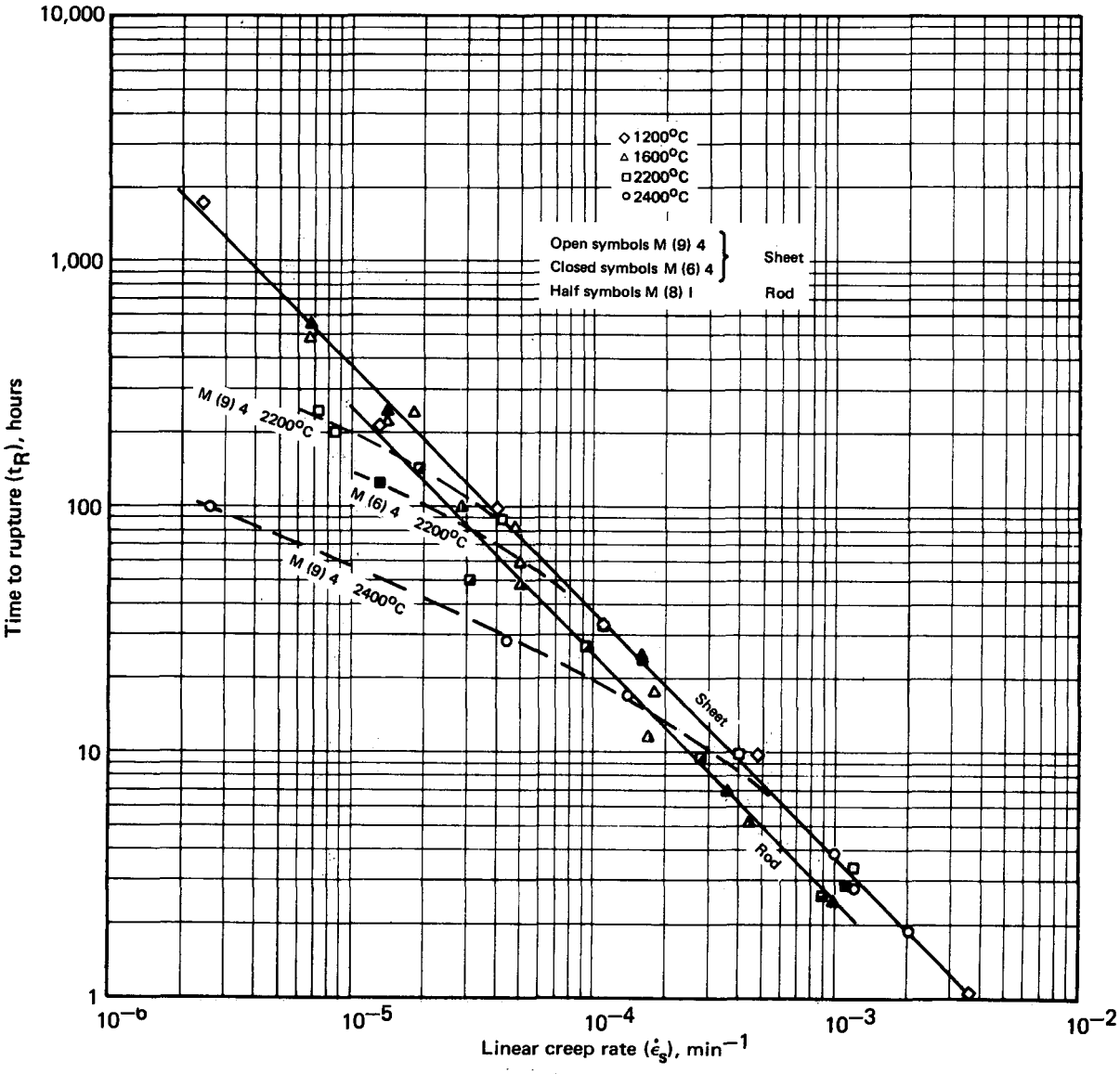

Fig. 1.34 — Rupture life versus creep rate for arc-cast molybdenum showing correlation of data to $t_R \dot{\epsilon}_s = C$

good agreement for the linear creep rate is shown in Figure 1.31. The data points in Figure 1.34 that deviate significantly from the straight lines are those showing deviations from the linear creep rate plot of Figure 1.31. The effect of the change in the creep curve shape is shown in this Monkman-Grant type of plot. Only those data at the lower stresses and higher temperatures, where no primary creep was observed, deviate from the lines in Figure 1.31.

Molybdenum-Base Alloys

Mo – 5Re and Mo – 5W – Creep-rupture data were reported[33] for PM Mo – 5Re and Mo–5W (both at. %) alloy sheet fabricated at GE-NMPO. Sheet thicknesses were 0.05 cm and 0.08 cm for Mo – 5W and Mo – 5Re, respectively, with testing performed at 1600°C and 2200°C in hydrogen. Data obtained in these tests are presented in Figures 1.35 and 1.36; the data for AC molybdenum are shown for comparison. Each alloy is seen to be stronger than unalloyed, AC

[33]GEMP-1002, p. 16.

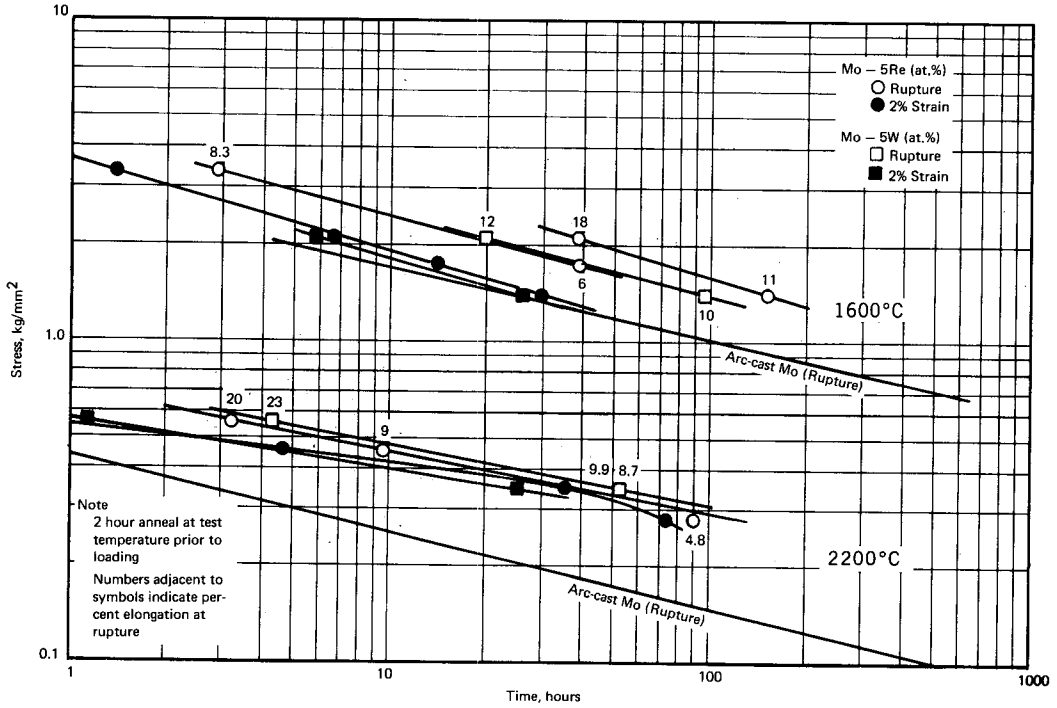

Fig. 1.35 – Stress-rupture data for powder-metallurgy Mo – 5Re and Mo – 5W alloy sheet tested in hydrogen

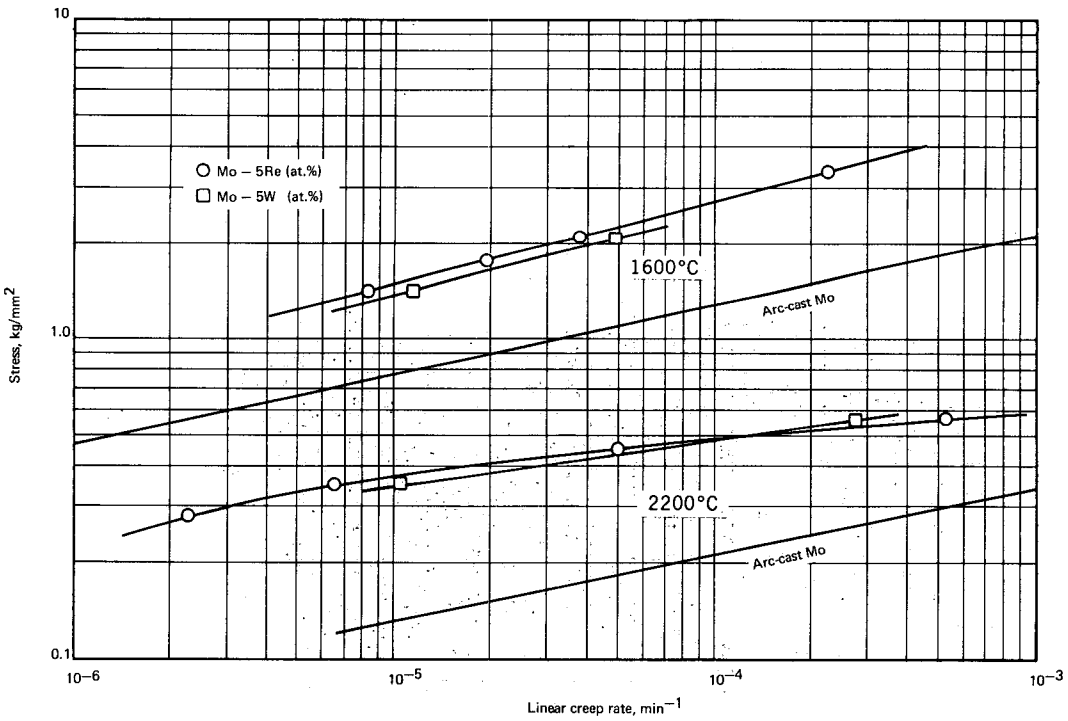

Fig. 1.36 – Linear creep rate data for powder-metallurgy Mo – 5Re and Mo – 5W alloy sheet tested in hydrogen

molybdenum. Two isotherms are presented for Mo – 5Re at 1600°C to reflect the different behavior observed in specimens from two different sheets of this material. Actually these two molybdenum alloys exhibit about the same creep-rupture behavior.

Mo – 50Re – Stress-rupture and creep data (constant load) for wrought, PM Mo – 50Re (wt %) alloy sheet were previously presented[34] for lot 1 material at 2200°C and for lot 2 material at 1600°, 2200°, and 2400°C. The lot 2 results were obtained using specimens from sheet 1. Additional tests were performed at 1600°, 2200°, and 2400°C using specimens obtained from sheet 2 of the lot 2 material. The objective was to compare results for two different sheets of the same wrought, powder-metallurgy material obtained from the same lot. In addition, the lot 2, sheet 1 results indicated that at the higher temperatures and lower stresses, diffusional creep may be the controlling mechanism based on the increased slope of the stress versus linear creep rate plot. Further studies were therefore performed to verify this.

Table 1.9 and Figures 1.37 and 1.38 give the stress-rupture and creep data obtained for the lot 2, sheet 2 material. The sheet 2 results appear to be consistent with the sheet 1 material in terms of stress-rupture, linear creep rate, and ductility at 2200°C and 2400°C. At 1600°C, the rupture life is greater whereas the linear creep rate and ductility are lower for the sheet 1 material.

Creep curves for lot 2, sheet 2 specimens tested at the lowest stress for each of the three temperatures involved are shown in Figure 1.39. At 1600°C, the curve shows third-stage-type creep from essentially time zero, while the 2200°C curve gives the more conventional type of creep curve. At 2400°C, the creep curve displays two regions of essen-

TABLE 1.9

CREEP-RUPTURE RESULTS[a] FOR WROUGHT, POWDER-METALLURGY Mo – 50Re SHEET[b] TESTED IN HYDROGEN (LOT 2, SHEET 2)

Specimen No.	Test Conditions: Temperature, °C	Stress, kg/mm²	Time to Indicated Strain, hr: 0.2%	0.5%	1%	2%	3%	5%	10%	Rupture: Time, hr	Elongation, %	Linear Creep Rate, min⁻¹
2-2	1600	3.37	0.05	0.10	0.16	0.25	0.32	0.46	0.74	2.02	102	–
-3	1600	2.81	0.18	0.40	0.61	0.95	1.23	1.67	2.45	5.25	92	8.0×10^{-5}
-4	1600	2.11	0.72	1.44	2.42	3.82	4.90	6.57	9.30	16.7	85	–
-5	1600	1.76	1.37	2.90	4.90	8.10	10.6	14.7	21.6	37.9	74	2.3×10^{-5}
-6	1600	1.41	2.85	6.85	12.4	20.0	25.5	33.8	47.2	81.0	60	1.3×10^{-5}
-1	1600	1.05	7.45	18.2	34.2	59.6	79.9	111.	162.	262.	58	4.5×10^{-6}
2-13	2200	0.352	0.29	0.83	1.87	3.76	5.51	8.48	12.6	14.8	21	9.5×10^{-5}
-15	2200	0.211	0.72	1.88	4.06	8.85	14.0	24.9	47.6	70.3	24	2.9×10^{-5}
-17	2200	0.141	1.03	2.77	5.52	14.4	23.2	42.0	88.2	145.	24	1.7×10^{-5}
-18	2200	0.105	1.28	3.50	7.60	16.5	26.2	46.7	94.1	174.	45	1.6×10^{-5}
2-8	2400	0.211	0.14	0.34	0.68	–	–	–	–	1.09[c]	1.8	2.5×10^{-4}
-30	2400	0.211	0.15	0.37	0.72	1.33	1.83	2.51	3.20	3.48	30	2.4×10^{-4}
-21	2400	0.141	0.24	0.57	1.12	2.19	3.13	4.63	6.75	8.65	32	1.5×10^{-4}
-25	2400	0.105	0.36	0.89	1.78	3.56	5.34	8.30	13.2	20.9	46	9.4×10^{-5}
-29	2400	0.070	0.61	1.48	2.94	5.84	8.75	14.6	27.5	70.0	44	5.7×10^{-5}[d]
-24	2400	0.035	0.97	2.66	5.50	11.3	18.4	33.6	97.7	224.	36	1.2×10^{-5} / 2.9×10^{-5}[d]
1-21	2200[e]	0.141	1.55	3.93	8.80	18.6	28.6	48.5	85.9	112.	20	1.7×10^{-5}

[a]Annealed at test temperature for 2 hours in hydrogen before testing.
[b]0.05-cm-thick sheet, 0.64-cm by 2.54-cm gage section.
[c]Test terminated; load train support failed.
[d]Diffusional creep rate.
[e]Annealed at 2400°C for 2 hours in hydrogen before testing (lot 2, sheet 1).

[34]GEMP-67, p. 15.

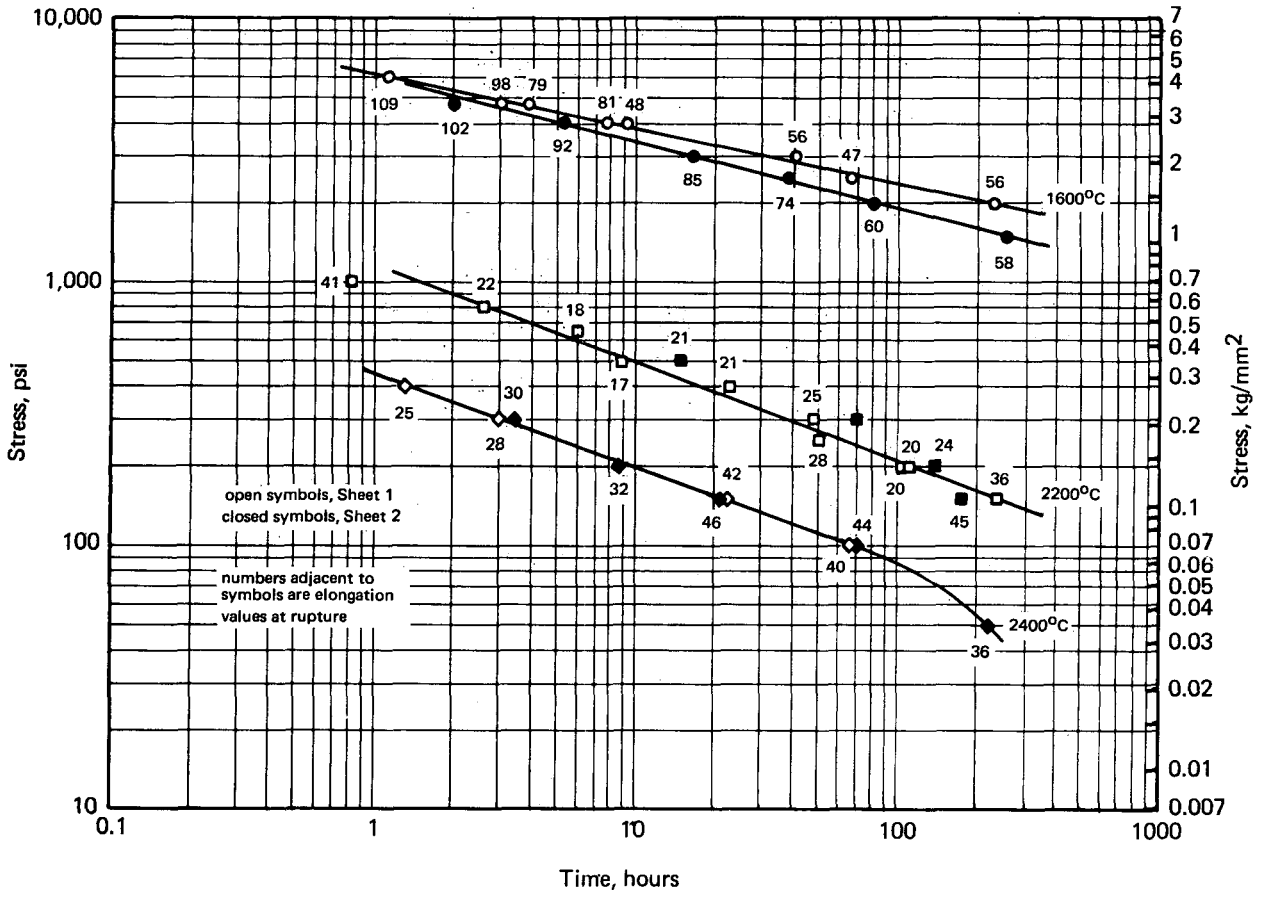

Fig. 1.37 — Stress-rupture results for wrought, powder-metallurgy Mo — 50Re (wt %) sheet (lot 2) tested in hydrogen

tially linear creep rate followed by third-stage creep. If these curves are analyzed in terms of the creep-rate curve given in Figure 1.38, it appears that the initial portion of the creep curve at 2400°C and 0.035 kg/mm^2 (Figure 1.39) is diffusion controlled since the creep-rate curve at 2400°C (Figure 1.38) yields a slope of essentially 1. This is consistent with the Nabarro-Herring[35] model for diffusional creep which indicates stress to be directly proportional to creep rate. This is further confirmed by the analysis approach proposed by Sherby[36] for polycrystalline metals above one-half the absolute melting temperature. Figure 1.40 shows good correlation of the results using this approach. The curve at the low-stress levels also yields a slope of 1 indicating diffusional creep. At the higher stress levels the curve slope is 2.7. According to Sherby, when a slope approximating 3 is obtained, the creep mechanism is dislocation glide based on the microcreep theory of Weertman.[37] He showed that when dislocation motion under stress is controlled by the velocity of solute drag along the dislocation line the creep rate is given by

$$\dot{\epsilon}_S = k\, D_S \frac{\sigma^3}{G^4} \qquad (1.14)$$

[35]Herring, loc. cit.

[36]Sherby, loc. cit.

[37]J. Weertman, "Steady-State Creep of Crystals," J. Appl. Phys., Vol. 28, 1957, p. 1185.

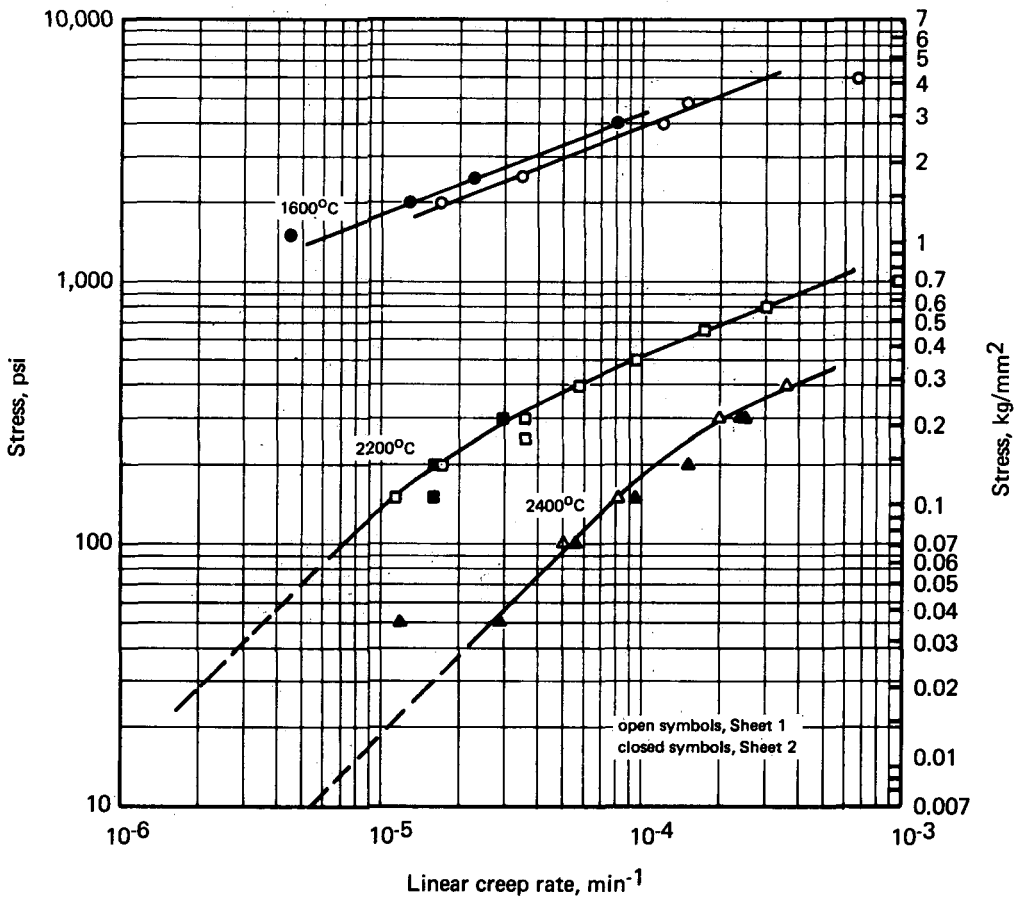

Fig. 1.38 – Creep rate results for wrought, powder-metallurgy Mo – 50Re (wt %) sheet

where k is a constant depending on the interaction force between the solute atmosphere and the dislocation, D_S is the solute diffusion coefficient, and G is the shear modulus. This equation predicts that the creep rate of solid solutions should be proportional to the third power of stress in contrast to the five power law dependence observed for pure metals.

Apparent activation energy calculations for creep were made based on the linear creep rate data obtained at the same stress level for two different temperatures. Data between 1600° and 2200°C gave a value of 84 kcal/mole and the data between 2200° and 2400°C gave a value of 121 kcal/mole.

A value of the diffusion coefficient for Mo – 50Re was calculated based on the Nabarro-Herring equation for creep rate:

$$\dot{\epsilon}_S = \frac{10\, D\, \sigma\, b^3}{k\, T\, L^2} \qquad (1.15)$$

where $\dot{\epsilon}_S$ is the steady-state creep rate in sec^{-1}, D is the diffusion coefficient in cm^2/sec, σ is the stress in dynes/cm^2, k is Boltzmann's constant (1.38×10^{-16} ergs per degree), T is the absolute temperature, L is the grain diameter in centimeters, and b is the lattice spacing in centimeters. Based on the test data obtained at 2400°C and 0.070 kg/mm^2 for lot 2, sheet 1 material, the value of the diffusion coefficient was calculated to be 1.143×10^{-7} cm^2/sec. The values of grain size and lattice spacing used were based on actual meas-

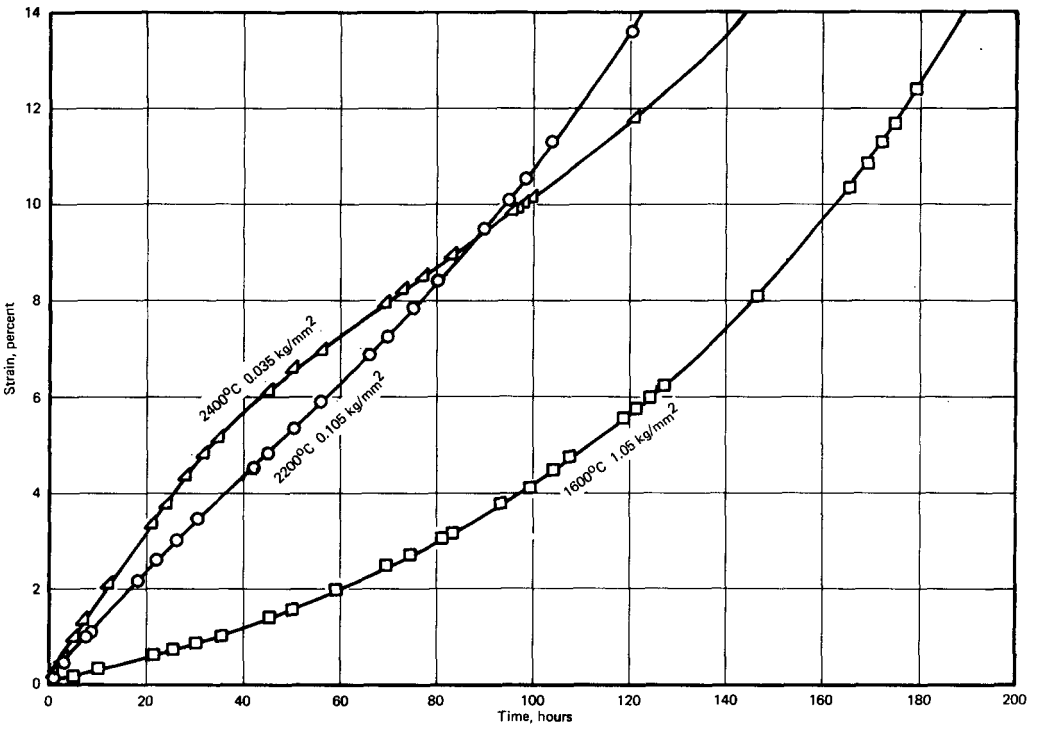

Fig. 1.39 – Creep curves for wrought, powder-metallurgy Mo – 50Re (wt %) sheet (Lot 2) tested in hydrogen

urements of 285 microns and 3.16×10^{-8} cm, respectively. The two activation energy values discussed above were applied to the conventional diffusion expression

$$D = D_0 e^{-\frac{Q}{RT}} \qquad (1.16)$$

where D is the self-diffusion rate of atoms, D_0 is a constant, Q is the activation energy for self-diffusion, R is the gas constant, and T is the absolute temperature. Diffusion rate values could then be expressed by the relations shown in Figure 1.40.

Mo – 30W – The stress-rupture characteristics for both wrought, unalloyed tungsten and molybdenum sheet were shown to vary above one-half the absolute melting temperature depending on whether the material was fabricated by an AC or PM process.[38,39] Results obtained for PM molybdenum varied depending on the material source (i.e., vendor); results for AC material were essentially identical independent of the source. Similar findings were observed for tungsten. When the stress-rupture test results for AC molybdenum and AC tungsten were analyzed in terms of homologous temperature, identical results were obtained;[40] this did not occur for the PM materials.

The phase diagram for the tungsten-molybdenum system reveals that these metals form solid solutions over the complete range of compositions. The rupture-strength relationship for alloys of the two metals may be expected to be the same as that for the elements on a homologous temperature basis except for the possible strengthening effect of the lattice dis-

[38] P. N. Flagella, "High-Temperature Stress-Rupture Characteristics of Mo and Mo Alloys," AIAA Journal, Vol. 5, 1967, p. 281.

[39] P. N. Flagella, "High Temperature Creep-Rupture Behavior of Unalloyed Tungsten," GE-NMPO, GEMP-543, August 1967.

[40] GEMP-475A, p. 16.

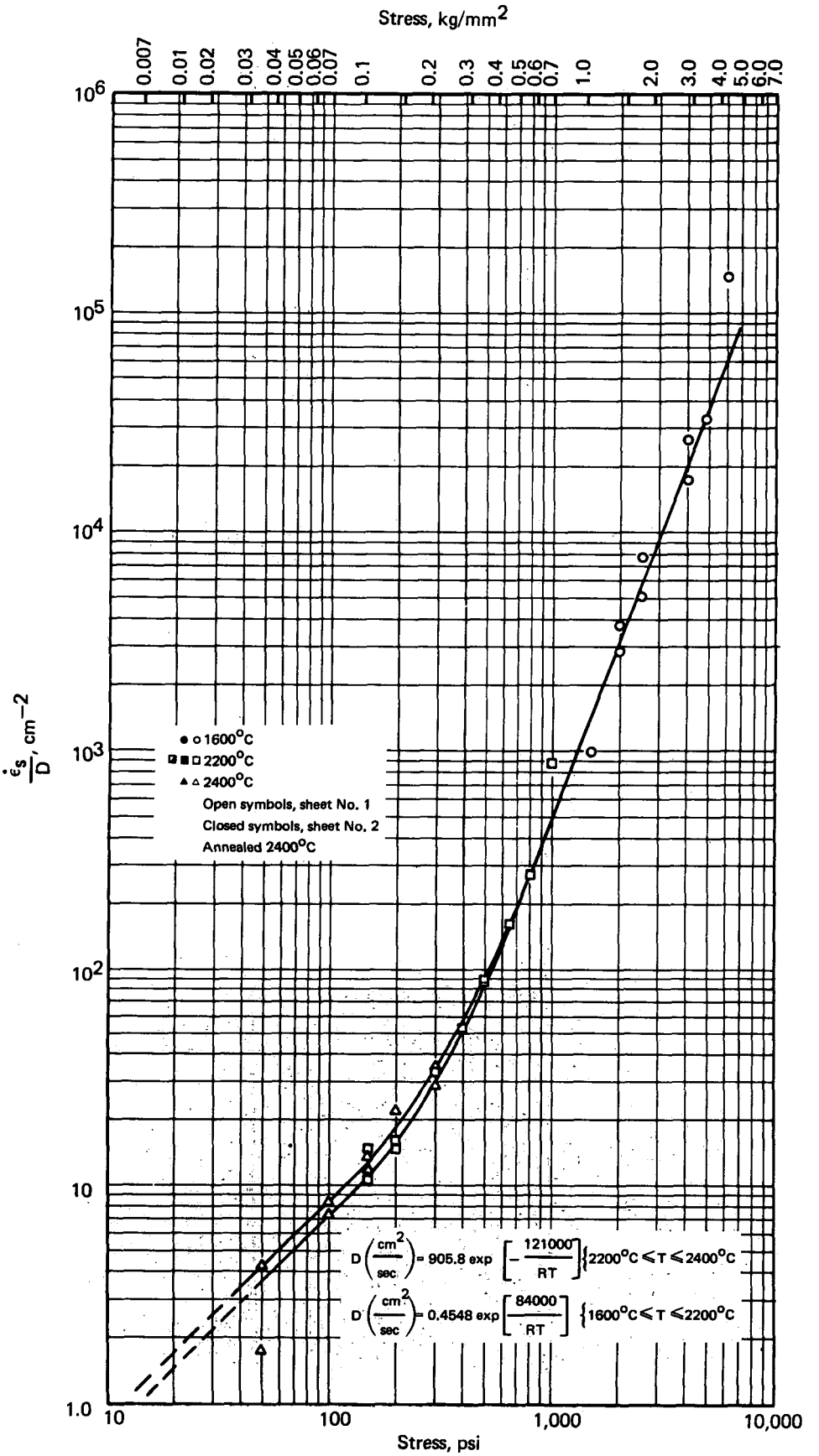

Fig. 1.40 — Correlation of creep rate data for wrought, powder-metallurgy Mo — 50Re (wt %) tested in hydrogen

tortion by the substitution of tungsten atoms for molybdenum atoms. Because of the similarity between tungsten and molybdenum, the stress-rupture characteristics of wrought, arc-cast Mo – 30W (wt %), purchased commercially (heat 30W 7694), were evaluated.[41]

The Mo – 30W alloy was of relatively high purity containing 69, 12, 1, and 41 ppm of C, O, H, and N, respectively. After rolling to sheet, with intermediate anneals, the material was stress-relieved for 1 hour at 1175°C in vacuum. Stress-rupture and creep tests were performed at 1600°C and 2200°C in hydrogen after annealing for 2 hours at the test temperature. Creep curves for this material are presented in Figure 1.41. For all stress levels indicated, at constant temperature, the strain is presented as a function of the time to give 10 percent strain. In this way the curve shapes over a wide range of stresses are easily shown and compared. All the creep curves for the Mo – 30W alloy display a third-stage-type creep from essentially time zero. As shown, the ratio of $t_R/t_{10\%}$ (Figure 1.41) decreases with decreasing stress at the same temperature. This is apparently not related to the fact that at 1600°C the elongation for the material at rupture decreases with decreasing stress since this is not the case at 2200°C.

Figure 1.42 gives the stress-rupture curves for the Mo – 30W material at 1600°C and 2200°C along with curves for wrought, AC, unalloyed W, Mo, and W – 25Re (wt %) for comparison. As expected, the addition of tungsten to molybdenum increases the rupture life. All the materials exhibit a linear relationship between log stress and log rupture time. Isotherms for the Mo – 30W and W – 25Re alloys are nearly parallel and have slopes greater than those shown for the unalloyed tungsten and molybdenum.

The 100-hour rupture data from Figure 1.42 are shown in Figure 1.43 in terms of the homologous temperature (percent of the absolute melting temperature). Agreement is shown between the tungsten and molybdenum data but the Mo – 30W data show a 17 percent increase in the rupture stress for the same percent of the absolute melting temperature. This may be due to the lattice distortion effect mentioned above. The W – 25Re data reflect a different behavior.

Figure 1.44 shows typical specimens after testing at 1600°C and 2200°C and the resulting photomicrographs. The effect of temperature on the grain size is quite apparent being 145 microns at 1600°C and 490 microns at 2200°C. Significant intergranular separation is also noted. For the specimen tested at 1600°C this appears to occur primarily transverse to the stress direction. At 2200°C, the effect is not apparent due to the large grain size involved.

RHENIUM

Studies of the creep-rupture behavior of wrought, PM (lot 2), unalloyed, rhenium sheet (0.05 cm thick) were reported[42,43] for tests at 1600°, 2200°, and 2600°C in hydrogen. Rupture data obtained in these evaluations are presented in Figure 1.45 along with some previously reported[44] data for lot 1 rhenium which had been obtained from the same vendor at an earlier date. Some slight difference between lots 1 and 2 is quite evident from Figure 1.45 and was attributable[43] to different sintering procedures which led to different grain sizes in the two lots of material. Cavitation was observed in the grain boundaries of the material from both lots at fracture. Linear creep rate data for the lot 2 material are presented in Figure 1.46. In terms of rupture strength, the lot 2 material has about the same strength as AC tungsten at 1600°C and is decidedly stronger than AC tungsten at all higher temperatures.

[41] GEMP-1002, p. 11.

[42] GEMP-67, p. 11.

[43] "AEC Fuels and Materials Development Program Progress Report No. 69," GE-NMPO, GEMP-69, September 29, 1967, p. 11.

[44] "Fourth Annual Report – High-Temperature Materials and Reactor Component Development Programs, Volume I – Materials," GE-NMPO, GEMP-334A, February 26, 1965, p. 23.

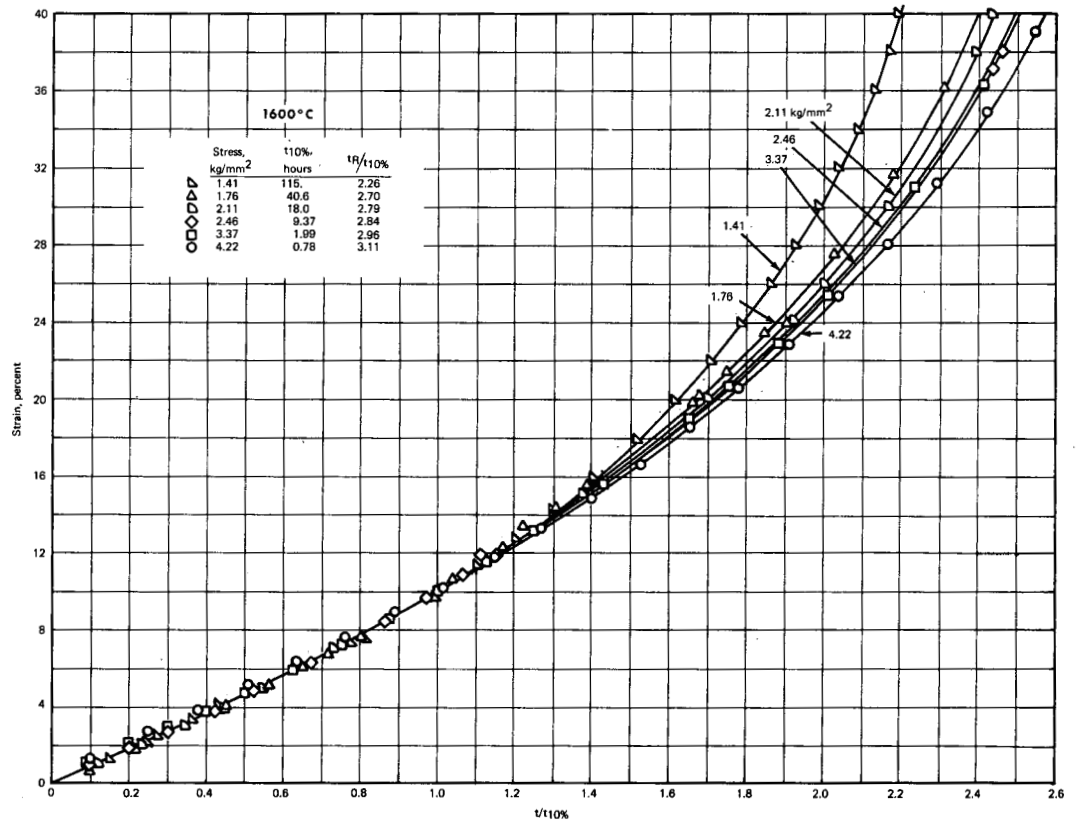

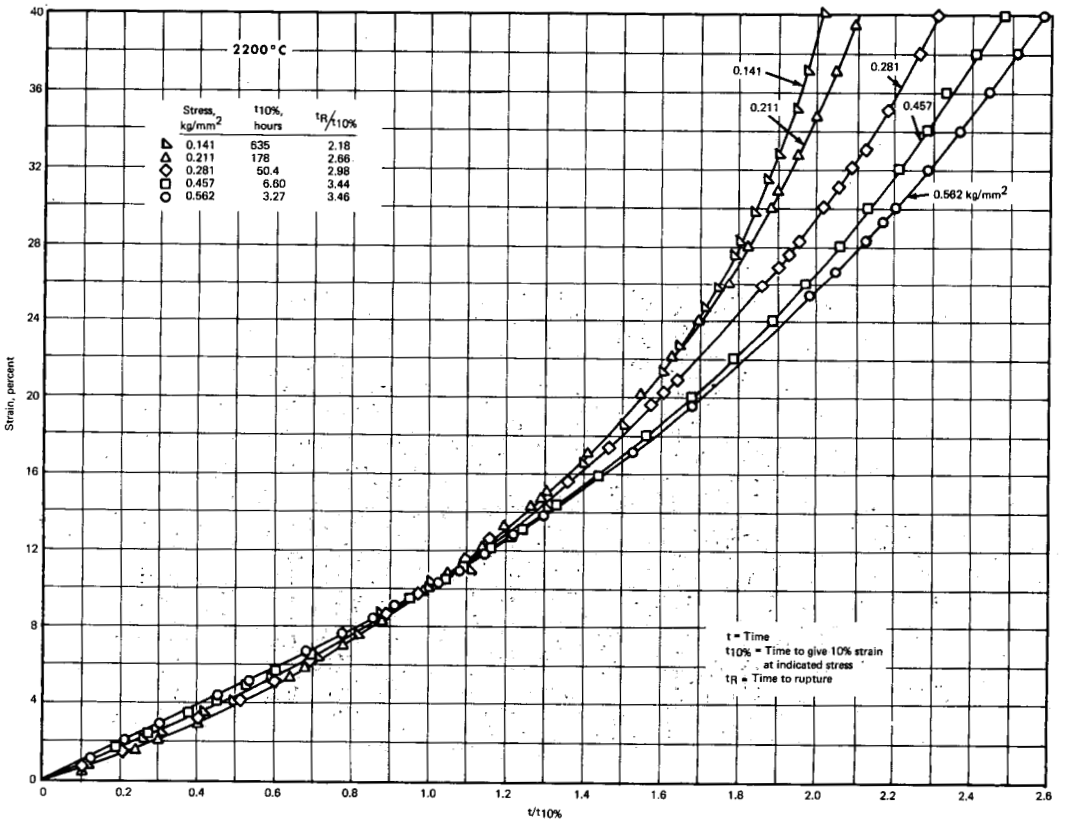

Fig. 1.41 — Creep curves for wrought arc-cast Mo — 30W (wt %) sheet tested in hydrogen

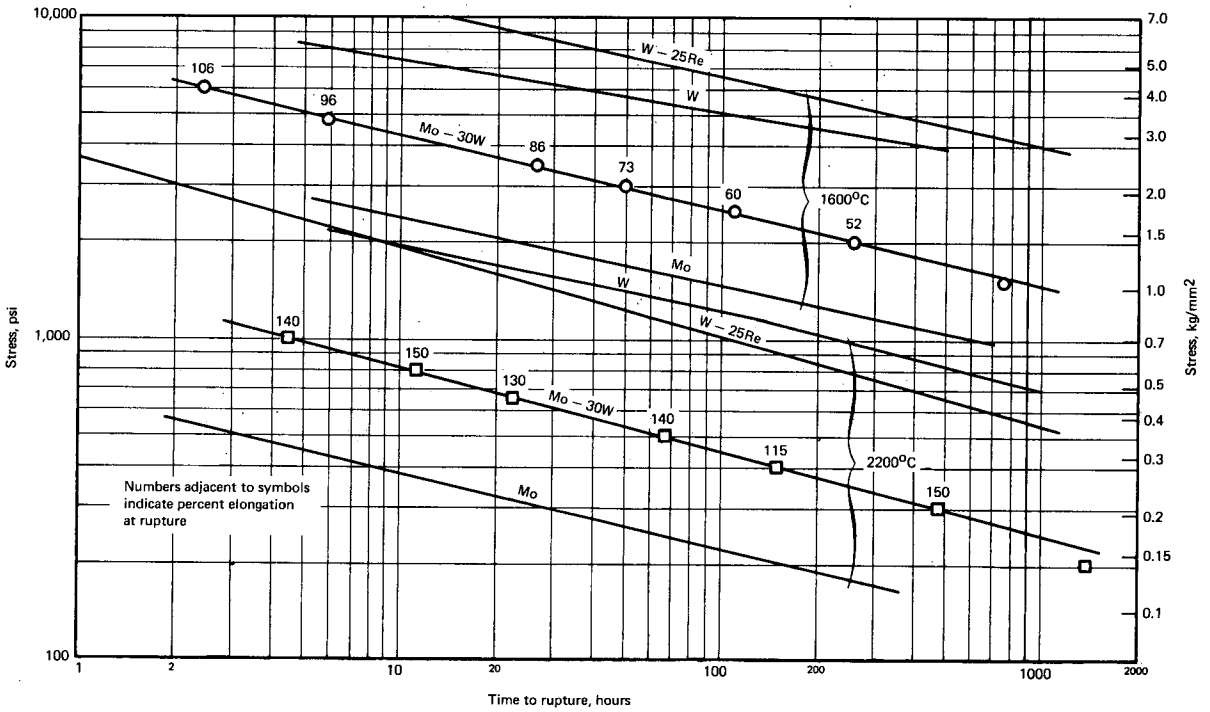

Fig. 1.42 – Stress-rupture results for wrought arc-cast Mo – 30W (wt %) sheet compared to W, Mo, and W – 25Re (wt %)

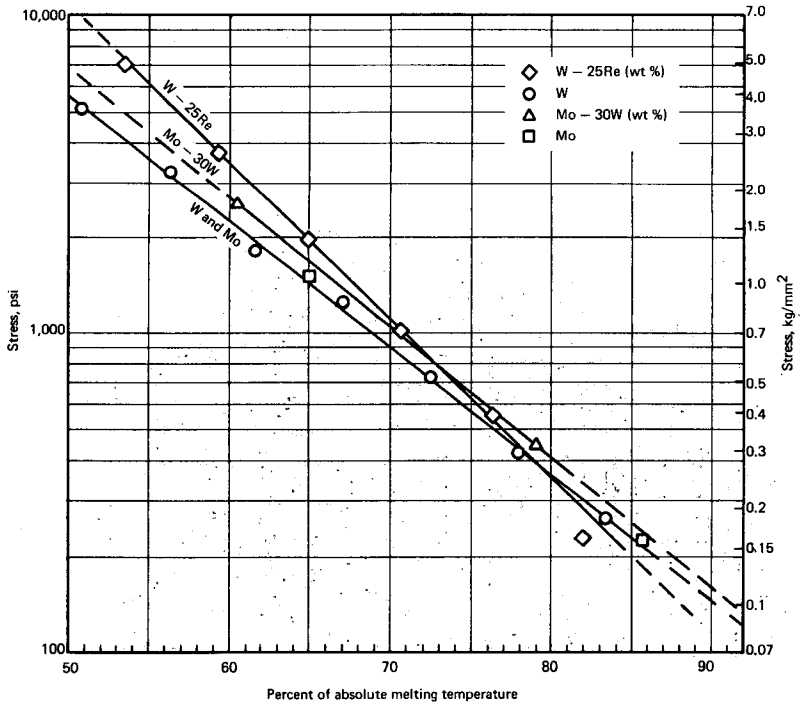

Fig. 1.43 – Stress required to cause rupture in W, Mo, Mo – 30W, and W – 25Re in 100 hours

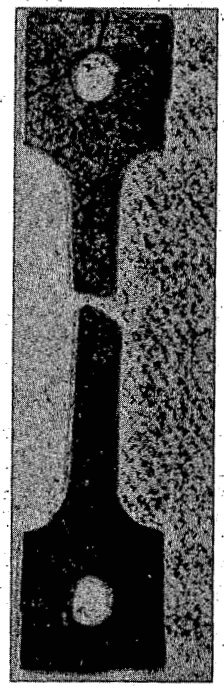

(Neg. P67-12-20D)

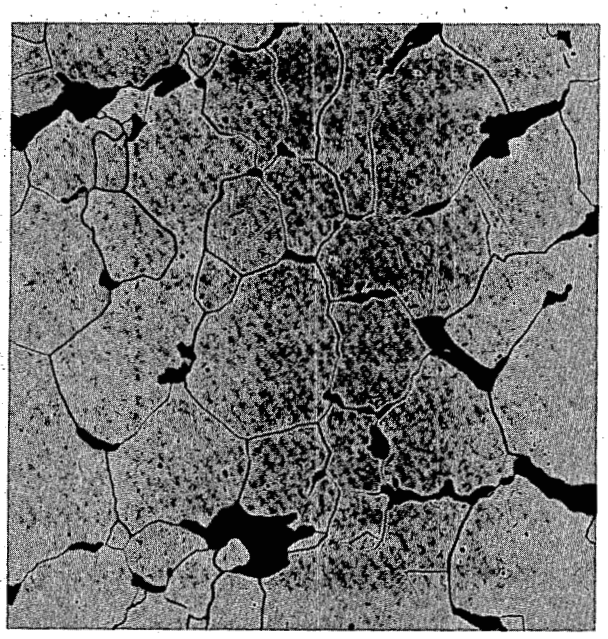

(Neg. 10191)
1600°C, 1.05 kg/mm^2
764 hours, 48%
145 microns

(100X etched)

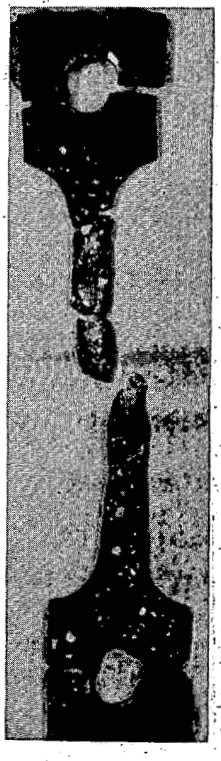

(Neg. P67-12-20F)

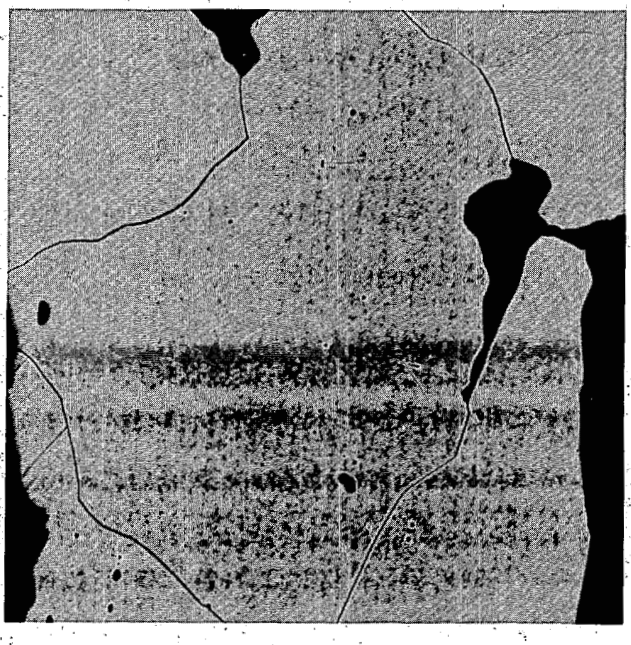

(Neg. 10187)
2200°C, 0.141 kg/mm^2
1388 hours, 72%
490 microns

(100X etched)

Fig. 1.44 — Mo — 30W (wt %) sheet samples after creep-rupture testing in hydrogen. Numbers below figures are: test temperature, stress, rupture time, elongation at rupture, and grain size.

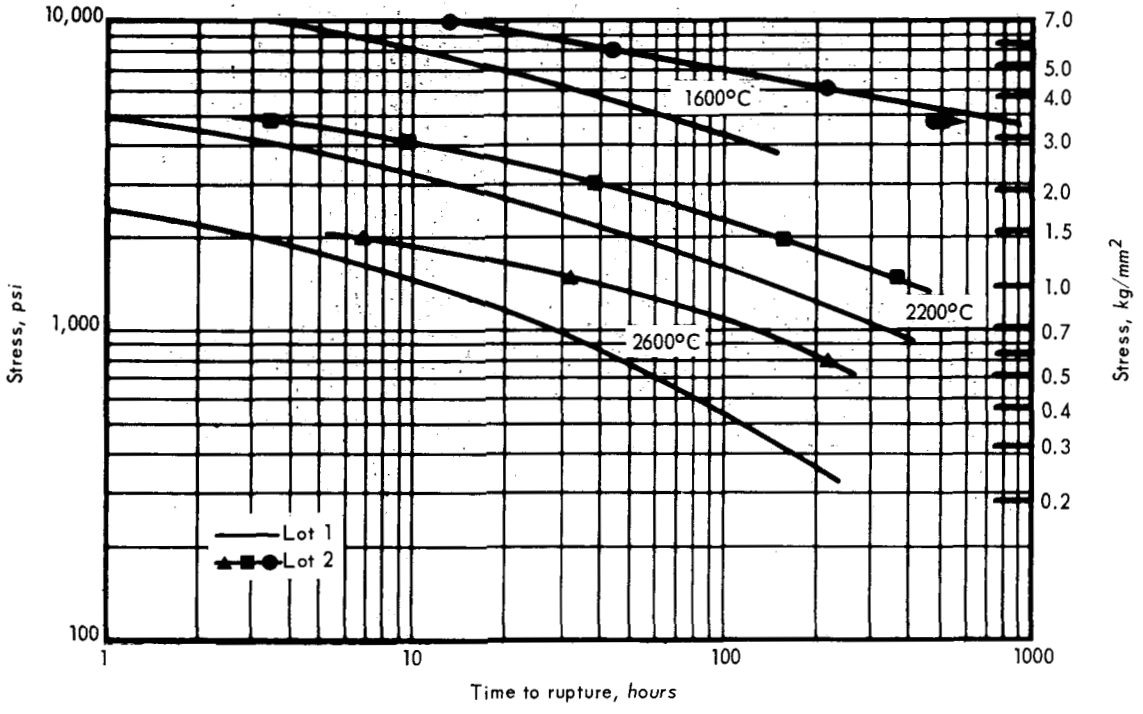

Fig. 1.45 — Stress-rupture data for lot 1 and lot 2 wrought, powder-metallurgy unalloyed rhenium sheet tested in hydrogen

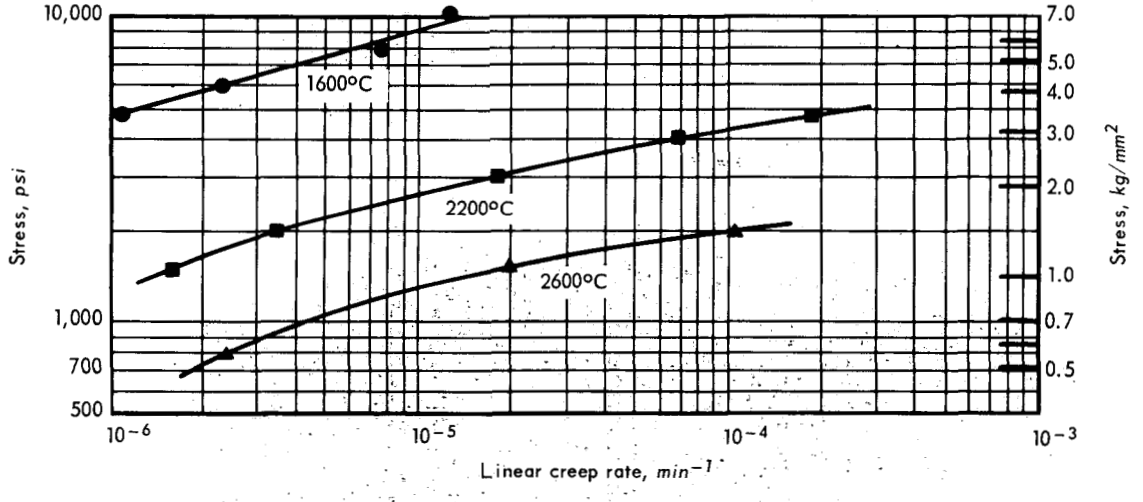

Fig. 1.46 — Linear creep rate data for lot 2 wrought, powder-metallurgy unalloyed rhenium sheet tested in hydrogen

NIOBIUM AND NIOBIUM ALLOYS

Creep-rupture testing of niobium was based on experience gained from tests[45] of tantalum at high temperatures, in either high-purity hydrogen or argon. These tests showed that the material becomes significantly contaminated with nitrogen and oxygen causing strengthening and embrittlement. The primary source of the contamination is not the test gas, since high-purity gas was used, but the result of the furnace components outgassing at high temperatures. Placing a protective tantalum foil around the specimen being tested decreased the contamination level but did not eliminate it. No such problem was encountered with the non-reactive refractory metals (W, Mo, Re) or their alloys. This is apparently due to the low level of solubility for interstitials.

Niobium, tantalum, and vanadium (Group V elements) are highly reactive and have a high solubility for the interstitial elements and hence are more difficult to evaluate in the uncontaminated condition. To overcome some of the contaminating problems associated with evaluating the creep-rupture properties of niobium, a test system was modified by incorporating an ion pump so that testing could be performed in a relatively high vacuum. In addition, modifications were incorporated to allow the system to outgas after reaching test temperature with the test specimen in a cold region of the furnace until outgassing had subsided and a good vacuum level was reached (~1 x 10^{-6} Torr). By operating the system at a higher temperature than required for testing, outgassing was accelerated and possible outgassing during test was reduced. After outgassing was complete and thermal equilibrium obtained at the test temperature, the test specimen was positioned in the hot zone of the furnace, annealed for 2 hours, loaded to the desired stress level and the creep-rupture test performed.

This procedure was used to test four wrought, AC, unalloyed niobium sheet samples and one alloy, Cb-753 (Nb-5V-1.25Zr, wt %), sample at 1600°C. Impurities in ppm for the as-received materials were as follows: for Nb; C = 22, O = 282, N = 16, H = 5; for Cb-753; C = 15, O = 208; N = 44, H = 2. The test results are given in Table 1.10 and the creep curves shown in Figure 1.47. The stress-rupture data are presented in Figure 1.48 including previously published[46] data for the alloy Cb-753. The greater rupture life for the alloy over the unalloyed niobium at 1600°C and 0.703 kg/mm^2 is obvious. The fact that the alloy showed considerable elongation at rupture (130%) after 342 hours at 1600°C is an indication of a high-purity non-contaminating environment. Additionally, the hardness of the alloy decreased

TABLE 1.10

CREEP-RUPTURE RESULTS[a] FOR WROUGHT, ARC-CAST, UNALLOYED NIOBIUM SHEET[b] AND ALLOY Cb-753 SHEET[c] AT 1600°C TESTED IN VACUUM[d]

Material	Specimen No.	Stress, kg/mm^2	Time to Indicated Strain, hours							Rupture		Linear Creep Rate, min^{-1}
			0.2%	0.5%	1%	2%	3%	5%	10%	Time, hr	Elongation, %	
Nb	1-4	0.211	0.95	2.60	5.50	12.2	20.0	35.3	70.0	182.	41	1.9×10^{-3}
	-3	0.352	–	0.03	0.18	0.86	1.88	4.28	9.60	19.3	30	5.1×10^{-3}
	-5	0.562	–	–	–	–	0.01	0.09	0.51	1.83	41	1.9×10^{-3}
	-1	0.703	–	–	–	–	–	0.04	0.18	0.54	30	1.7×10^{-5}
Cb-753	1	0.703	0.79	2.52	6.00	14.4	23.6	42.8	90.0	342.	130	1.4×10^{-4}

[a]Annealed at 1600°C for 2 hours in vacuum before testing.
[b]0.053-cm-thick sheet, 0.64-cm x 2.54-cm gage section.
[c]0.15-cm-thick sheet, 0.64-cm x 2.54-cm gage section.
[d]From 1 to 2 x 10^{-6} Torr.

[45]"High-Temperature Materials Program Progress Report No. 25," GE-NMPO, GEMP-25A, July 31, 1963, p. 12.

[46]Union Carbide Corp., Stellite Division, F-30, 269-1, September 1964.

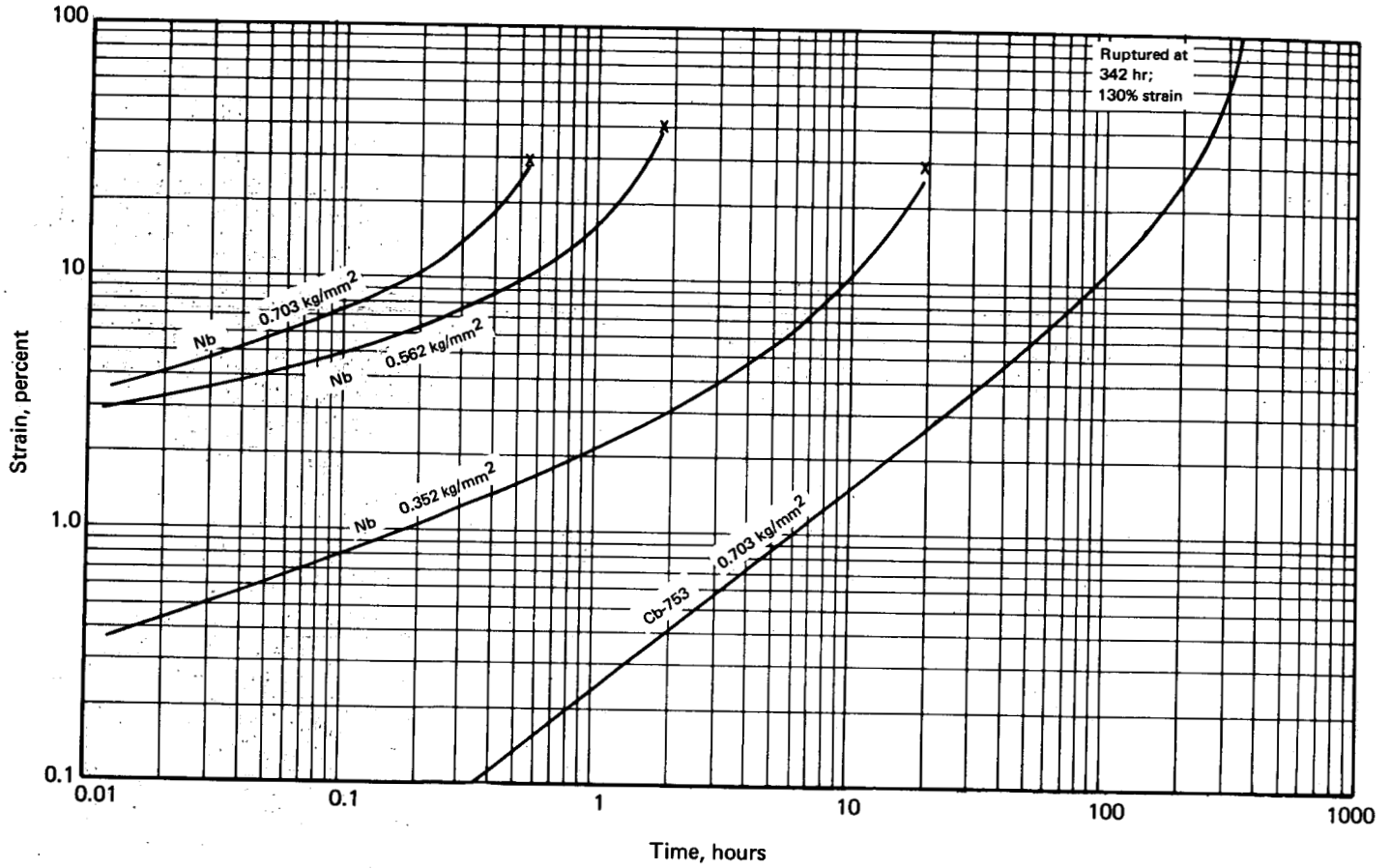

Fig. 1.47 – Creep-rupture curves for wrought, arc-cast niobium and alloy Cb-753 sheet tested at 1600°C and in a vacuum of 1×10^{-6} Torr

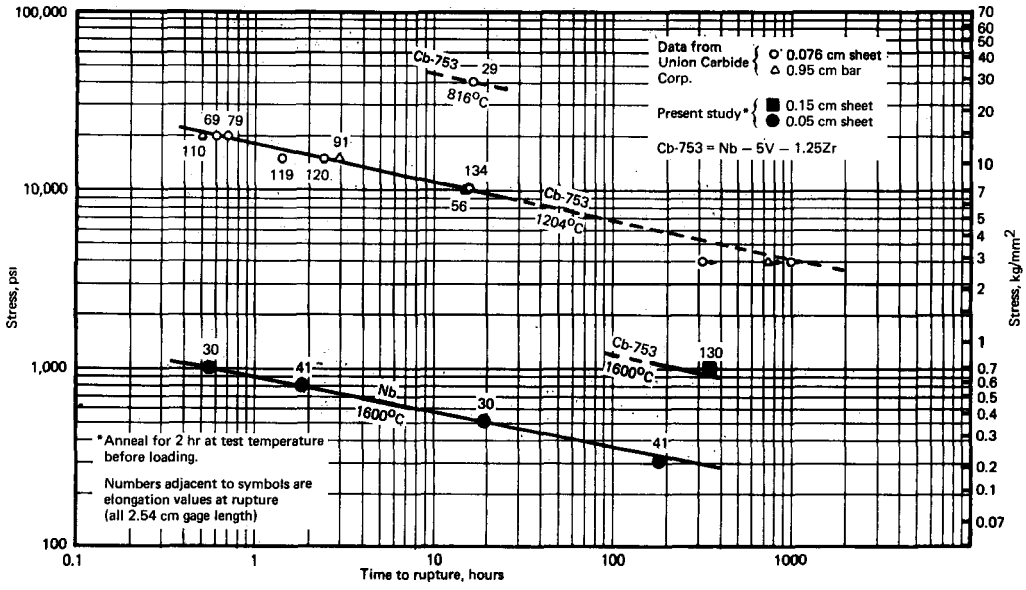

Fig. 1.48 – Stress-rupture results for unalloyed niobium and alloy Cb-753

from 183 DPH before test to 160 DPH after test. Chemical analysis and metallographic evaluations are planned for all samples to determine the extent of any otherwise undetected contamination.

CONSTANT-STRESS CREEP TESTING

All stress-rupture and creep data reported in this program to date have been obtained by constant-load testing. As the test specimen elongates, the cross-sectional area decreases and the stress increases. Most data reported in the literature are obtained in this manner, but to better understand the basic characteristics and mechanisms involved in creep, test data obtained at constant stress are desirable.

One high-temperature creep-rupture test stand was modified to perform tests at constant stress. Figure 1.49 shows a schematic diagram of the system. The electro-optical strain measuring system[47] automatically records strain versus time for the test specimen. On the basis of the strain measurement, the automatic load-control unit decreases the load on the specimen to maintain a constant stress. The assumption involved with this approach is that the strain occurs uniformly over the gage length of the specimen and that the increase in strain is proportional to the decrease in cross section (i.e., constant volume deformation). This is a valid assumption until local necking occurs which, on the basis of constant stress, does not occur until third-stage creep is observed.

Several constant-stress creep tests were performed to evaluate the system. Unalloyed molybdenum sheet specimens were tested at 1600°C and a constant stress of 2.11 kg/mm^2 in hydrogen and compared to the results obtained at constant load for the same material. One such comparison is shown in Figure 1.50. As expected, due to the continually decreasing load with increasing strain, the constant-stress tests show a longer time to reach the same values of strain observed in the constant-load tests.

Previous evaluations of equation forms have shown that a third-degree polynomial in $t^{1/3}$ describes the primary and secondary stages of creep for a constant-load test very well. This

[47] W. L. McCullough and P. N. Flagella, "Experimental Techniques Employed in Stress-Rupture and Creep Measurements to 3000°C," GE-NMPO, GE-TM 65-5-10, April 1965.

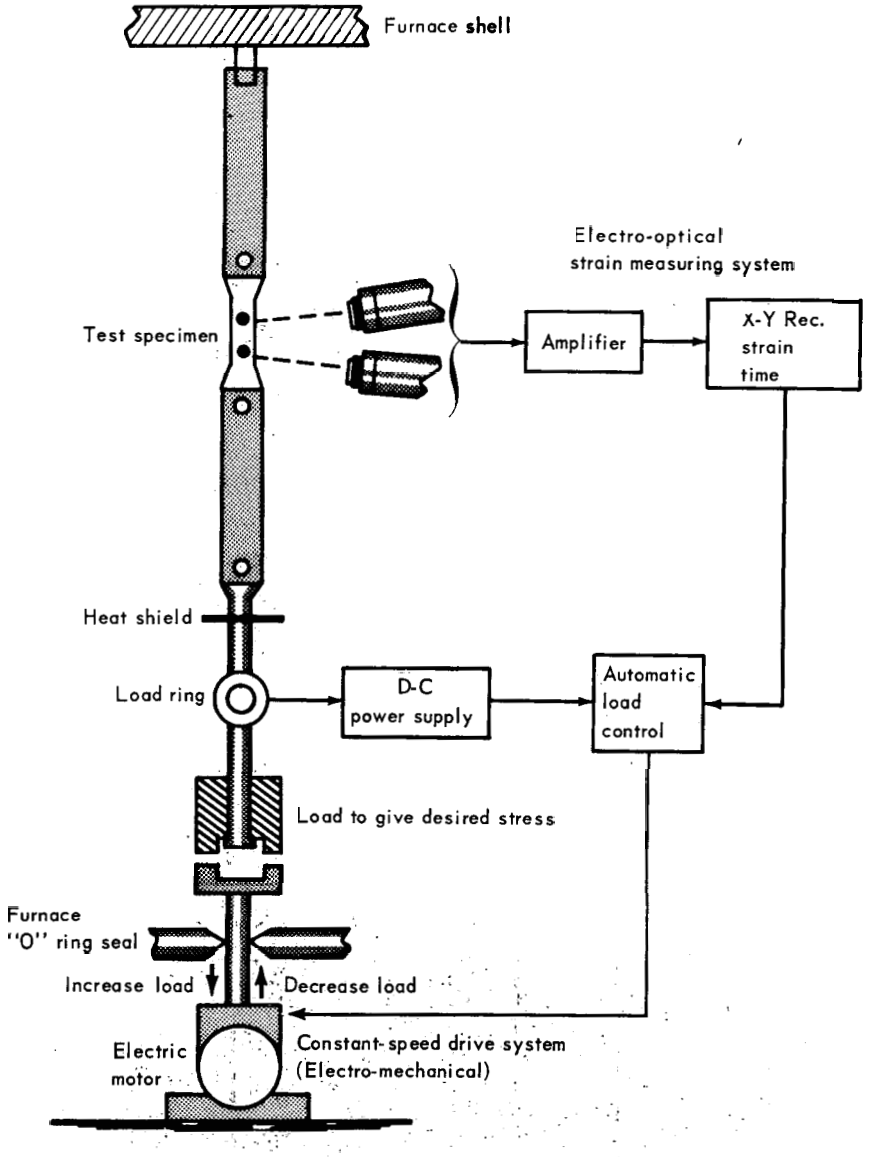

Fig. 1.49 – Schematic diagram of constant stress creep system

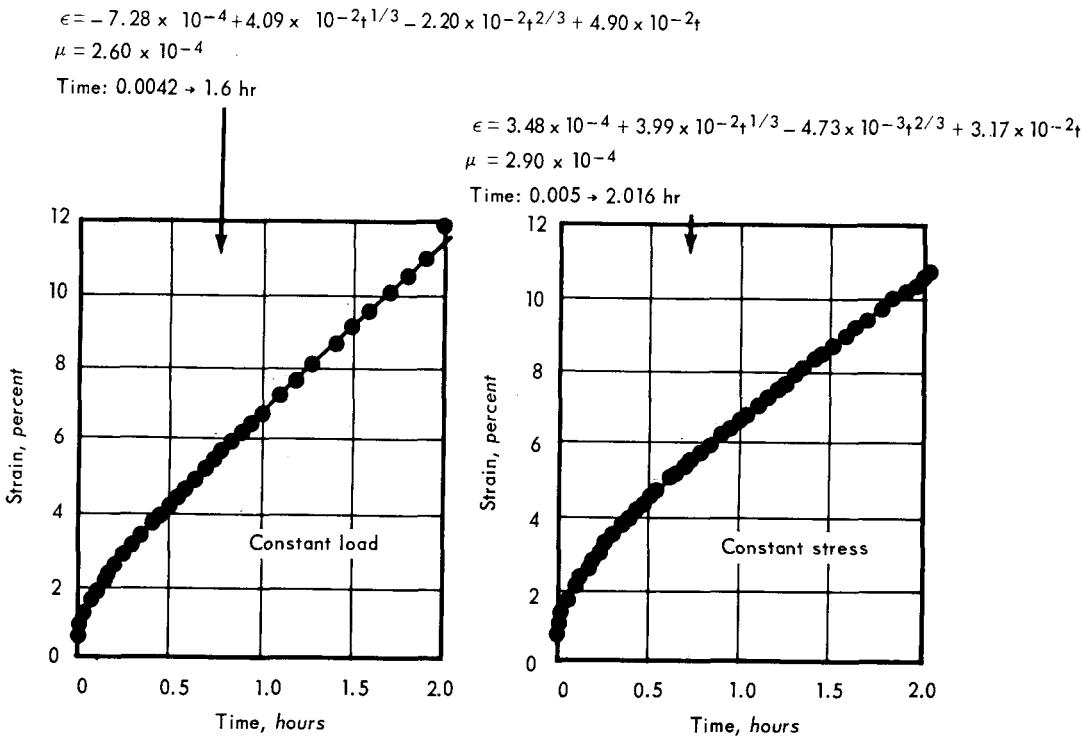

Fig. 1.50 — Comparison of constant-load and constant-stress creep tests of Mo sheet at 1600°C and 2.11 kg/mm^2 in hydrogen

same equation form is effective in describing the constant-stress test as shown in Figure 1.50.

Additional tests of wrought, AC molybdenum sheet were performed at both 1600°C and 2200°C in hydrogen to compare the second-stage creep rates. Figures 1.51 and 1.52 show the creep curves obtained with the time scale normalized to the time required to give 10 percent strain. This permits a more direct comparison of the creep curves to evaluate the effect of stress on the strain. Although small differences are observed between the constant-load (increasing stress) and constant-stress creep curves, the differences are not significant until approximately 15 percent strain is obtained which is beyond the region of the linear creep rate for the constant-load test. The linear creep rates for the two types of tests are essentially the same. This being the case, constant-load creep test results may be analyzed in terms of the linear (secondary) creep rate with no significant error.

The creep curves presented in Figures 1.51 and 1.52 for AC molybdenum, display the classical form at constant load and, therefore, permit analysis, correlation, and interpretation of linear creep rate behavior. Any conclusions reached in this type of analysis should be consistent with those based on an analysis of constant-stress data. Some materials, notably solid-solution alloys such as W – 25Re, Mo – 30W, and some tantalum alloys, have displayed creep curves consisting of only third-stage creep when tested at constant load. Similar curves were obtained for AC molybdenum at 2400°C (0.93 T_m) as shown in Figure 1.32. These data do not permit an analysis to be performed on the basis of linear creep rate.

To evaluate the difference due to constant-stress testing, constant-stress tests of Mo–30W (wt %) were performed at 2200°C and 0.352 kg/mm^2. Creep curves for two constant-stress tests and one constant-load test are shown in Figure 1.53. The results show a marked dif-

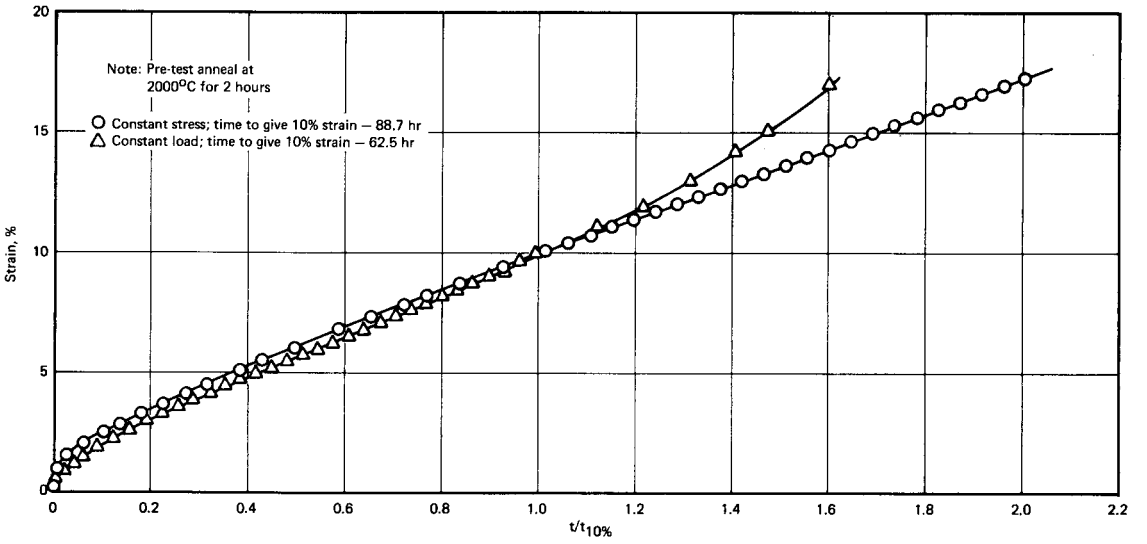

Fig. 1.51 – Comparison of constant-load and constant-stress creep curves for arc-cast Mo sheet tested at 1600°C and 0.844 kg/mm^2 in hydrogen

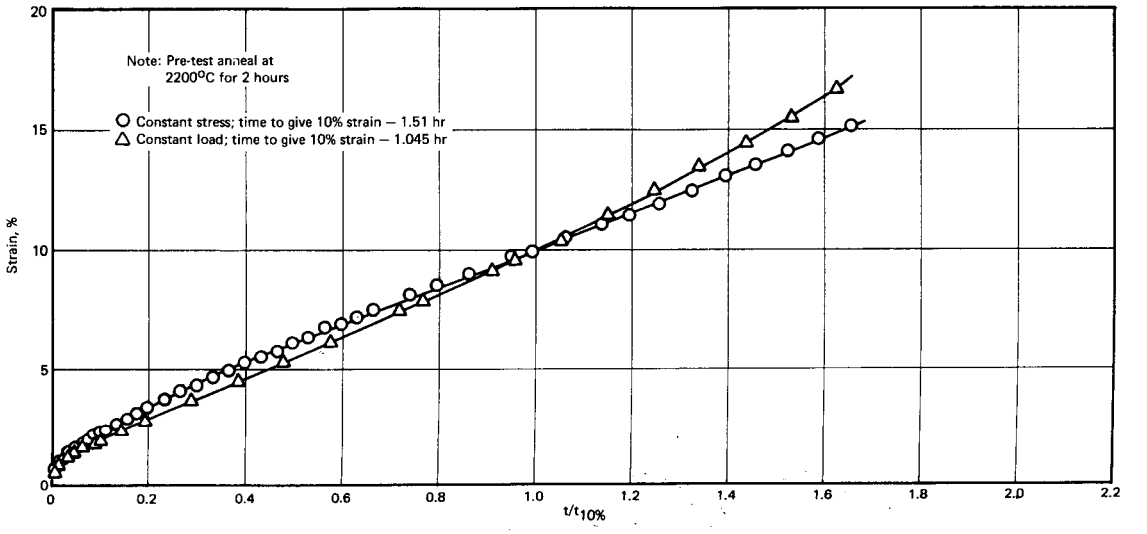

Fig. 1.52 – Comparison of constant-load and constant-stress creep curves for arc-cast Mo sheet tested at 2200°C and 0.35 kg/mm^2 in hydrogen

ference in the curve shapes. Whereas, the constant-load test displays a curve of increasing creep rate from time zero, one of the constant-stress tests gave essentially a linear creep curve to a strain of 65 percent. This indicates that uniform deformation over the length of the gage section occurred to at least this strain level. Strain measuring beyond this level was not possible with the test equipment and the test was terminated. The lower constant-stress creep curve in Figure 1.53 shows a decreasing rate of deformation after approximately 25 percent strain. This was caused by a greater load removal rate than actually needed to maintain constant stress. Deformation of the specimen from this test was quite uniform over the total length of the gage section (2.54 cm) after 36 percent strain as shown in Figure 1.54. The same observation was made for the sample tested to 65 percent strain.

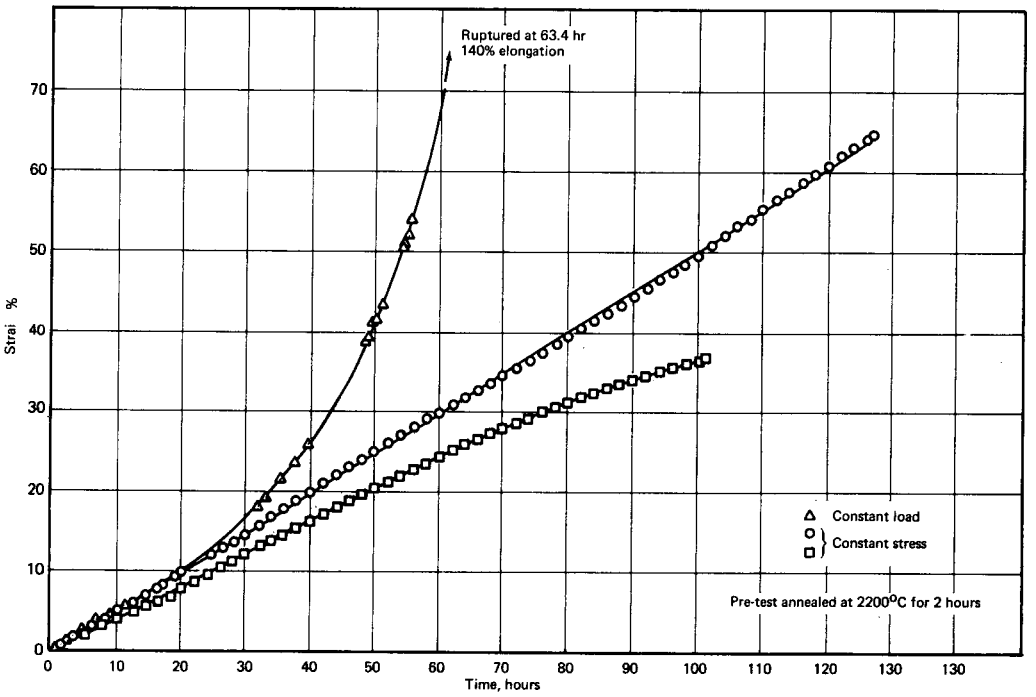

Fig. 1.53 — Comparison of constant-load and constant-stress creep curves for arc-cast Mo — 30W (wt %) tested at 2200°C and 0.352 kg/mm^2

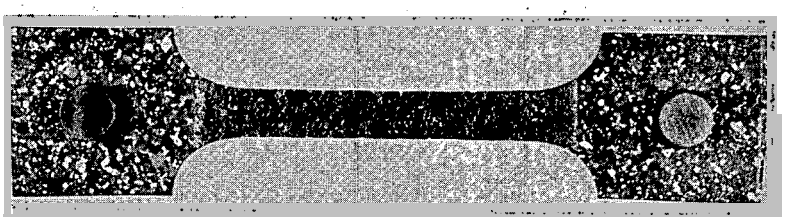

Fig. 1.54 — Mo — 30W (wt %) creep sample after testing at 2200°C and 0.352 kg/mm^2 showing 36% strain (2.54-cm gage length)(Neg. P68-1-12B)

Computer analysis procedures were developed to analyze constant-load creep tests in terms of instantaneous creep rate and instantaneous stress (see creep analysis section under Tungsten) to determine the dependence of strain rate on stress. This technique was employed to analyze the experimental results obtained at constant stress. Figure 1.55 shows the results for both types of testing. The constant-load test of this one sample shows the creep rate to be proportional to stress to the 4.6 power over the range from 0.35 to 0.5 kg/mm^2. The data points for the two constant-stress tests show reasonably good agreement with the constant-load test in terms of creep rate. The difference in the two constant-stress tests is probably due to experimental variations associated with precise temperature measurement at 2200°C, the normal precision being ±10°C at 2200°C.

Experimental creep data obtained at both constant-load and constant-stress indicate that constant-load creep data may be analyzed in terms of constant stress with no significant error due to the increasing stress as the result of strain until non-uniform deformation occurs. This appears to apply for materials exhibiting the conventional creep curve, consisting of the three stages of creep, as well as a material exhibiting only third-stage-type creep.

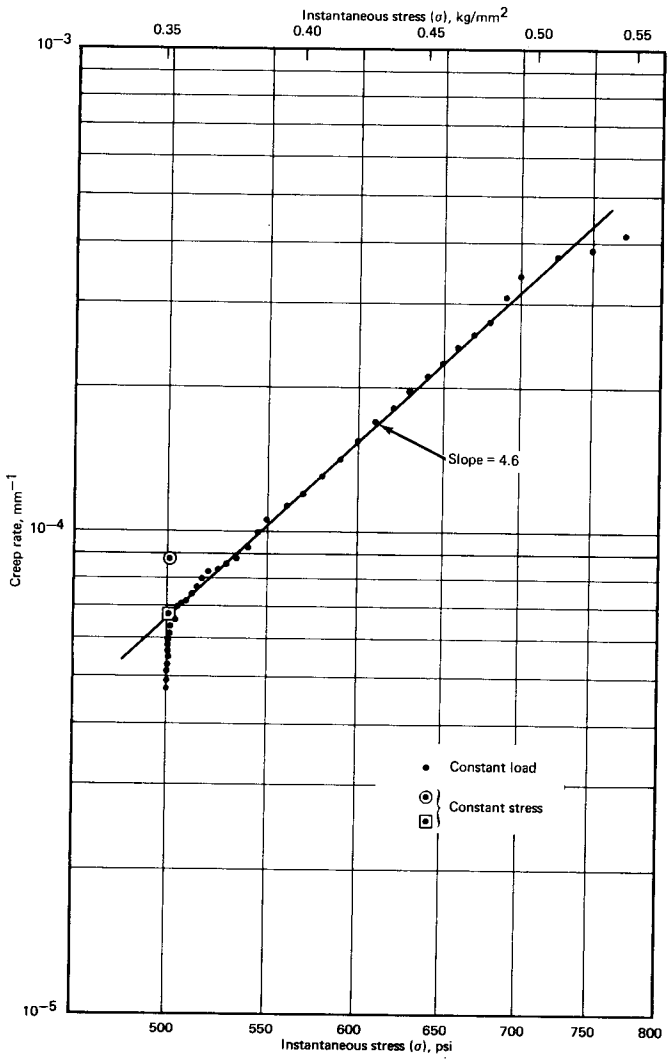

Fig. 1.55 — Comparison of constant-load and constant-stress creep tests in terms of creep rate for Mo – 30W (wt %) at 2200°C and 0.352 kg/mm^2

SINGLE CRYSTALS

Unalloyed, powder-metallurgy tungsten sheet straps, 0.05 cm thick by 1.9 cm wide by 19 cm long, are used to support the sheet-type test specimens during creep testing at 1600° to 3000°C in hydrogen. During testing, large grains are sometimes developed in the straps with the sizes apparently dependent on temperature, time, and stress. One such test performed at 2200°C for 315 hours produced a single crystal of tungsten over approximately one-half the length of a strap. Using the Laue back-reflection X-ray diffraction technique, it was confirmed that the strap was a single crystal and had a nearly perfect (114) orientation with the stress axis along the (110) direction.

Creep-rupture tests of polycrystalline tungsten have been shown to exhibit correlatable characteristics consistent with other pure materials. The creep characteristics of single crystals are not understood, in general, and no data at high temperatures seem to be available for single-crystal tungsten. A creep-rupture test of the single-crystal sheet material was performed in hydrogen on a specimen having a 0.64-cm-wide by 2.54-cm-long gage section fabricated by the electrical discharge machining process (Elox). Table 1.11 lists the test conditions and results. These data show the single-crystal material to be stronger than polycrystalline, wrought, AC tungsten.

Figure 1.56 shows the single-crystal test specimen before and after testing. The significant observation is that essentially no deformation occurred prior to rupture other than that occurring locally at the 0.01-cm holes used as fiducial marks for strain measurements. The mode of fracture is not clear but near the center of the gage length there is an indication of slip along some plane of the crystal. Investigations are underway to study this region of the specimen using X-ray diffraction, metallography, and the electron microscope. These studies should provide some explanation of the mode of deformation in single-crystal, PM tungsten at extremely high temperatures.

TABLE 1.11

CREEP RESULTS OF SINGLE-CRYSTAL, UNALLOYED TUNGSTEN SHEET TESTED IN HYDROGEN

Temperature, °C	Stress, kg/mm^2	Time, hr	Strain,[a] %
2400	0.46	22	0 (5.0)
2400	1.05	22	0 (rupture at 3.1 hr – 85%)
2600	1.05	22	0 (rupture on loading)
2800	1.05	53.6	Rupture

[a]Values in parentheses refer to data for polycrystalline arc-cast tungsten.

STRESS-RUPTURE PARAMETER ANALYSIS

A comprehensive study of stress-rupture parameters was completed.[48] In addition to a detailed treatment of the three most common parameters, Larson-Miller, Dorn, and Manson-Haferd, appropriate attention was given the Graham-Walles, Murry, Chitty-Duval, and Brozzo parametric approaches. In each case, special consideration was given to the mathematical procedures employed in identifying parameter constants and in developing an analytical expression relating parameters to stress. Also, a detailed comparison was made of the relative effectiveness of these parameters in the correlation and extrapolation of experimental data. As part of this comparison, mathematical optimization procedures were employed to re-evaluate numerous sets of experimental data which have appeared in the literature.

[48]J. B. Conway, "Stress-Rupture Parameters: Origin, Calculation and Use," GE-NMPO, GEMP-555, June 30, 1967.

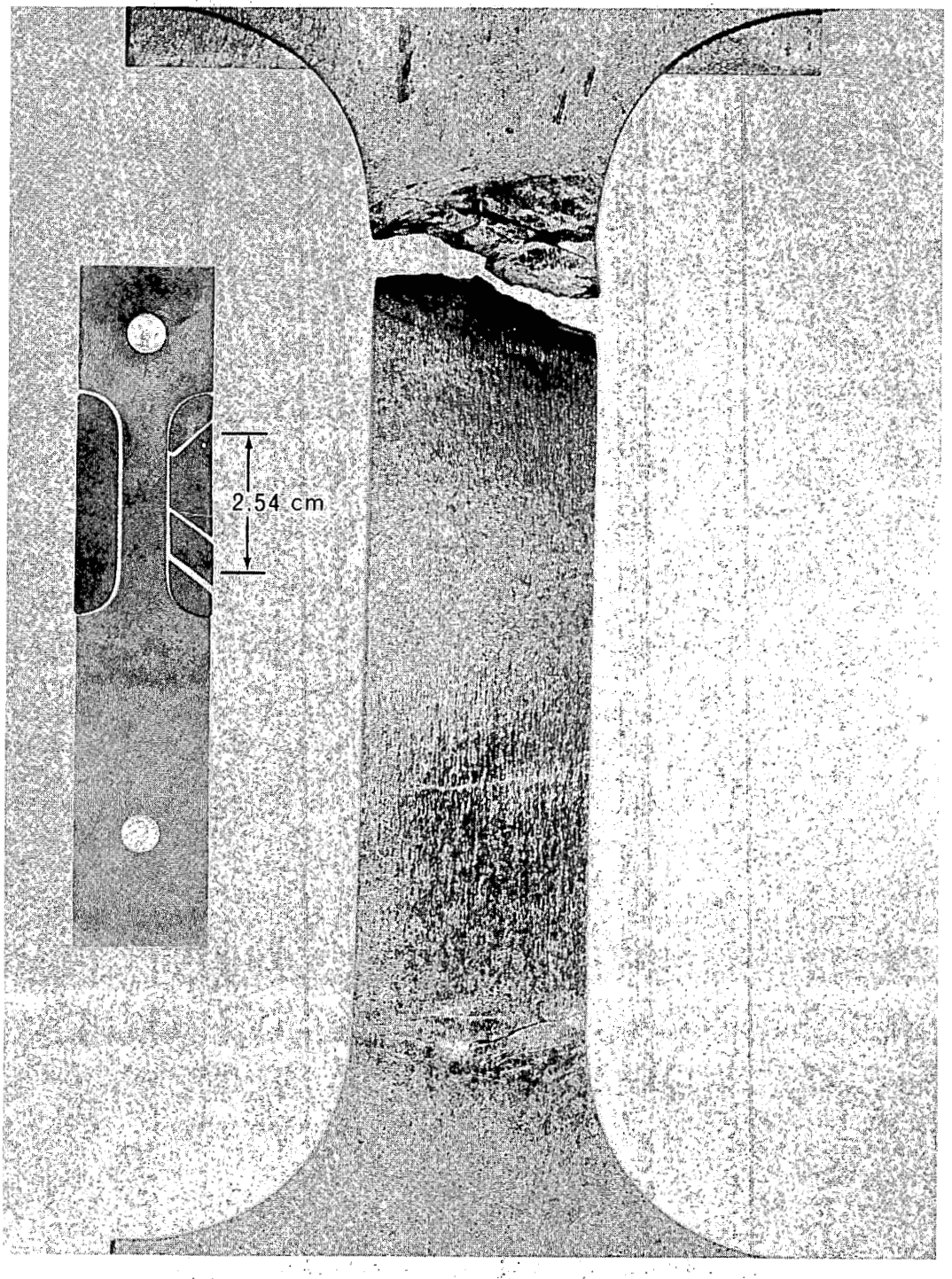

Fig. 1.56 – Single-crystal, unalloyed W sheet before and after rupture testing for 53.6 hours at 2800°C and 1.05 kg/mm^2 (Neg. P67-4-23A; Inset, Neg. P67-3-44A)

Several typical developments evolved during the above study are presented below.

Timken 35-15 Stainless Steel

In a recent study by Clauss,[49] the stress-rupture data for Timken 35-15 stainless steel were correlated in terms of the Larson-Miller parameter using a constant C = 20. A plot of this correlation is shown in Figure 1. 57a indicating a high degree of scatter about an average behavior given by the solid curve. Dashed lines are used to demonstrate that the data at each temperature seem to describe a separate line and, hence, poor correlation is indicated. Obviously, when the solid curve is used for extrapolation to lower stresses at a given temperature, rupture times are predicted which are much higher than those actually observed.

When these same data were analyzed using the optimization procedures described previously,[50] the results shown in Figure 1. 57b were obtained. In this case, the Larson-Miller constant is found to be 12. 2 and results in a very excellent correlation. Extrapolation of these results to lower stresses would seem to be capable of yielding fairly acceptable results.

In Figure 1. 57c, the correlation obtained when C = 5 is presented. Here, too, when the C value is different from the optimum an extremely poor correlation results. It is apparent that as the C value is decreased, the isotherms assume different positions with respect to the average parameter curve until, at the optimum C value, all isotherms appear to be coincident with an average curve which can be drawn through all the points. Actually, the solid curve in Figure 1. 57b represents a polynomial developed in the least-squares optimization procedure applied to the Larson-Miller parameter.

Arc-Cast W, Mo, and W – 25Re

A linear relationship was identified[50] for the stress-rupture data of Hastelloy N when the natural logarithm of the Dorn parameter was plotted as a function of the natural logarithm of sinh ($C\sigma$), where C is a constant and σ is the stress. A similar approach was employed in analyzing the stress-rupture data for arc-cast W, Mo, and W – 25Re. As shown in Figure 1. 58, linear relations are obtained. Such plots can be compared to the standard master-rupture plots which usually yield a curved relationship.

When the hyperbolic sine approach is employed, it is possible to define the linear type of relationships shown. With this approach it would appear that extrapolation beyond the experimental stress range can be effected with more confidence than when the master rupture plot is curved.

In a similar analysis the Larson-Miller parameter was employed, and, as in Figure 1.58, a linear relationship was defined using the hyperbolic sine stress function. These results are presented in Figure 1. 59 where excellent linearity is seen to exist.

Timken 25-20 Stainless Steel

In an evaluation of the rupture data for Timken 25-20 stainless steel, Clauss employed the Larson-Miller approach, with C = 20, and found that a very unsatisfactory correlation resulted. On the parameter plot, data for each temperature described individual lines and no general correlation was noted. In the present study, these same data were analyzed using optimization procedures with the results shown in Figure 1. 60. It can be seen that all three parameters appear equally effective in the representation of these data, at least if the stand-

[49] F. J. Clauss, "An Examination of High-Temperature Stress-Rupture Correlating Parameters," Proc. of ASTM, Vol. 60, 1960, p. 905.

[50] "High-Temperature Materials Program Progress Report No. 63," GE-NMPO, GEMP-63, December 30, 1966, p. 13.

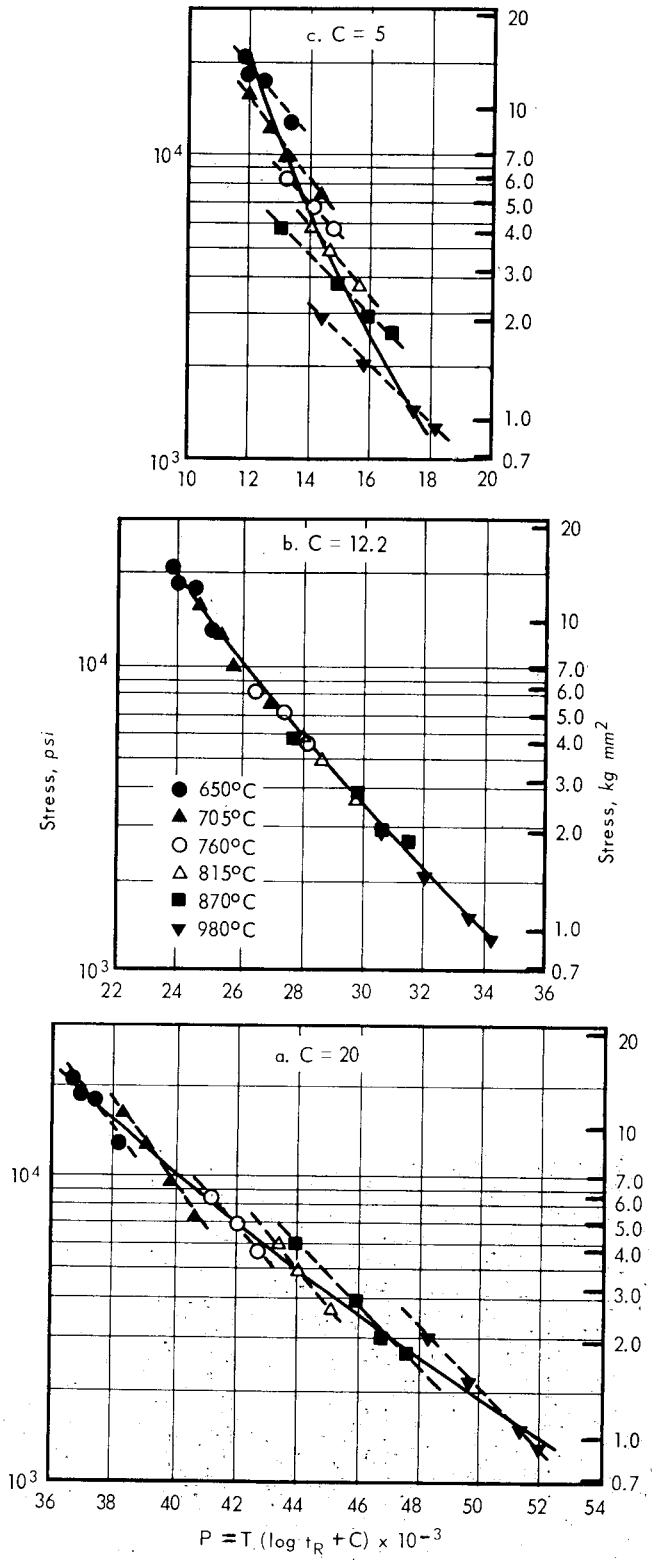

Fig. 1.57 — Larson-Miller plots of Timken 35-15 data illustrating effect of various C values

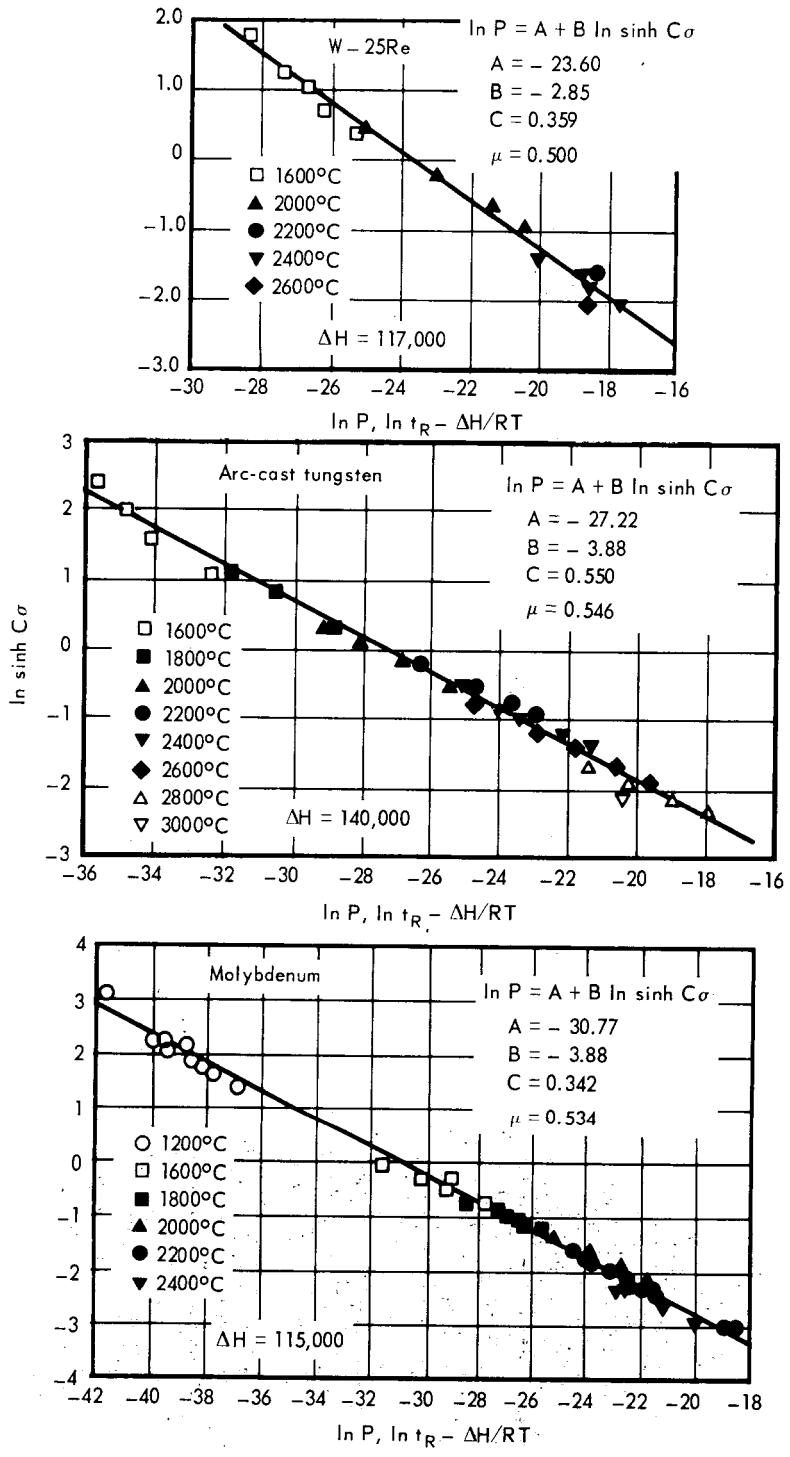

Fig. 1.58 – Dorn parameter plot for arc-cast W, Mo, and W – 25Re using hyperbolic sine stress function

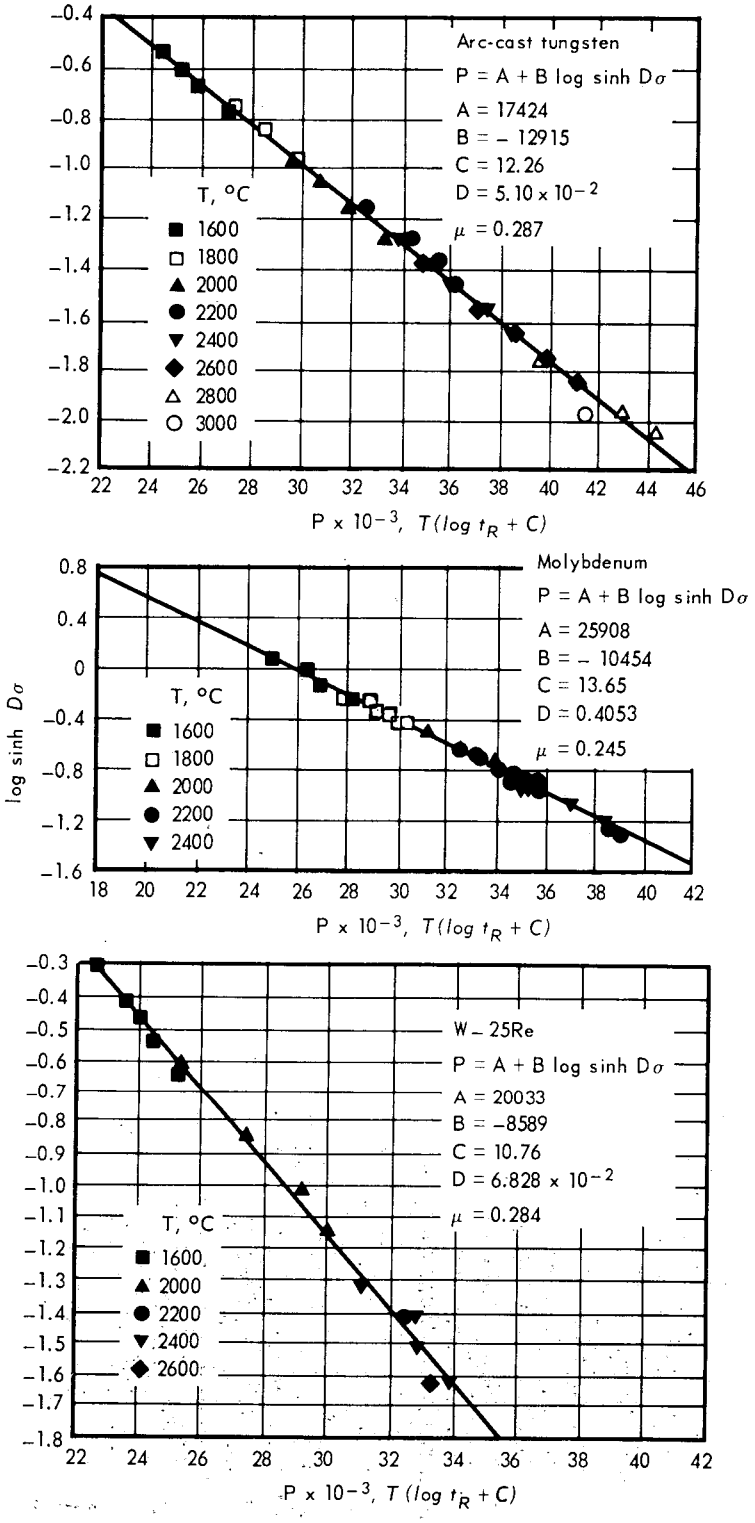

Fig. 1.59 — Larson-Miller parameter plot for arc-cast W, Mo, and W — 25Re using hyperbolic sine stress function

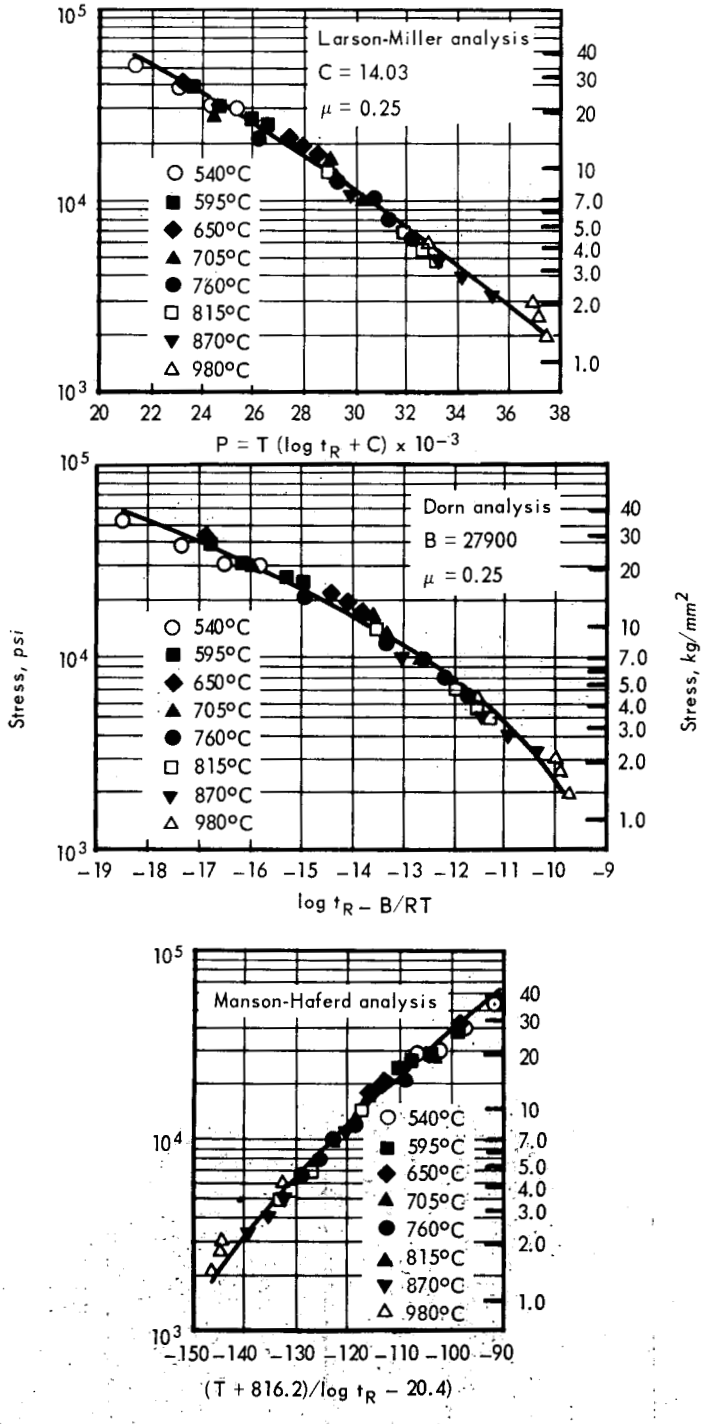

Fig. 1.60 — Rupture data for Timken 25-20 stainless steel analyzed in terms of various parameters

ard deviation, μ (based on log time) is used as a guide. For the Larson-Miller approach, the optimized C value of 14.03 yields a much better correlation than that observed in the Clauss analysis.

S-590 Alloy

Some indication of the relative extrapolative effectiveness of the Larson-Miller, Dorn, and Manson-Haferd parameters was provided in an analysis of the rupture data for S-590.[51] Employing optimization procedures, and assuming a second-degree polynomial relating the parameter to log stress, master-rupture plots were prepared for the three parameters. In one case, the analysis was based on data points below 10,000 hours while in a second evaluation only data points below 2000 hours were included.

Using the master rupture plots, the predicted rupture times corresponding to conditions beyond the range of data used in making the analysis were compared to actual experimental values. This comparison is presented in Table 1.12 where the standard deviations (based on log time) for each set of results indicate the Dorn parameter to be the most effective in the case of the 10,000-hour data with the Manson-Haferd slightly less effective. Rather poor results are seen for the Larson-Miller parameter. In the 2000-hour analysis, approximately equal effectiveness is seen for the Dorn and Manson-Haferd parameters with the Larson-Miller parameter again somewhat less effective. While these results identify certain parameters as being more effective than others, it cannot be concluded that this is a general result. For other data, the Larson-Miller parameter may give the best extrapolations.

TABLE 1.12

COMPARISON OF PREDICTED AND EXPERIMENTAL RUPTURE TIMES FOR S-590 ALLOY FOR LARSON-MILLER, DORN, AND MANSON-HAFERD PARAMETERS

Stress		Temperature,	Experimental Rupture	Predicted Rupture Times, hr		
kg/mm^2	psi	°C	Time, hr	L-M	Dorn	M-H
Based on S-590 data, $t_R < 10{,}000$ hours						
17.6	25,000	1200	43,978	62,248	42,958	41,698
21.1	30,000	1200	11,937	11,999	9,977	10,085
12.3	17,500	1350	16,964	19,508	13,493	16,378
7.0	10,000	1500	15,335	34,465	17,436	21,870
7.0	10,000	1500	11,257	34,465	17,436	21,870
				μ = 0.278	0.105	0.151
Based on S-590 data, $t_R < 2{,}000$ hours						
35.2	50,000	1100	3,149	1,661	1,614	1,467
24.6	35,000	1200	2,243	2,582	2,206	2,304
14.1	20,000	1350	9,529	5,921	4,234	5,143
8.8	12,500	1500	5,052	6,428	4,076	5,084
17.6	25,000	1200	43,978	50,747	29,856	29,860
21.1	30,000	1200	11,937	10,069	7,518	7,715
12.3	17,500	1350	16,964	17,761	10,332	13,067
7.0	10,000	1500	15,335	35,918	13,873	19,445
7.0	10,000	1500	11,257	35,918	13,873	19,445
				μ = 0.244	0.195	0.190

[51] R. M. Goldhoff, "Comparison of Parameter Methods for Extrapolating High Temperature Data," ASME Trans. J. of Basic Engrg., Vol. 81, 1959, p. 629.

COMPARISON OF TEST DATA

During the last few years, stress-rupture and creep data have been obtained for a number of refractory metals and alloys from 1600° to 2800°C. Stresses required to cause rupture in 1, 10, 100, and 1000 hours at 1600°C and 2200°C are given in Table 1.13 for a number of materials. Items of note are (1) at 1600°C arc-cast W – 25Re has the highest 100-hour rupture stress, whereas at 2200°C powder-metallurgy rhenium has the highest value followed by tungsten; (2) available data have indicated different behavior for arc-cast and powder-metallurgy forms of the same material. Figures 1.61 and 1.62 give isochronal stress-rupture data as a function of temperature for 1 and 100 hours. The change in rupture life with respect to temperature and time is readily seen.

TABLE 1.13

STRESS TO CAUSE RUPTURE AT TIMES INDICATED FOR VARIOUS REFRACTORY METALS AND ALLOYS

Material[a,b]	1600°C Stress,[b] kg/mm², at hours indicated				2200°C Stress,[b] kg/mm², at hours indicated			
	1	10	100	1000	1	10	100	1000
Tungsten								
AC	7.7*	5.2	3.6	2.5	2.0*	1.3	0.88	0.49
PM	0.84	5.5	3.5		2.3	1.6	1.1	
Molybdenum								
AC	2.5	1.5	0.98	0.62	0.46	0.28	0.17	0.098*
PM			1.3		0.70	0.59	0.38*	
Rhenium								
PM No. 1		5.6	3.1		3.5	2.2	1.2	
PM No. 2		7.4	4.8	3.2*	4.2*	2.8	1.7	
Niobium								
AC	0.63	0.39						
W–25Re (wt %)								
AC	15.*	8.8	4.9	2.8	2.5	1.3	0.70	0.38
PM	15.*	7.9	4.1		1.9	1.1	0.44*	
Mo–30W (wt %)								
AC	5.2*	3.0	1.8	1.0	1.0*	0.57	0.32	0.17
Mo–50Re (wt %)								
PM No. 1	4.3	2.7	1.7	1.1*	0.81	0.35	0.15	0.063*
PM No. 2	4.3	2.4	1.3	0.75*	0.81	0.35	0.15	0.063*
W–30Re–30Mo (at. %)								
AC		5.9*	2.8*			0.70*	0.42	0.25*
		4.2	2.2			0.74*	0.32	
Mo – 5W (at. %)								
PM	4.7*	2.5	1.3		0.75*	0.48	0.31	
Mo – 5Re (at. %)								
PM	4.7*	2.5	1.3		0.69*	0.46	0.31	
Re – 10Os (at. %)								
PM		6.7	4.5			2.7	1.1	
Ta – 10W (wt %)								
AC		7.7	4.9*		2.1*	1.2*		
Mo–TZM								
AC					0.48	0.28		
Tantalum								
AC	1.4				0.34*			
PM								
Cb-753[c]								
AC			0.84					

[a]Values with asterisk are based on extrapolations.
[b]Wrought sheet material, AC = arc-cast, PM = powder metallurgy.
[c]Nb – 5V – 1.25Zr (wt %).

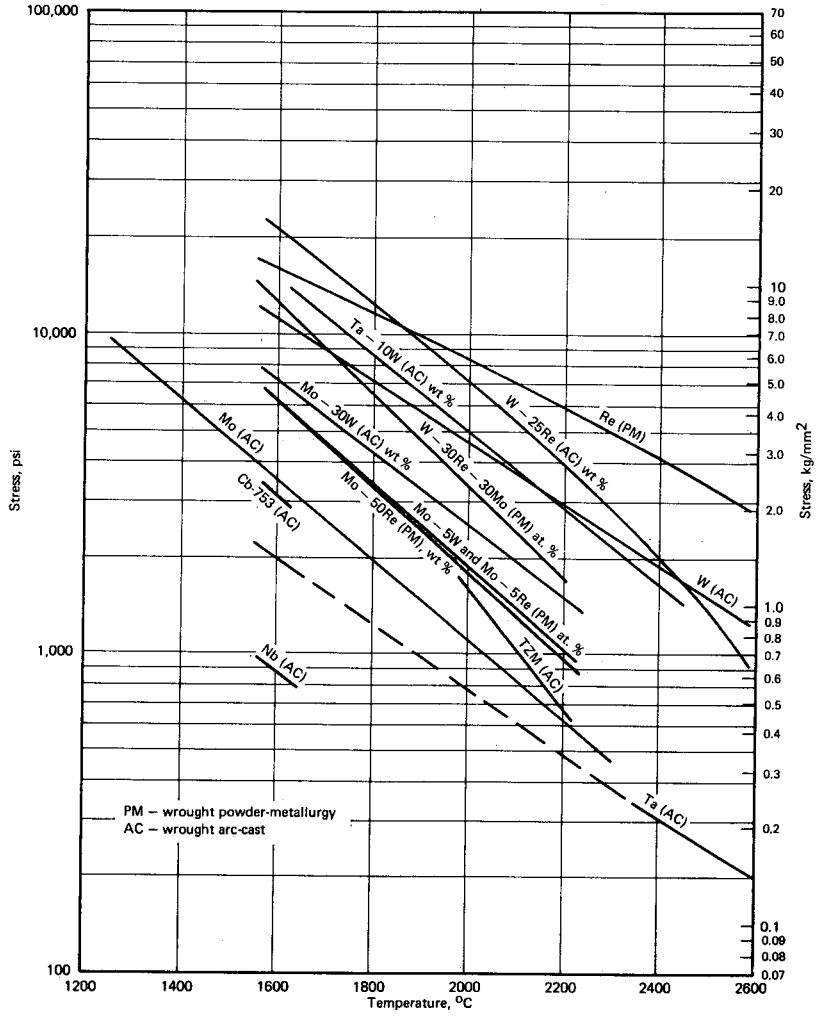

Fig. 1.61 — 1-hour isochronal stress-rupture data for various refractory metals and alloys

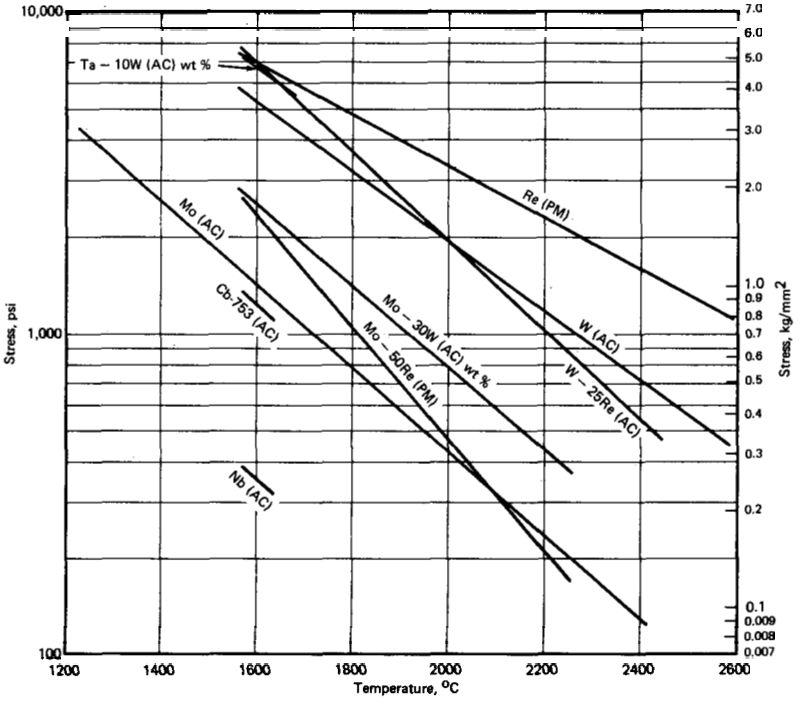

Fig. 1.62 – 100-hour isochronal stress-rupture data for various refractory metals and alloys

1.2 THERMAL PROPERTY EVALUATIONS

ELECTRICAL RESISTIVITY AND THERMAL CONDUCTIVITY

Measurements of the electrical resistivity of W – 26Re (wt %) and unalloyed tungsten were made from room temperature to 1600 °C in argon plus hydrogen. These data[52] are presented in Figure 1.63 along with some representative literature values.[53-57] A least squares analysis of these data yielded the following relationships:

W – 26Re

$$\rho = 1.86430 \times 10^{-5} + 3.37090 \times 10^{-8}T - 1.29457 \times 10^{-12}T^2 \qquad (1.17)$$

$$\mu = 2.43036 \times 10^{-7} \text{ ohm-cm}$$

Tungsten

$$\rho = 4.33471 \times 10^{-12}T^2 + 2.19691 \times 10^{-8}T - 1.64011 \times 10^{-6} \qquad (1.18)$$

$$\mu = 3.03318 \times 10^{-7} \text{ ohm-cm} \qquad 300°K \leq T < 1240°K$$

[52] GEMP-1002, pp. 26–31.

[53] D. L. McElroy, "High Temperature Materials Program Quarterly Report for Period Ending April 30, 1966," ORNL-TM 1520, Part 1, pp. 53–58.

[54] J. P. Moore, R. S. Graves, W. Fulkerson, and D. L. McElroy, "The Physical Properties of Tungsten," 1965 Conference on Thermal Conductivity, Denver, Colorado, October 1965, by permission.

[55] R. P. Tye, "Preliminary Measurements on the Thermal and Electrical Conductivities of Mo, Nb, Ta, and W," from Niobium, Tantalum, Molybdenum, and Tungsten, A. G. Quarell, Editor, Elsevier Publishing Co., Amsterdam, 1961.

[56] A. G. Worthing and E. M. Watson, "Resistance and Radiation of Tungsten as a Function of Temperature," J. Opt. Soc. A., Vol. 24, 1934, p. 114.

[57] V. S. Gumenyuk and V. V. Lebedev, "Investigating Heat and Electro-Conduction of Tungsten and Graphite at High Temperatures," Fizika Metallov and Metalovedeniye (2 Jan. 1961), Nr. 1, pp. 29–33, Translation USAEC-NP-TR733.

and

$$\rho = -4.06012 \times 10^{-12} T^2 + 4.6093 \times 10^{-8} T - 1.97071 \times 10^{-5} \qquad (1.19)$$

$$\mu = 1.56328 \times 10^{-6} \text{ ohm-cm} \qquad 1240°K < T < 2570°K$$

where:

ρ = electrical resistivity, ohm-cm
T = temperature, °K
μ = standard deviation

Previously reported data[52] for the thermal conductivity of W – 26Re (density close to 98 percent of theoretical) are summarized in Figure 1.64. Using the resistivity data reported above, the thermal conductivity data were analyzed to yield:

$$k = 2.443 \times 10^{-8} \frac{T}{\rho} + \frac{1}{0.7493 + 7.3427 \times 10^{-3} T} \qquad (1.20)$$

(standard deviation = 4.5818×10^{-2} watt/cm °C)

where:

k = thermal conductivity, watt/cm°C
T = temperature, °K
ρ = electrical resistivity, ohm-cm

Also shown in Figure 1.64 are data for W – 25Re reported by Jun and Hoch[58] and other data estimated by McElroy.[53] Fairly good agreement is noted between these data and those obtained in the NMPO studies.

THERMAL DIFFUSIVITY

A pulse-type diffusivity technique[59] based on the use of a laser was employed to measure the thermal diffusivity of commercial, powder-metallurgy W – 25Re in the temperature range from 300° to 1000°C. Specimens were in the form of discs 0.63 cm in diameter by 0.18 cm in thickness. A platinum-wound muffle furnace was used to provide the desired test temperatures and an oscilloscope was employed to determine the temperature – time transient of the specimen following the laser pulse. The time required for the back surface of the specimen to reach a temperature corresponding to one-half the maximum rise was then used in the usual manner to calculate diffusivity values. Data obtained for the W – 25Re alloy are presented in Figure 1.65. Also shown in this figure are diffusivity values calculated from the thermal conductivity data for the W – 26Re composition shown in Figure 1.64. As shown the agreement is quite excellent.

Diffusivity data were also obtained for arc-cast and powder-metallurgy tungsten using specimens 0.152 and 0.203 cm in thickness and 0.63 cm in diameter. All diffusivity values were in good agreement indicating no effect due to specimen thickness or material form. Average diffusivity values obtained in these tests are presented in Figure 1.66; all experimental data were within ±2 percent of this average curve. Also shown in Figure 1.66 are diffusivity data for tungsten calculated from some recent thermal conductivity data[60] reported for this material. Except at 300°C where a difference of slightly greater than 10

[58] C. K. Jun and M. Hoch, "Thermal Conductivity of Tantalum, Tungsten, Rhenium, Ta – 10W, T-222, W – 25Re in the Temperature Range 1500° – 2700°K," Third International Symposium on High-Temperature Technology, Stanford Research Institute, September 17–20, 1967. To be published.

[59] R. J. Freeman, "Thermal Diffusivity Measurements on Pre- and Post-Irradiated BeO," GE-NMPO, GEMP-452, November 15, 1966.

[60] Moore, Graves, Fulkerson, and McElroy, loc. cit.

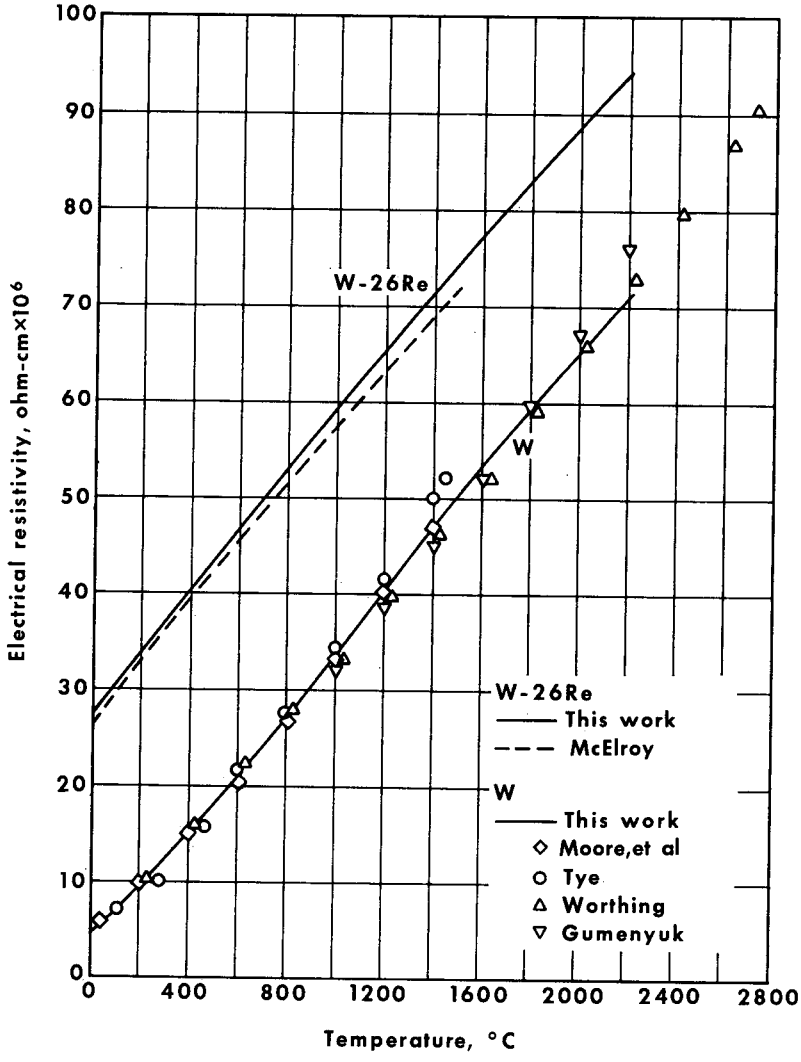

Fig. 1.63 — Electrical resistivity versus temperature for W — 26Re alloy and unalloyed W (AS-745B)

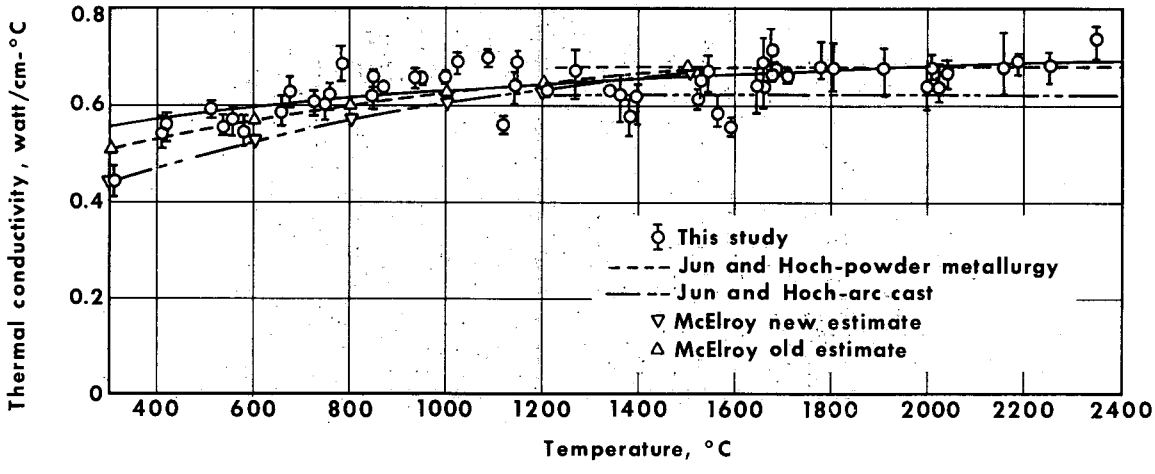

Fig. 1.64 — Thermal conductivity versus temperature for W — 26Re alloy (AS-745D)

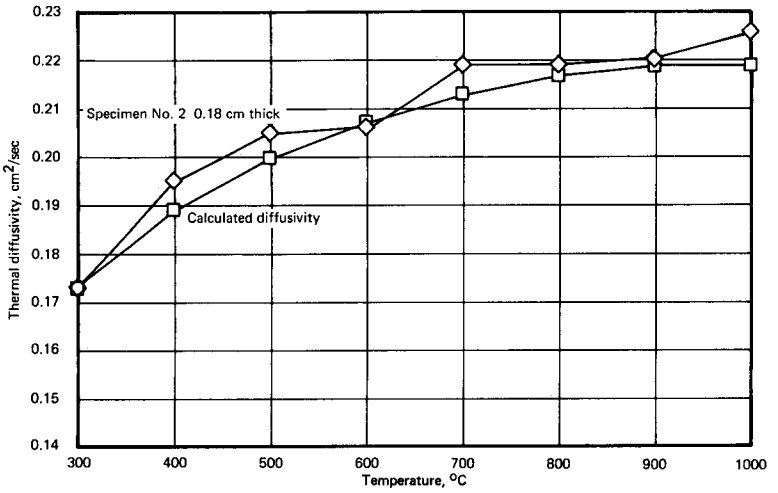

Fig. 1.65 – Thermal diffusivity versus temperature for W – 25Re (wt %) from 300° to 1000°C in argon atmosphere

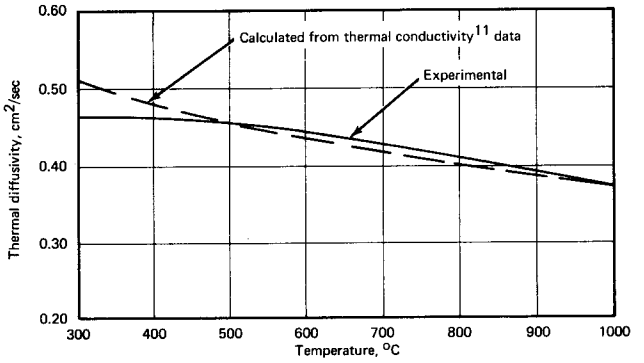

Fig. 1.66 – Average thermal diffusivity of tungsten from 300° to 1000°C in argon atmosphere (specimen thickness, 0.152 and 0.203 cm)

percent is indicated, agreement between measured and calculated diffusivity values is within 5 percent. This is excellent agreement considering the thermal conductivity data were obtained using a radial-flow steady-state technique, whereas the measured diffusivities were obtained by a transient procedure.

Diffusivity data were also obtained for 304L stainless steel in the temperature range from 300° to 1100°C. Testing was performed in argon using specimens 0.63 cm in diameter and 0.127 and 0.152 cm in thickness. The chemical composition of this material was: 18.37% Cr, 9.89% Ni, 0.024% C, 1.31% Mn, 0.70% Si, 0.014% P, 0.012% S, 0.09% Mo, and 0.05% Cu. A plot of the diffusivity data for this material is presented in Figure 1.67. It is important to note that for both specimen thicknesses the diffusivity increased slightly after the first heating to reveal an annealing effect.

ENTHALPY

Modifications were made to the drop calorimeter to permit enthalpy measurements to be made to 3000°C. Enthalpies of commercially pure (99.94%), powder-metallurgy tung-

sten were measured[61] to 3250°K and are summarized in Figure 1.68. A least squares analysis of these data yielded:

$$H_T - H_{298°K} = -1579.3 + 5.406T + 5.047 \times 10^{-4}T^2 + 271485X \qquad (1.21)$$

where:

X = exp. (-35629.5/RT)
H_T = enthalpy in cal/mole
R = 1.9869 cal/mole - °K
T = °K

applicable temperature range 1200° to 3250°K.

Differentiating the heat content equation yields the heat capacity equation:

$$C_p = 5.406 + 10.094 \times 10^{-4}T + 96728 \times 10^5 X/RT^2 \qquad (1.22)$$

where:

C_p = cal/mole - °K

A comparison of the heat capacities obtained in this study with those reported in the most recent literature[62-65] is given in Figure 1.69. Between 1200° and 2400°K agreement within 4 percent is shown for most of the data; however, this study is about 8 percent higher than that reported by Kirillin, et al.[63] at 3100°K. A slightly different equation was applied to Kirillin's data by West[65] to yield a slightly better representation; however, it only affected the C_p by about 2 percent (higher) at 3100°K.

1.3 SUMMARY AND CONCLUSIONS

Stress-rupture and creep data for wrought, arc-cast tungsten are presented for temperatures from 1600° to 3000°C and rupture times approaching 4000 hours. Good correlation is shown when analyzed in terms of the diffusion-compensated creep rate versus the modulus-compensated stress. The rupture ductility for arc-cast tungsten is a maximum (~20%) in the 2200° to 2400°C temperature range, whereas powder-metallurgy material shows a decrease in ductility (from 70%) with increasing temperature. Based on the counting of free dislocations for samples creep tested above one-half the absolute melting temperature, a power stress law is shown to apply indicating creep by dislocation climb or the glide of jogged screw dislocations. Optical microscopy and electron fractography studies of creep-rupture tested (1600° to 2800°C) powder-metallurgy and arc-cast tungsten indicate different mechanisms of failure operating in the two types of materials. The powder-metallurgy and arc-cast tungsten indicate different mechanisms of failure operating in the two types of materials. The powder-metallurgy material showed pronounced grain boundary separation and cavitation, whereas the arc-cast material showed no tendency to form cavities.

Stress-rupture and creep data are presented for wrought, arc-cast, unalloyed molybdenum sheet for temperatures from 1200° to 2400°C. Good correlation between the time to rupture and linear creep rate is shown except for the extremely high temperatures

[61] GEMP-1002, p. 34.

[62] M. Hoch and H. L. Johnston, "A High Temperature Drop Calorimeter. The Heat Capacities of Tantalum and Tungsten Between 1000° and 3000°K," J. Phys. Chem., Vol. 65, 1961, pp. 855–860.

[63] V. A. Kirillin, et al., "Thermodynamic Properties of Tungsten at 0° – 3500°K," Zhurnal Fizi Khimii, Vol. 37, No. 10, 1963, pp. 2249–2257.

[64] G. C. Lowenthal, "The Specific Heats of Metals Between 1200°K and 2400°K," Aust. J. Phys., Vol. 16, No. 1, 1963, pp. 47–67.

[65] E. D. West and S. Ishihara, National Bureau of Standards, Washington, D.C., Preliminary Data of the Enthalpy of Tungsten – private communication.

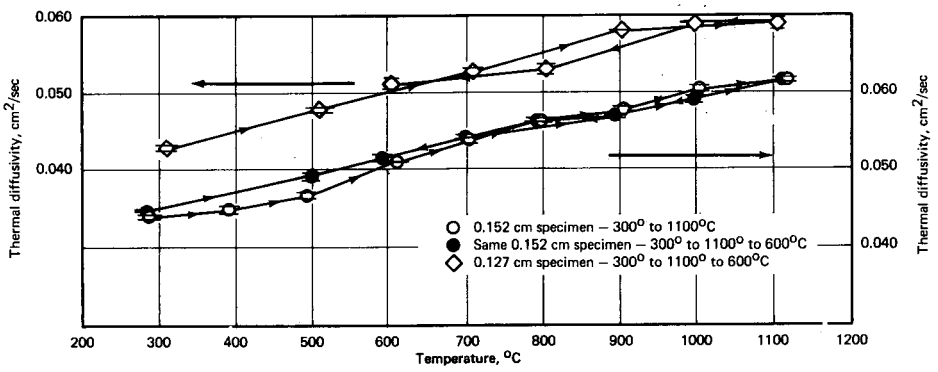

Fig. 1.67 – Thermal diffusivity of 304L stainless steel from 300° to 1100°C in argon atmosphere

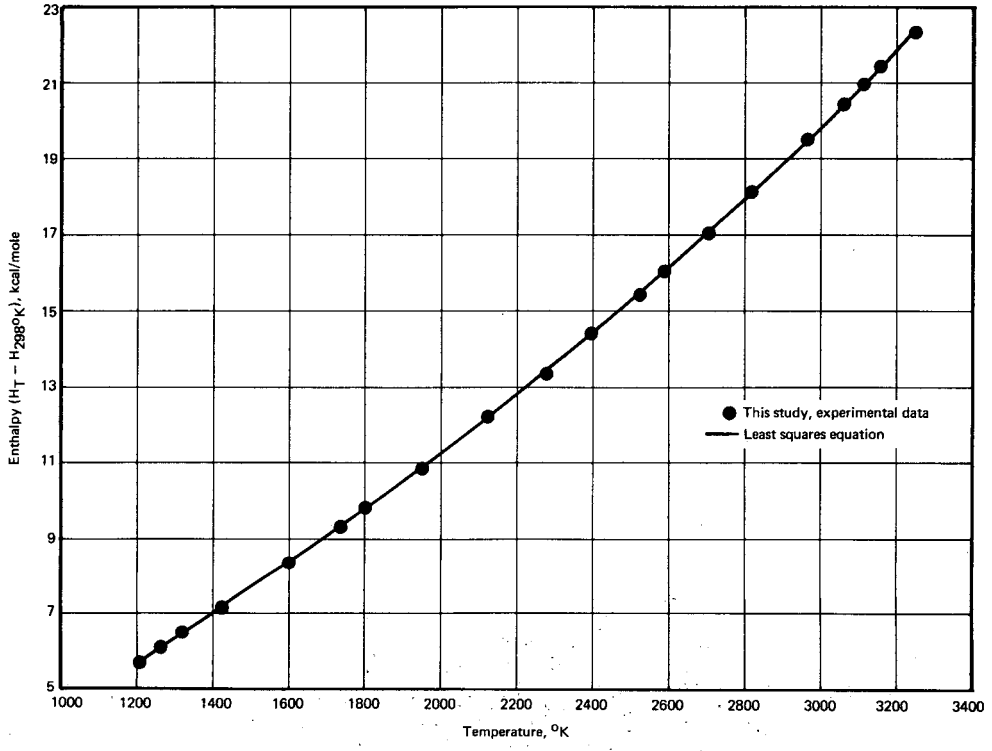

Fig. 1.68 – Enthalpy versus temperature for tungsten (99.94% purity)

and low stresses. The deviation appears to be related to a change in the creep mechanism indicated by a change in the form of the creep curve.

Creep-rupture data are presented for Re, W – 30Re – 30Mo (at. %), Mo – 30W (wt %), and W – 25Re (wt %) sheet tested in hydrogen at temperatures from 1600° to 2600°C.

Creep-rupture properties for powder-metallurgy Mo – 50Re (wt %) are presented for temperatures of 1600°, 2200°, and 2400°C. Diffusional creep is indicated at the higher temperatures and low stresses based on the creep rate versus stress relationship yielding a slope of unity. The diffusion coefficient for Mo – 50Re at 2400°C and 0.07 kg/mm^2 was calculated to be 1.14×10^{-7} cm^2/sec.

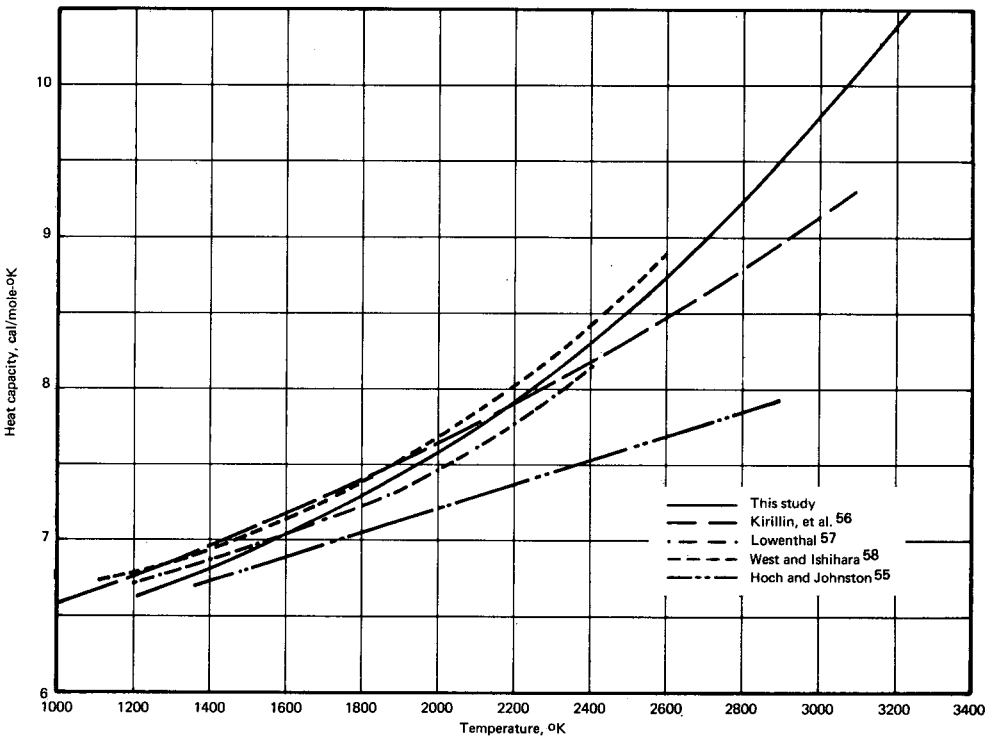

Fig. 1.69 – Heat capacity versus temperature for tungsten

Creep-rupture tests of Mo – 30W at 2200°C under constant load display a creep curve consisting only of third-stage-type creep with the elongation at rupture exceeding 100 percent. Identical tests performed at constant stress display a linear (secondary) creep rate to a strain of 65 percent.

Creep-rupture tests of powder-metallurgy tungsten at 2800°C and 1.05 kg/mm^2, in single-crystal form, displayed no detectable creep with fracture being brittle in nature. This result appears to be consistent with creep deformation observations for most powder-metallurgy, polycrystalline materials tested at high temperatures in that cavitation and/or grain boundary separation are the predominant mechanisms.

A comprehensive study of stress-rupture parameters was completed with special consideration given to the mathematical procedures employed in identifying parameter constants. Detailed comparisons were made of the relative effectiveness of these parameters in the correlation and extrapolation of experimental data.

Based on experimental measurements of thermal conductivity and electrical resistivity for W – 26Re (wt %), an expression describing the thermal conductivity from 400° to 2400°C is presented.

Enthalpies of unalloyed tungsten were measured from 1200° to 3450°K. Equations for heat content and heat capacity were determined from the data using a least squares analysis.

1.4 PLANS AND RECOMMENDATIONS

Stress-rupture and creep studies will be continued for commercially available and developmental refractory metal alloys as well as materials having potential application to

the LMFBR program. Evaluations will be performed in inert, reducing, and vacuum environments.

In an attempt to identify the mechanisms associated with creep resistance and deformation, optical and transmission electron microscopy studies of tested samples will be performed.

Creep tests at constant stress will be performed to afford a comparison with data obtained under constant load. The results will assist in determining the stress dependence of more complex materials.

Some physical properties will be determined for materials of interest. Properties such as enthalpy, thermal expansion, and thermal conductivity will be determined to temperatures approaching the melting point for design purposes as well as hazards evaluation. Some thermal diffusivity measurements to 1000°C are also planned.